STUDIES ON HYDRODYNAMIC DELIVERY AS A TREATMENT FOR ACUTE KIDNEY INJURY

by

Alexander Kolb

A Dissertation

Submitted to the Faculty of Purdue University

In Partial Fulfillment of the Requirements for the degree of

Doctor of Philosophy

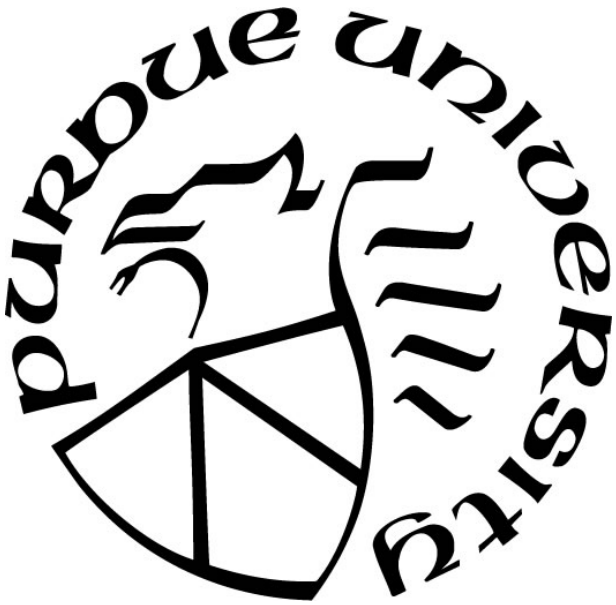

Department of Biology

Indianapolis, Indiana

August 2017

THE PURDUE UNIVERSITY GRADUATE SCHOOL
STATEMENT OF COMMITTEE APPROVAL

Dr. Simon Atkinson, Chair
Department of Biology

Dr. Robert Bacallao
Department of Medicine, Division of Nephrology, Indiana University School of Medicine

Dr. David Basile
Department of Cellular and Integrative Physiology, Indiana University School of Medicine

Dr. Guoli Dai
Department of Biology

Dr. Daniel Szymanski
Department of Agronomy

Approved by:

Dr. Theodore Cummins
Head of the Graduate Program

I dedicate this dissertation to Kelly and our little one Clara. Your patience, dedication, and love made this all possible. Thank you for believing in me and pushing me to succeed.

ACKNOWLEDGMENTS

I would like to thank Dr. Simon Atkinson, Dr. Robert Bacallao and Weimin Xu for their help, insight, and guidance over the past four years. Your dedication, time, and patience molded me into the researcher I am today. I started this journey more than four years ago with little research experience and the time you invested in me will never be taken lightly, never be forgotten, and will continuously to be passed on to future generations. Thank you for passing on your gifts to future scientists.

I would like to thank Dr. David Basile and Dr. George Rhodes. Thank you for spending time teaching me animal surgeries and how to critically evaluate my data. The time you invested and the discussions we had are very much appreciated.

I would like to thank Dr. Guoli Dai and Dr. Daniel Szymanski for serving on my dissertation committee. The discussions we had helped me shape my research and thesis.

I would like to thank past members of the Atkinson laboratory: Dr. Mark Hallett, Dr. Peter Corridon, Shijun Zhang, and Michelle Lu. I enjoyed our conversations and the time spent working together.

I would also like to thank my family. Your support and love made this possible.

TABLE OF CONTENTS

LIST OF TABLES

LIST OF FIGURES

ABBREVIATIONS

AKI- Acute Kidney Injury

AMP- Adenosine Monophosphate

ATP- Adenosine Triphosphate

BCL-2- B-Cell Lymphoma Type 2

CKD- Chronic Kidney Disease

ESRD- End Stage Renal Disease

ETC- Electron Transport Chain

$FADH_2$- Flavin Adenine Dinucleotide

FCCP- Carbonyl cyanide-*4*-(trifluoromethoxy)phenylhydrazone

FITC- Fluorescein Isothiocyanate

GFR-Glomerular Filtration Rate

GSK3-β- Glycogen Synthase Kinase 3-beta

GTP- Guanosine-5'-Triphosphate

HIFD- Hydrodynamic Isotonic Fluid Delivery

HPLC- High Pressure Liquid Chromatography

HRP- Horseradish Peroxidase

IDH2- Isocitrate Dehydrogenase II (NADP+), Mitochondrial

IPC- Ischemic Preconditioning

IRI- Ischemia Reperfusion Injury

MCA- Multiplex Cell Authentication

MDCK- Madin-Darby Canine Kidney

MPTC- Murine Proximal Tubule Cells

MPTP-Mitochondria Permeability Transition Pore

NAD(P)H- Nicotinamide Adenine Dinucleotide Phosphate

NADH- Nicotinamide Adenine Dinucleotide

OCR- Oxygen Consumption Rate

PAPS- Phosophoadenosine-5'-phosophosulfate

PFA- Paraformaldehyde

PGC1-α- Peroxisome Proliferator-Activated Receptor Gamma Coactivator 1-alpha

PI-Propidium Iodide

RISK- Reperfusion Injury Salvage Kinase

ROS- Reactive Oxygen Species

S3- Segment 3

SAFE- Survivor Activating Factor Enhancement

SCr- Serum Creatinine

SRC- Spare Respiratory Capacity

STAT 3- Signal Transducer and Activator of Transcription 3

STR- Short Tandem Repeat

SULT1C2- Sulfotransferase 1 C2

TCA- Tricarboxylic Acid Cycle

TFAM-Transcription Factor A, Mitochondria

TMRM-Tetramethyl Rhodamine Methyl Ester

Ψ_m- Mitochondria Membrane Potential

ABSTRACT

Author: Kolb, Alexander, L. Ph.D.
Institution: Purdue University
Degree Received: August 2017
Title: Studies on Hydrodynamic Delivery as a Treatment for Acute Kidney Injury
Major Professor: Simon Atkinson

Hydrodynamic delivery is a powerful tool that allows delivery of macromolecules to the kidney culminating in gene expression. This finding is important in the fight against kidney disease. Current therapy for kidney injury, specifically acute kidney injury, is lacking. Supportive care in the form of IV fluids and medications aimed at restoring Glomerular Filtration Rate (GFR) and urine output are currently used. However, even with these treatments, prognoses of patients diagnosed with this disease remains poor. We believe that hydrodynamic delivery provides a mechanism that can be used to reverse and prevent AKI. Hydrodynamic delivery following ischemic injuries leads to reductions in serum creatinine and infiltrating mononuclear cells, as well as increased renal blood flow and survival. These changes are due to reductions in vascular congestion and inflammation typically seen following injury. To determine the underlying mechanisms of gene delivery preventing AKI, we used candidate genes identified in a proteomic screen on kidneys that recovered from AKI. We selected Isocitrate Dehydrogenase II (IDH2) and Sulfotransferase 1C2 (SULT1C2) for study and found that delivery prior to injury prevents serum creatinine increase and reduces cell death. We found that gene delivery of *IDH2* prevents a glycolytic shift typically seen following ischemic injuries. The mechanism underlying the prevention of this shift are seen in increased ATP stores and spare respiratory capacity allowing the cell to remain in an

oxidative state. Additionally, we show that SULT1C2 post-translationally modifies the mitochondria membrane, increasing oxidative phosphorylation providing the cell with additional energy needed in times of oxidative stress. These candidate genes allow cells to remain in an oxidative state preventing the activation of cell death pathways typically activated following injury, thereby preserving normal kidney function.

CHAPTER 1: INTRODUCTION

1.1 The Kidney

1.1.1 Why Study the Kidney

The kidney is a dynamic organ. Its functions range from waste excretion to electrolyte balancing, to maintaining a hormone balance that is important for regulating blood pressure, contributing to red blood cell development, and aiding in bone formation and turnover (2-6). The kidney's regulation is pivotal for human life. At rest, kidneys utilize >25% of cardiac output at any given moment and any slight change in that output has the potential to reduce kidney function leading to disease (2). Similarly, if urine output decreases, this is also an indication of kidney disease. It is important that the filtration of waste from the blood into the urine be maintained at constant and consistent rates to prevent kidney disease and diseases elsewhere. If homeostasis cannot be maintained, treatment may be required. The costs and the length of hospital stays for patients suffering from kidney injury, specifically acute kidney injury (AKI), are on the rise. Patients diagnosed with AKI not requiring dialysis spend an extra 7,900 dollars and stay three additional days in the hospital. Patients requiring dialysis spend an extra 42,000 dollars and stay an extra twelve days (3). As of 2017, patients diagnosed with AKI accrue more in hospital costs then patients suffering from myocardial infarctions and gastrointestinal bleeding (2-4). Currently, patients hospitalized for kidney disease have one treatment option, renal replacement therapy (dialysis or transplant). Patients who are initially hospitalized with this disease category are supported with fluids and medications,

such as steroids or ionotropes, with the sole purpose of reestablishing normal glomerular filtration rates. Once diagnosed with kidney disease, patients are afflicted their entire life and progression from acute to chronic to end stage disease is likely. Novel therapies are needed for patients suffering not just from AKI but other forms of kidney disease in order to prevent additional increases in both cost of care and length of stay.

1.1.2 Renal Physiology

As mentioned previously, the kidney is involved in balancing electrolytes and hormones, regulating blood pressure, and excreting waste. These processes occur in the nephron. The nephron is composed of two major units, each of which serves specific and distinct functions. The first unit, the renal corpuscle, is composed of the glomerulus and Bowman's Capsule. The second unit, known as the tubule unit, consists of proximal, distal, and connecting tubules in addition to the Loop of Henle (Fig 1)(7).

The main role of the renal corpuscle and its components is filtration. The glomerulus is responsible for filtering blood, regulating filtrate pressure to ensure normal glomerular filtration rate, and controlling what is filtered from the blood. The glomerulus is made up of three units that work together to regulate filtration- filtrated endothelial cells, podocytes, and extracellular membrane. Together these three units work as a sieve, regulating the flow of water and small solutes while retaining proteins, sugars, and other electrolytes in the body (8-13). Damage to any one of these three components has the potential to cause kidney disease.

The second unit of the nephron is the tubule unit. The main function of the tubule is filtrate and water reabsorption back into circulation (7). The proximal tubule, for

example, is involved in reabsorption of water, glucose, amino acids, Na^+, Cl^-, urea, and K^+, among other ions. The loop of Henle is also important in water and sodium chloride reabsorption. The varying permeability in the loop regulates where (ascending or descending limb) and what (water or solutes) is reabsorbed into circulation. Once past the Loop of Henle, the filtrate passes through the distal tubule. The distal tubule is involved in Ca^{2+} reabsorption and regulation of urine pH. Once through the distal tubule, the filtrate collects in the collecting duct and then exits the body as urine (12-15).

1.1.3 Renal Diseases Classification

Renal diseases can be classified into three main categories and each has its own criteria. These three categories are Acute Kidney Injury (AKI), Chronic Kidney Disease (CKD), and End Stage Renal Disease (ESRD). AKI is defined as a sudden decrease in glomerular filtration rate and urine output coupled with increases in blood urea nitrogen and serum creatinine. To be diagnosed with AKI patients must present with a 1.5-2-fold increase in serum creatinine (SCr) or 50% reduction in GFR, or a urine output of <0.5 mL/kg for twelve hours. CKD on the other hand is similar in presentation to AKI with the exception that patients present with deteriorating kidney function for periods greater than one month and typically higher SCr. Finally, ESRD is classified by complete renal failure for greater than three months and a dependence on dialysis for that time period. Once diagnosed with kidney disease, the progression from AKI to CKD to ESRD is likely. While current treatment methods are lacking, what is known is that AKI maybe reversible and a likely area for successful treatment (16-18).

1.2 Acute Kidney Injury (AKI)

1.2.1 Establishing the Definition of AKI

There is not a singularly agreed upon definition of AKI. The aspects of AKI that make it difficult to classify are the dynamic nature of the kidney and the patients that present with the disease. Essentially, clinicians refer to AKI as a rapid loss of kidney function with a simultaneous decrease in glomerular filtration and increases in serum creatinine and/or blood urea nitrogen (2, 19, 20). Clinicians established this definition of AKI during the Acute Dialysis Quality Initiative (ADQI) where they were able to lay the foundations for categorizing kidney injury. The criteria for these categories are laid out using the acronym RIFLE: Risk, Injury, Failure, Loss, and End stage renal disease and are used in determining various stages of kidney disease (Table 1) (17). These criteria have gone through modifications over the past decade and a half. The first was in 2005 during the Acute Kidney Injury Network (AKIN) coalition meeting; this modification included patients that present with changes in kidney function, but fell below the initial risk category (Table 2) (17). In 2012, during Kidney Disease: Improving Global Outcomes meeting, it was established that changes made to the RIFLE criteria guidelines set up by ADQI and AKIN were successful in diagnosing patients with kidney injury all over the world (Table 3).

1.2.2 Scope of Clinical Issues

Acute Kidney Injury (AKI) present in 2-7% of hospitalized patients, but increases to over 15% for patients admitted to the ICU. Once hospitalized for AKI, mortality rates

increase to over 50% (2, 3). The critical issue with AKI is that there is no known cure; only supportive care can be provided. Even with supportive care, relapse is likely and progression to ESRD likely. Aside from the progression of AKI to CKD or ESRD, there are other complications that can arise from AKI such as metabolic acidosis, high potassium levels, uremia, and changes in fluid balance (2, 19, 21). The only treatment option following the progression of AKI is renal replacement therapy. Of the three mentioned kidney diseases AKI is the only type that is reversible. Recent findings have indicated that gene therapy may play a crucial role in reversing the progression of AKI (22).

1.2.3 AKI: The Causes and Types

Once diagnosed with Acute Kidney Injury, the next step is to determine the type of acute injury and the potential cause of that injury. AKI is divided into three etiologies: prerenal, renal, and postrenal. Prerenal, as the name describes, is an acute injury associated with changes outside the kidney prior to renal circulation. Prerenal injuries are associated with decreases in cardiac output of >25%. Causes of prerenal acute injury include hypovolemia from fluid loss, congestive heart failure, and decreases in vascular resistance due to sepsis or anaphylaxis to name a few.

Renal acute injury entails injuries that occur directly to the kidney itself that can lead to damage to tubules, interstitium, vasculature, or glomeruli. This damage can result in acute tubular necrosis, glomerulonephritis, and acute interstitial nephritis.

The final type of acute injury is caused by post renal injury, or changes in urine output. These changes in urinary output can be the result of prostate cancer or

inflammation, cervical cancer, catheter obstructions, kidney stones, or growths that cause changes in the bladder or urethra (2, 7, 23-26).

1.2.4 Mechanisms of AKI

Much like the definition of AKI, its causes are complex and diverse. Causes of AKI range from sepsis, to systemic inflammation, to an ischemic insult. The complexities of these causes are difficult to parse thus making determination of injury onset arduous. (Table 3) (7).

Sepsis, an uncontrolled immune response to infection leading to organ failure, is the most common cause of AKI in critically ill patients and is diagnosed as the cause of AKI in 40-50% of these patients (27, 28). Causes of sepsis-induced-AKI include hypo-perfusion, microvascular dysfunction, inflammation, and tubular epithelial cell reprogramming (differentiation into a new cell type or self–renewal). Septic AKI was once believed to be the result of changes in perfusion, mainly hypoperfusion. However, recent studies have indicated that even in the absence of abnormal flow, septic AKI can still occur. The models now point to changes in tubular cell behavior, cellular response to inflammatory cytokines, and endothelial communication as potential causes of septic AKI (29-36).

Systemic inflammation is also a cause of AKI. Mechanistically, the inflammatory response is brought about during cellular reprograming in response to stress. In this case, the stressor can lead to apoptosis and necrosis. In the kidney, the cells most susceptible to stress are the tubular epithelial cells (37-41). During a necrotic event, the epithelial cells release damage associated molecular patterns, DAMPs, which lead to the activation of

pattern recognition receptors, such as Toll-like receptors or other inflammatory receptors (37-41). The activation of these receptors allows recruitment and activation of immune cells such as monocytes, dendritic cells, and macrophages that then release their chemokines. The release of chemokines such as CXCL1 or CXCL5 contributes to the activation of immune and inflammatory responses. To maintain a pro or anti-inflammatory state requires specific pro or anti-inflammatory cytokines, and it is the balance between the two that regulates inflammation. During an ischemic event, the balance between the cytokine population changes allowing an accumulation of pro-inflammatory cytokines, leading to inflammation. This inflammation causes changes in vascular permeability and blood flow (37-41).

Another common model for AKI is an ischemic injury. During ischemic injury, renal blood flow decreases leading to decreased oxygen supply to the kidney and a buildup of waste products such as ureic nitrogen and creatinine. The buildup of these waste products and the lack of oxygen lead to reductions in both oxidative phosphorylation and ATP levels in the cell. As stated previously, reductions quickly lead to cellular reprogramming and apoptotic or necrotic cells. In the case of renal ischemia, the cell type that is most affected is the proximal tubular epithelial cell. ATP depletion in this cell type quickly leads to changes in cellular polarity and signaling, typically followed by cell death.

In addition to the epithelium, the endothelium and its cells are also critical in regulating AKI. As previously mentioned, changes in microcirculatory flow in the kidney lead to poor endothelial barrier function, the recruitment of inflammatory cells, and reductions in vasodilators (NO for example). Taken together, damage to the endothelium

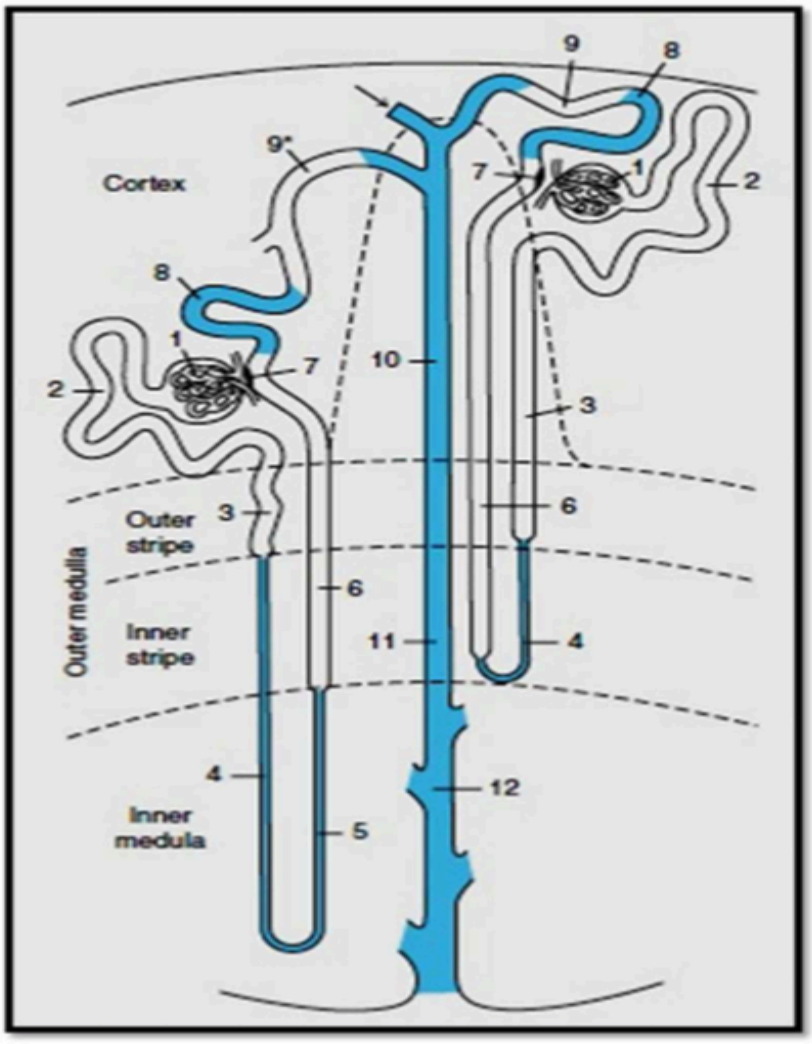

Figure 1: Schematic Illustration of a Nephron (7). 1- Renal corpuscle consisting of Bowman's capsule and the glomerulus; 2-Proximal Convoluted Tubule; 3-Proximal Straight Tubule; 4- Descending Thin Limb of the Loop of Henle; 5- Ascending Thin Limb of the Loop of Henle; 6- Think Ascending Limb of the Loop of Henle; 7- Macula Densa; 8- Distal Convoluted Tubule; 9- Connecting Tubule; 10- Cortical Collecting Duct; 11- Outer Medullary Collecting Duct; 12- Inner Medullary Collecting Duct.

can lead to cellular coagulation: reductions in vascular space leading to reductions in blood flow and culminating in ischemic injury (6, 8, 9, 42, 43).

1.2.5 Managing AKI

Currently the options for clinical management of AKI are limited. Patients admitted to the hospital are treated on a symptom-by-symptom basis. The goal of treatment is to reestablish homeostasis by restoring blood flow to the kidney and restoring a normal GFR. The care provided is supportive only. This is accomplished by providing fluids, electrolytes and controlling pH. If this fails, or if patients are suffering from a severe injury, renal replacement therapy is the only option.

1.3 Ischemic Preconditioning (IPC)

1.3.1 Background of IPC

Ischemic preconditioning was first observed by Murry *et al* in 1986 (44). Since the original observation that applying non-lethal doses of ischemia to target organs can confer protection against subsequent injury, it has been thought that a full understanding of this phenomenon would offer an entree to therapy for ischemic injury. Following Murry *et al's* demonstration of this phenomenon, studies were conducted on different organs such as the heart, brain, liver, and kidney to name a few (9, 44-47). The conclusions drawn from these studies were similar to what Murry *et al* demonstrated in 1986, that ischemic episodes to these organs protected them from future injury.

Table 1: RIFLE Criteria for AKI Classification

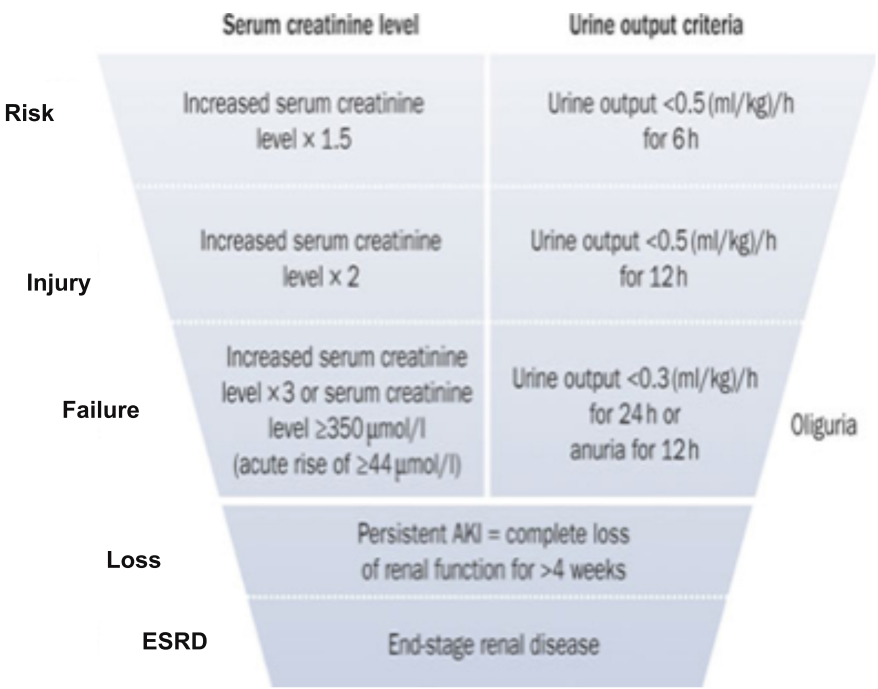

Table 2: AKIN Staging System for AKI from Murugan and Kellum (17).

AKIN-2007

Medscape® www.medscape.com

Stage	Serum creatinine criteria	Urine output criteria
1	Increase of ≥26.4 µmol/l (0.3 mg/dl) OR to 150–200% of baseline (1.5–2.0-fold)	<0.5 ml/kg/h for >6 h
2	Increase to >200–300% of baseline (>2–3-fold)	<0.5 ml/kg/h for >12 h
3[a]	Increase to >300% of baseline (>3-fold; or serum creatinine ≥354 µmol/l [4.0 mg/dl] with an acute rise of at least 44 µmol/l [0.5 mg/dl])	<0.3 ml/kg/h for 24 h OR anuria for 12 h

Only one criterion (creatinine or urine output) needs to be fulfilled to qualify for a stage. [a]Patients who receive renal replacement therapy are considered to have met the criteria for Stage 3, irrespective of the stage that they are in at the time of commencement

Table 3: Potential Pathways Implicated in the Development of AKI.(7)

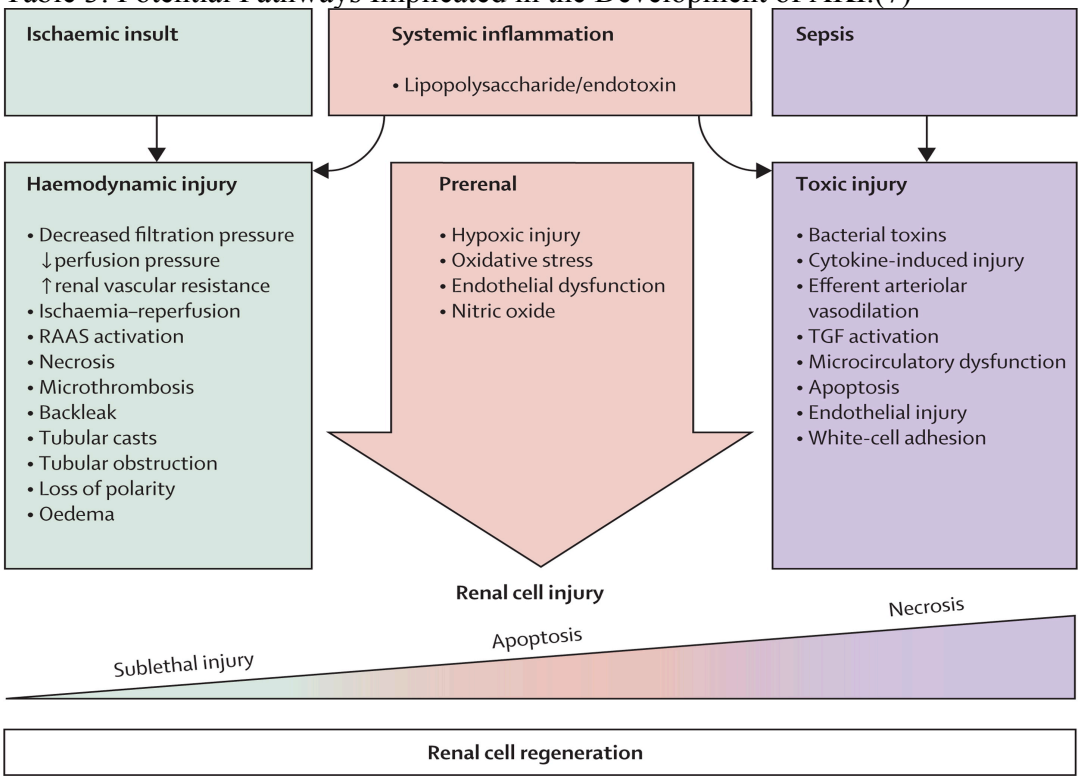

1.3.2 Mechanism of IPC

While the exact mechanisms of IPC are not well understood, what is known is that non-lethal doses of ischemia can confer protection to the target organ. Studies conducted on IPC have also shown that IPC reduces apoptotic cell death, endothelial dysfunction, oxidative stress production and inflammation (48-52). Two possible pathways that are implicated in IPC and its protective effects are the RISK, Reperfusion Injury Salvage Kinase, and SAFE, Survivor Activating Factor Enhancer pathways.

The RISK pathway relies on the activation of G-protein-coupled ligands and the pro-survival kinases AKT and ERK. The combination of these kinases prevents the activation of pro-apoptotic factors and prevents mitochondria Permeability Transition Pore (mPTP) opening promoting cell survival (Figure 2) (49). Studies have demonstrated that stimulation of this pathway prior to ischemia confers protection.

The second pathway, the survivor activating factor enhancer (SAFE) pathway, behaves similarly to the RISK pathway in that it promotes cellular survival (Figure 3) (53). Unlike the RISK pathway, the SAFE pathway is activated by Tumor Necrosis Factor alpha, TNFα, leading to the activation of the JAK-STAT pathway. The activation of the STATs, particularly STAT 3 leads to the activation of pro-survival and proteins such as BCL-2, and reductions in pro-apoptotic proteins such as Bad. There is also data that indicates STAT 3 may even regulate mitochondria activity through mitochondria connexin 43 which is involved in releasing stored biochemical energy such as ATP, GTP, and NAD(P)H during stress (53-56).

The result of both pathways is cell survival. Both pathways have been implicated in promoting survival through the upregulation of anti-apoptotic genes and the

downregulation of pro-apoptotic genes in addition to regulating mitochondria activity. These areas are potential targets for therapies that mimic IPC to prevent cell and organ death.

1.3.3 IPC in the Kidney

Ischemic preconditioning in the kidney was first studied by Zager *et al* (57). This work laid the foundation for studying IPC in the kidney. Using this foundation, Joo *et al*. demonstrated that IPC consists of two protective windows (58). These protective windows consist of an acute window, which begins immediately following IPC and extends for several hours and a late window which begins around 24 hours and lasts up to several weeks following recovery from injury. Acute IPC may be mediated by mechanisms related to ion channels and cell signaling such as the RISK and SAFE signaling pathways (48, 49, 53, 55, 59, 60). The late phase involves transcriptional activation and translation of cytoprotective proteins such as hypoxia induced transcription factors or heat shock proteins. Because mitochondria impairment represents an early step in the pathogenesis of renal injury, IPC may be mediated in part by preserving mitochondria function in response to IRI by preserving cellular ATP levels, reducing ROS production and inhibiting cell death pathways (60-62).

1.3.4 Involvement of Mitochondria in IPC

Mitochondria involvement in ischemic preconditioning was first noted by Murry *et al* in 1986 and further analyzed in 1989. Murry and colleagues hypothesized two possible biochemical scenarios that led to ischemic injury, metabolite loss or catabolite

accumulation (63). Both of these biochemical processes focus on mitochondria and its involvement in IPC. They concluded that mitochondria protect cells from ischemia by conserving ATP and reducing the catabolite accumulation responsible for ischemic cell death. Future study conducted by other investigators revealed that Murry's conclusions laid the foundation for the involvement of mitochondria proteins and signaling as regulators in IPC and therefore potential targets for therapy. To determine the mitochondria enzymes involved in IPC we conducted a proteomic analysis to determine protein targets for potential therapeutic use. One such protein, Isocitrate Dehydrogenase II (IDH2) is involved in the citric acid cycle and reactive oxygen species reduction and was upregulated during IPC. IDH2 was shown to mimic the effects of IPC when delivered to the rodent kidney.

1.4 Mitochondria

1.4.1 Structure

Mitochondria are the powerhouse of the cell. These organelles are responsible for cellular energy production and regulation. To protect mitochondria and ensure normal function, they are surrounded by two membranes, an inner and outer membrane with different levels of permeability. The outer membrane contains protein pores and pumps, which regulate the flow of proteins, carbohydrates, ions, and other small molecules into mitochondria. The inner mitochondria membrane is less permeable than the outer membrane, as it is primarily responsible for housing the components of the electron transport chain (ETC). As a result, this membrane closely regulates the flow of ions from

the inner membrane space into the mitochondria matrix. The inner membrane folds into units called cristae to increase surface area to allow maximal ATP generation.

The final component of mitochondria is the mitochondria matrix. This matrix is found inside the inner membrane and is the location of the citric acid cycle (TCA) its constituents (Fig 4).

The combination of these mitochondria components allows for the establishment of the chemiosmotic mechanism. The mechanism relies on a closed system (membranes) to allow the flow of electrons down an electrochemical gradient to generate the energy needed to form ATP (64-66).

1.4.2 Bioenergetics

The generation of energy in the form of ATP or GTP in the mitochondria relies on the formation of reduction equivalents, NAD(P)H and $FADH_2$. The formation of these molecules drives the generation of ATP by substrate level phosphorylation, also known as phosphate group transfer. The formation of NADH and $FADH_2$ occurs during the TCA and their energy is used by the ETC to generate ATP. While these are not the only pathways that are regulated by mitochondria they will be the focus of this investigation. Previously mentioned, a major source of reduction potential is generated by the TCA. The cycle uses substrates generated from beta-oxidation and glycolysis via Pyruvate Dehydrogenase. During beta-oxidation, fatty acids are broken down by enzymes to form acetyl-coA which then enters the citric acid cycle.

Glycolysis, through various enzymatic steps, converts a glucose molecule into two pyruvate molecules. These molecules then undergo oxidative decarboxylation carried out

by pyruvate dehydrogenase to generate acetyl- coA, which then enters the TCA. The TCA cycle (Figure 5) consists of eight steps that lead to the generation of 1 GTP, 3 NADH molecules, and 1 $FADH_2$ molecule per molecule of acetyl-coA.

The four major dehydrogenases: Isocitrate, alpha-Ketogluterate, Succinate, and Malate Dehydrogenase are responsible for the generation of the NADH and $FADH_2$ that feed into the ETC. Of these four enzymes, it is Succinate Dehydrogenase that forms the sole $FADH_2$ molecule. In addition to the generation of NADH and $FADH_2$, GTP is generated by substrate level phosphorylation during the conversion of Succinyl CoA to Succinate by Succinyl CoA Synthetase. The reduction potential generated from the TCA is then passed into the ETC (65, 66). Succinyl CoA Synthetase. The reduction potential generated from the TCA is then passed into the ETC (65, 66).

The ETC consists of five major components (Figure 6). NADH and $FADH_2$ carry electrons from the TCA cycle into the ETC. The electrons from NADH are carried into Complex I, NADH:Ubiquinone Oxidoreductase, while the electrons from $FADH_2$ are carried into Complex II, Succinate Dehydrogenase by Succinate. From these complexes, the electrons are transferred by Ubiquinone to Complex III, Cytochrome bc1. From Complex III, the electrons are carried by Cytochrome c to Complex IV, Cytochrome Oxidase. The final electron acceptor is Oxygen, which is reduced to water upon receiving the electrons from Complex IV. As mentioned previously, the flow of electrons down a gradient is called chemiosmosis. The flow of electrons is governed by the reduction potential of the carrier and recipient molecules. Electrons flow from low reduction potential to high reduction potential and each component in the ETC has a higher

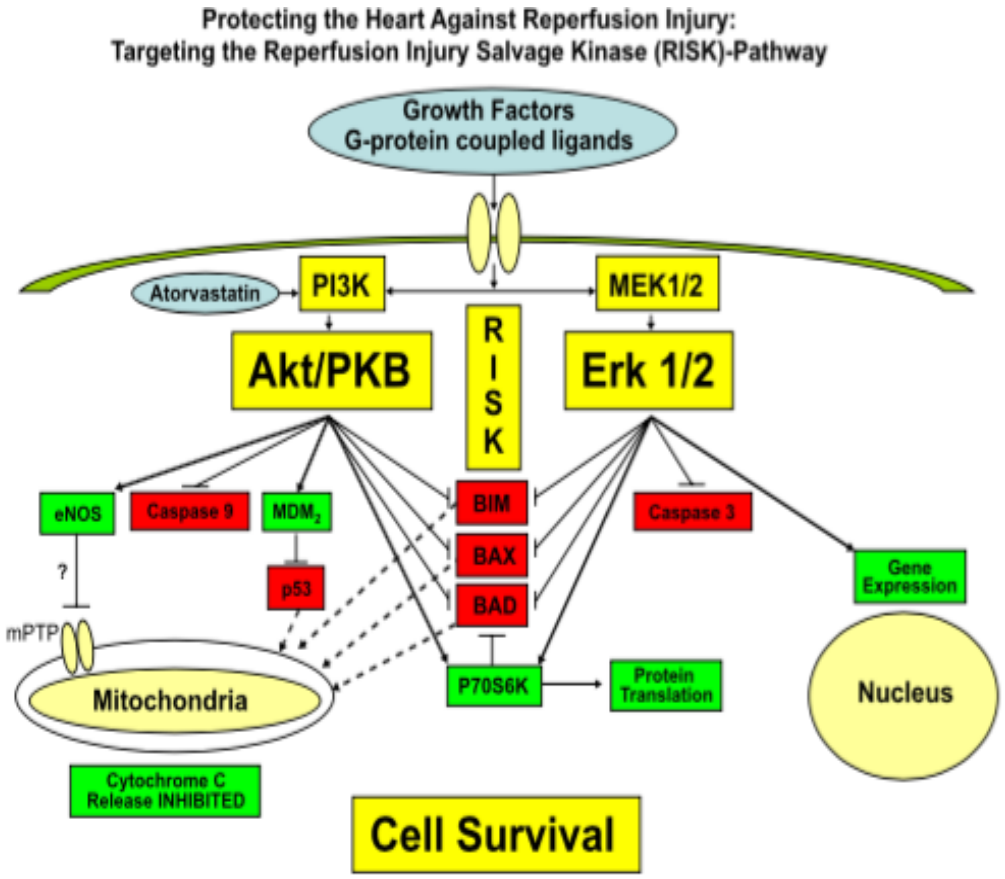

Figure 2: Reperfusion Injury Salvage Kinase (RISK) Pathway (49).

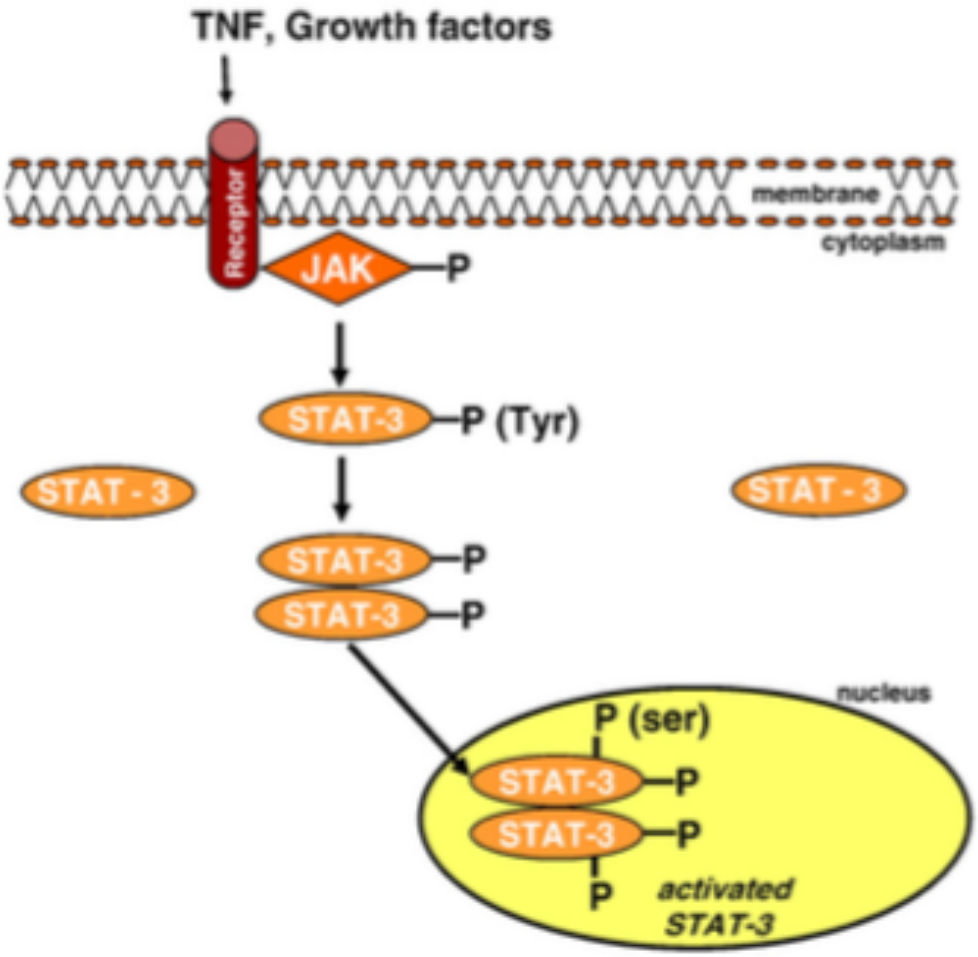

Figure 3: Survivor Activating Factor Enhancer (SAFE) Pathway (53).

reduction potential then the previous, thus allowing electron(s) to move from one component to the next. Coupled with the flow of electrons is the pumping of protons into the inner membrane space by Complexes I, III, and IV. Complex II, succinate dehydrogenase, is not a proton pump, and as a result electrons that initiate the chain at this complex generate fewer protons and thus less ATP than NADH. The protons from the inner membrane space then cycle through a proton channel in complex V, F_1F_o ATP Synthase, which drives the formation of ATP (65, 66).

Mitochondria membranes are dynamic and fluid. The proteins and lipids that make up each membrane are constantly being turned over. Damage to the mitochondria membrane may alter membrane potential and thus the ability to produce ATP, leading to the activation of cell death cascades (67). For this reason, it is important to study methods that can alter membrane potential in order to understand how to target mitochondria for potential treatments.

1.4.3 Mitochondria and Disease

Mitochondria are critically important regulators of cell homeostasis. Cells lacking mitochondria or that contain mitochondria where the amount of mutated DNA is greater than wild type DNA (mtDNA) initiate apoptotic pathways or succumb to necrosis due to poor ATP generation. For example, individuals with mutant Apolipoprotien L (*APOL-1)* have damaged mitochondria and are prone to cancer, renal disease and poor transplant reception (68-70). Cells with mitochondria that have alterations in permeability are also prone to cell death (67). Two qualities of mitochondria critical to understanding disease pathology are their maternal inheritance and that they contain their own genome (71-73).

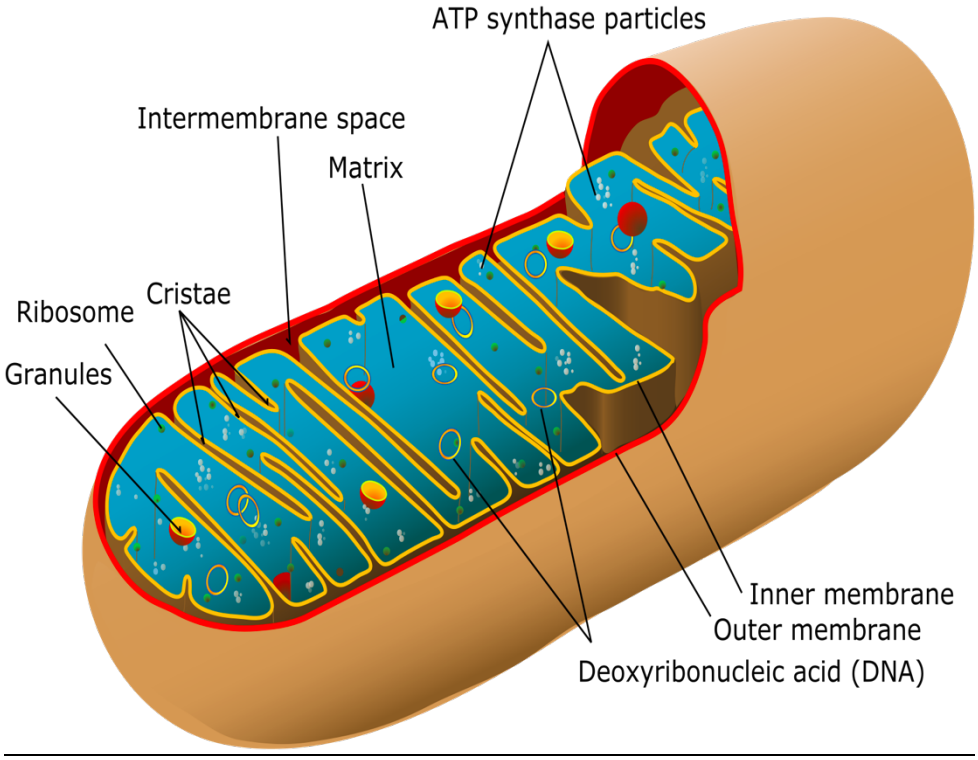

Figure 4: Mitochondria Structure (64)

Genes regulating mitochondria structure are predominately nuclear (roughly 900). However, the genes regulating respiration are encoded by mitochondria DNA. Damage to, or loss of these genes is associated with mitochondria disease. These diseases are typically associated with loss of normal electron transport chain structure and changes in respiratory capacity. These disease types tend to manifest in tissues that are highly aerobic such as: brain, skeletal muscle, and kidney (71, 74). Examples of diseases which effect brain and skeletal muscle include: MERRF, Myoclonic Epilepsy associated with Ragged Red Fibers, or MELAS, Mitochondrial Encephalomyopathy, Lactic Acidosis. Patients that present with these diseases suffer from seizures, muscle weakness, and infarctions and these symptoms are progressive. Similar to the brain and skeletal muscle, the kidney, and in particular proximal tubule epithelial cells, are highly aerobic and ATP dependent. De Toni-Debré-Fanconi syndrome, or proximal tubulopathy, occurs when sodium-potassium pumps fail due to low ATP levels. This disease is characterized by tubular proteinuria, glycosuria, hypercalciuria, and acidosis. In addition to tubulopathy, the glomerulus is also affected by mutated mtDNA. Patients with glomerular mitochondria defects present with glomerular lesions and sclerosis leading to poor glomerular filtration (74). Regardless of the disease type or organ affected, treatments for mitochondria disorders are lacking (71, 72, 74). A potential course of treatment would be to deliver the gene or genes that are missing to drive respiration and ATP generation. We show that hydrodynamic gene delivery to the kidney allows for the potential to treat these mitochondria diseases.

1.5 Isocitrate Dehydrogenase II and Sulfotransferase 1C2

1.5.1 Isocitrate Dehydrogenase

Isocitrate Dehydrogenases are a class of enzymes that catalyze the oxidative decarboxylation of isocitrate to alpha ketoglutarate. In humans and higher forms of eukaryotes this enzyme exists in three isoforms: IDH1, IDH2 and IDH3. Of the three isoforms only IDH3 reduces NAD+ and is found mainly in the mitochondria matrix and is a key regulator of the TCA cycle. IDH1 and 2 reduce NADP+ and play prominent roles in lipid metabolism, glucose sensing, reactive oxygen species (ROS) regulation and oxidative respiration (75-80).

IDH1 contains signaling sequences that target this particular isoform to the peroxisome where it functions in ROS regulation and oxidative mechanisms such as beta-oxidation. Studies have indicated that IDH1 is found in particularly high levels in the liver. IDH2, on the other hand, contains signaling sequences that target it to mitochondria, and is involved in oxidative phosphorylation and glucose sensing. This isoform is found in high levels in lymphocytes, heart, and skeletal muscle. Of particular interest is the role IDH2 plays in response to cellular stress. Due to its localization in the mitochondria, IDH2 has been found to function in ROS regulation and the reduction of glutathione. Glutathione reduction is critical in the reduction of H_2O_2 to water. Studies have indicated that loss of IDH2 activity leads to increases in oxidative DNA damage, peroxide generation, and increases in cell death (81-85).

Proteomic analysis of mitochondria lysates following IPC has implicated IDH2 as an activator of recovery pathways following injury. Han *et al* demonstrates that loss of

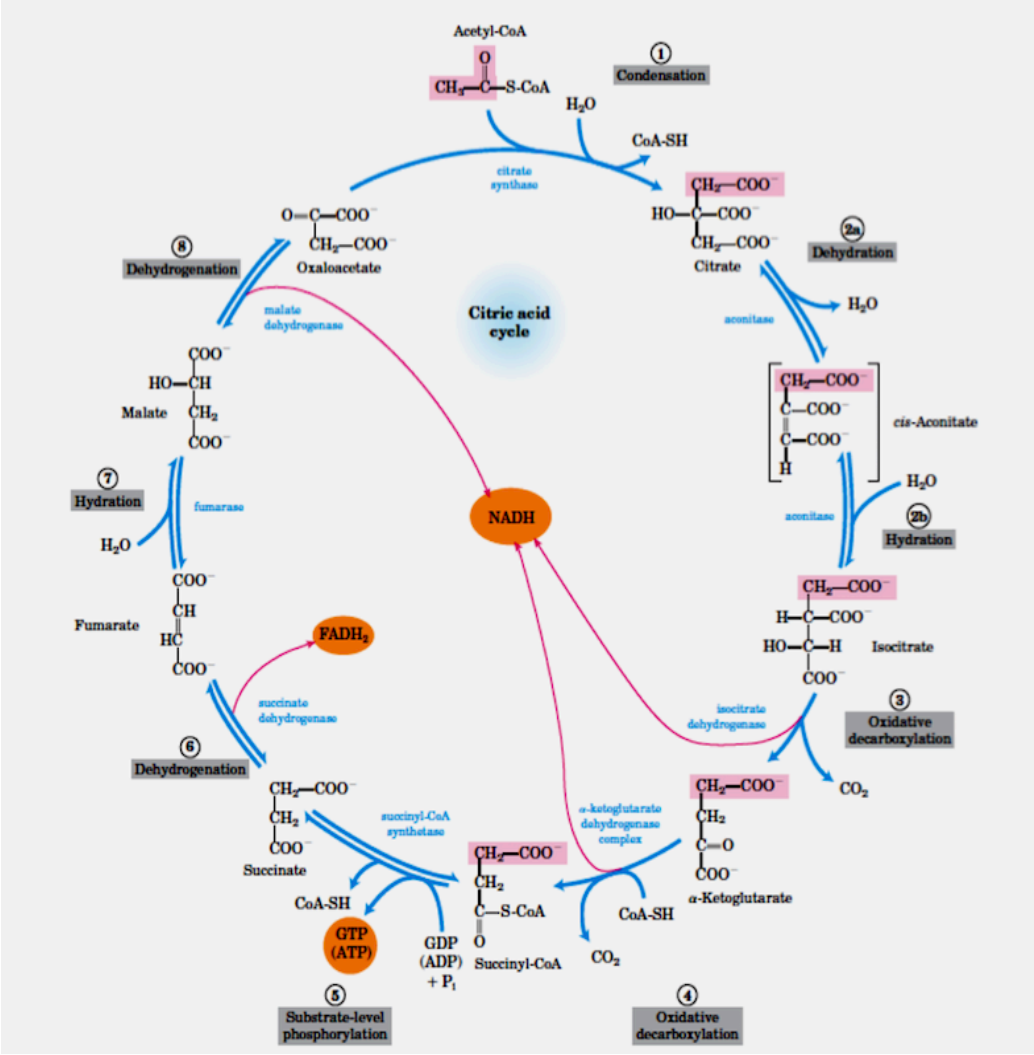

Figure 5: The Citric Acid Cycle (65)

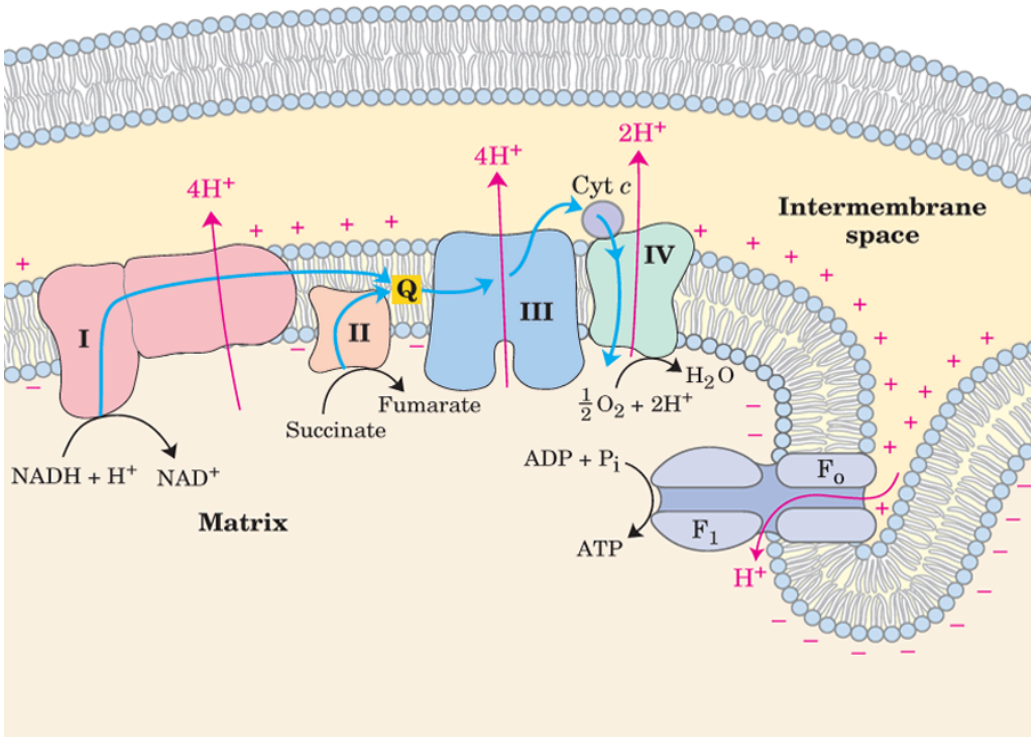

Figure 6: The Electron Transport Chain(65)

IDH2 exacerbates the disease state and detail the importance of IDH2 in these recovery pathways (86). Of importance now is to determine the exact mechanism(s) of action so IDH2 may be used as a therapeutic agent to treat ischemic diseases.

1.5.2 Structure and Function

Isocitrate Dehydrogenase is a class of enzyme that carries out a critical step in the TCA. Specifically, IDH is responsible for the conversion of isocitrate into alpha-ketoglutarate (Figure 7) (75, 87). The function of this enzyme is highly dependent upon the cofactor $Mg^{2+.}$ Studies show that in the absence of Mg^{2+} the structural changes needed for the catalytic activity of the enzyme do not occur and the enzyme fails to function properly (75). Aside from the substrate output, IDH is responsible for the production of key electron carriers necessary for the electron transport chain, ATP production, fatty acid synthesis, and alleviation of ROS. These enzymes can reduce either NAD^+ to NADH or $NADP^+$ to NAD(P)H. Isocitrate dehydrogenases are found both in mitochondria and the cytosol and the enzymes found in the mitochondria reduce either cofactor (88).

1.5.3 IDH2's Role in IPC

As previously mentioned, IPC is the application of non-lethal doses of ischemia to a target organ to protect that organ from more significant ischemic episodes. In the kidney, the application of these non-lethal doses of ischemia has proven to protect the kidney from future ischemic events. While the exact mechanism of IPC is unclear, one possible mechanism of protection entails changes to mitochondria or cytosolic protein

expression. Mitochondria protein lysates were analyzed by Liquid Chromatography-Mass Spectroscopy (LC/MS) two weeks following IPC. To ensure that these animals did in fact receive an ischemic injury, serum creatinine measurements were taken pre- and post-injury. As a normal byproduct of muscular metabolism, and a compound that is easily excreted by the kidney, serum creatinine is the gold standard for measuring changes in kidney function. The proteomic analysis carried out by Drs. Witzmann, Basile, and Bacallao indicated unique changes in the mitochondria proteome (Table 4). The protein most over expressed in preconditioned kidneys, sulfotransferase 1C2, is a cytosolic protein; its presence in the mitochondria proteome reflects the nature of the mitochondria isolation which aimed for preserving mitochondria function instead of a pure mitochondria isolation preparation. IDH2 is the second most over expressed protein (Table 4) and due to its function in the TCA cycle and as a branch point enzyme for precursor production, we chose this protein for further study.

1.5.4 Sulfotransferase 1C2 (SULT1C2)

Sulfotransferases are a class of enzymes that add sulfate groups to various targets resulting in activation of detoxification pathways of various molecules. These detoxification pathways lead to formation of water soluble compounds that are then excreted by the kidneys. Three families of sulfotransferases have been identified in humans: SULT1, SULT2, and SULT4. These families then fall into two groups: membrane bound and cytosolic (89-91). The membrane bound sulfotransferases are found in the Golgi, and are responsible for adding sulfate groups to proteins, lipids, and glycosaminoglycans. The addition of the sulfate group to these molecules leads to

changes in structure and function. The second group, the cytosolic group, is responsible for the metabolism of xenobiotics and other compounds such as steroids and neurotransmitters (89-91). SULT1C2 is a cytosolic sulfotransferase that is located in the kidney, liver, and stomach. Currently, the physiological role of SULT1C2 is unknown (92). We report here that SULT1C2, while found in the cytosol, is a critical component of mitochondria recovery from IRI (Chapter 5).

1.6 Delivering Genes to the Kidney

1.6.1 Choosing the Vector

When first conceived, the idea of gene therapy was to replace mutant or defective genes. This idea first originated in the late 1960s and early 1970s. It was not until the early 1990s that the first human clinical trial was conducted. This trial involved the replacement of a key enzyme, adenosine deaminase, to control proper regulation of the immune system (93, 94). The absence of this gene proves fatal. The results of this first clinical trial proved successful and the idea of gene therapy expanded from that point. A key dilemma in gene therapy is determining how to deliver the gene of interest. Currently two models of gene delivery exist: viral and non-viral delivery. When determining the viral route to use, it is important to consider what criteria make an ideal vector. The six criteria include: high concentration to allow many cells to be infected, convenience and reproducibility of production, ability to integrate in a site-specific location or to be maintained at that location, a transcriptional unit that can be regulated by regulatory

elements, the ability to target to a particular cell type, and avoidance of an immune response (93, 94).

1.6.2 Non-viral Vectors

In the case of non-viral delivery, DNA is paired with cationic lipids, polysaccharides or polypeptides that help DNA pass through the cell membrane. Issues that arise with the use of non-viral vectors include poor transfection efficiency and potential toxicity. In order to increase the transfection efficiency of non-viral delivery, dosage was increased, but this leads to cellular toxicity. To combat the toxicity and immune stimulation issues, models have been designed that allow conjugation of the DNA to PEI or PEG (polyethylenimine/polyethylene glycol) polyplexes or lipoplex (95-100). The formation of these complexes occurs due to positively charged lipids or polymers associating with negatively charged DNA. The benefits of forming these DNA polymer complexes include: preventing serum inactivation and enzymatic degradation of the DNA, and allowing the complex to enter the cell and the nucleus (95-97, 101-105).

1.6.3 Viral Vectors

Viral vectors are classified into 5 categories: retroviruses, lentiviruses, adenoviruses, adeno-associated viruses, and herpes simplex-1virus. Retroviruses are a group of viruses that utilize RNA as their gene delivery vector and integrate into their host genome. These viruses depend on their RNA genome being converted into DNA

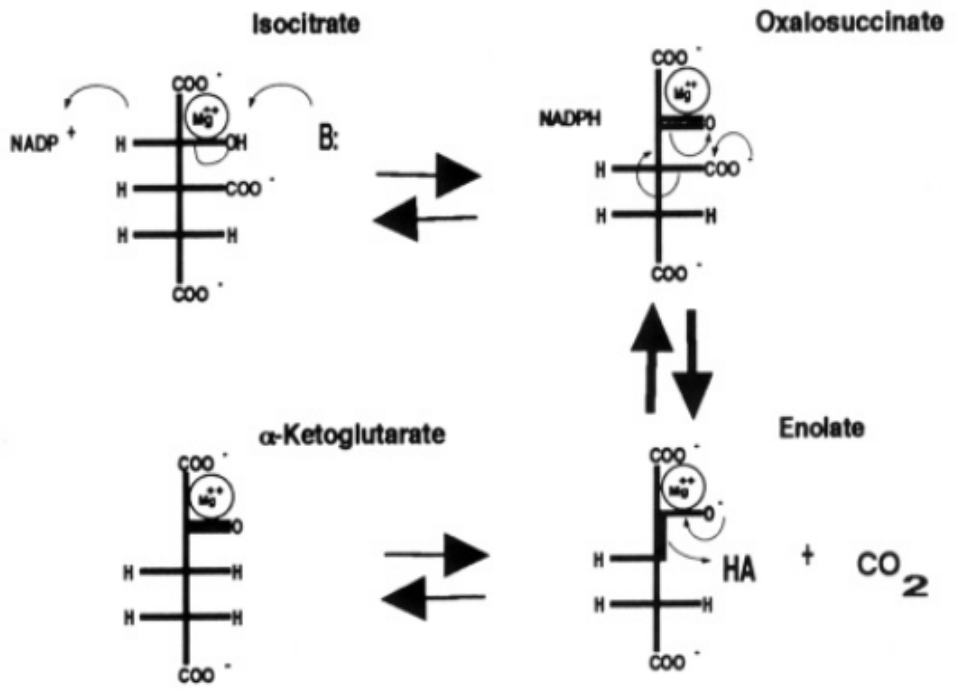

Figure 7: Schematic Depicting the Conversion of Isocitrate into alpha-Ketoglutarate. The conversion of Isocitrate into alpha-Ketoglutarate is an important step in the Citric Acid Cycle. Two important cofactors play a role in the generation of alpha-Ketoglutarate, Mg^{2+} and $NADP^{+.}$

upon entry into the cell. In order to accomplish this delivery, these viruses are composed of Gag, Pol, Env, and LTRs genes that are critical for integration into the host cell genome. This virus also depends on the packaging sequence (ψ) for its viral RNA to be distinguishable from cellular RNA. Advantages of retroviral vectors include a high efficiency of gene transfer into dividing cells and their ability to transfer genes precisely. Limitations with the use of retroviral vectors include failure to infect non-dividing cells and insertional mutagenesis leading to the activation of oncogenes. These viruses cannot be synthetically made. They must be cultured in cells for propagation, and due to their nature of integrating into dividing cells, these viruses can be gradually silenced over time (93, 94, 106, 107). Lentiviruses are a unique form of retroviruses which have the ability to infect dividing or non-dividing cells. A prime example of a lentivirus is HIV. The genome of a lentivirus includes accessory proteins, which allow its entry into either a dividing or non-dividing cell. Unlike other retroviruses, lentiviruses are not subjected to silencing which allows gene expression to continue for extended periods of time. Instances of six months of gene expression have been reported (93, 94, 107-109).

The next groups of viruses are adeno and adeno-associated viruses. Unlike retroviruses, they do not integrate into their host genome and can infect either dividing or non-dividing cells. Since these viruses do not integrate into the host genome, their replication occurs as episomal replication in the cell nucleus, dependent upon cellular replication machinery. For gene transfer, the E1 gene, which is essential for viral replication, is replaced with the gene of interest and an enhancer-promoter element. This reduces the possibility for wild-type reversion and viral propagation. Advantages of this vector type include: higher titer

Table 4: Mitochondria Proteomic Analysis

Gene Symbol	Gene Name	Fold Difference
SULT1C2	SULFOTRANSFERASE 1C2-LIKE	2.4
IDH2	ISOCITRATE DEHYDROGENASE (NADP+) MITOCHONDRIAL	2.2
HIST1H2BC	HISTONE H2B	2.0
C1QBP	COMPLEMENT COMPONENT1Q SUBCOMPONENT-BINDING PROTEIN	1.9
ACSL1	LONG CHAIN FATTY ACID COA LIGASE 1	1.7
ACOT2	ACYL-COENZYME ATHIOESTERASE 2, MITOCHONDRIAL	1.5
THUMPD2	THUMPD DOMAIN CONTAINING 2 ISOFORM 1	-3.0
MTCH2	MITOCHONDRIAL CARRIER HOMOLOG 2	-1.9
HSDL2	HYDROXYSTEROID DEHYDROGENASE LIKE PROTEIN 2	-1.6
SLC25A13	SOLUTE CARRIER FAMILY 25, MEMBER 13	-1.6
NDUFA5	NADH DEHYDROGENASE (UBIQUINONE) 1α SUBCOMPLEX SUBUNIT 5	-1.6
SUCLG1	SUCCINATE COA LIGASE, ALPHA SUBUNIT	-1.6

volumes (>10^{11}), the ability to carry large segments of DNA, and the ability to infect either dividing or non-dividing cells. Disadvantages of using adenoviruses include: stimulating an immune response and very limited expression time due to lack of chromosomal integration (93, 94, 107, 110). Adeno-associated viruses eliminate the issue of an immune response typically seen with adenoviruses. This virus is relatively simple. It is composed of a single strand of DNA, a cap gene which encodes the coat protein, and rep gene for replication and cell integration. Disadvantages of this vector are that it requires additional viral genes to aid in its replication and unlike adenoviruses, the adeno-associated virus cannot be propagated directly from cells. Although viral titer levels are similar to adenoviruses, only a small number of particles are infectious (94, 111, 112).

1.6.4 Non-viral Delivery Techniques

The difficulty with non-viral gene delivery is that in the absence of the viral mechanisms which enable host infection, non-viral DNA has difficulty gaining access to the cell. In order to gain access to the cellular genome, methods have been established that allow passage through both the cell and nuclear membranes allowing access to DNA. Methods that have been developed include electroporation/stimulation, gene gun, ultrasound-facilitated transfer, and hydrodynamic delivery (113-117).

Electrical stimulation of the cell membrane is thought to change the membrane permeability barrier, allowing the entry of plasmid DNA. While the exact mechanism is not known, it is hypothesized that electrical stimulation leads to formation of hydrophobic pores. After formation of the pores the plasmid moves down an electrochemical gradient and into the cell. Studies of electrically stimulated gene uptake

have been conducted in the skin, kidney, liver, lung, and different muscle types. While these studies seem promising, the major drawback of this technique is the damage to tissues and cells associated with applying an electrical shock and subsequent thermal heating. Additional limitations to this technique include a limited transfection area, and it is invasive. This damage leads to decreased transfection efficiency (118-120).

Yang *et al* established gene expression with the gene gun in the late 1980s (121, 122). The principle behind this technique involves DNA attached to gold particles being shot from a highly-pressurized gun with the momentum from gold particles driving penetration into cells or tissue. While gene expression has been reported, the highly pressurized direct onslaught of the cell or tissue surface leads to membrane damage, decreased gene expression, and potentially cell death (121, 122).

Other techniques for gene delivery include direct intramuscular injection. Wolff *et al* demonstrated this method is possible and they show gene expression for two months (116). However, the ability to recapitulate this work has proven difficult and those that have accomplished this feat report only localized gene expression (116). Another technique that utilized direct injection is the micropuncture technique. The micropuncture technique was established in the 1920s by Wearn and Richards and successfully conducted in the kidney in 1941 by Walker *et al* (123, 124). Still used today, micropuncture allows the direct injection of compounds in various compartments in tissue. In kidneys, for example, direct injection of various fluorescent proteins (either viral or non-viral) has been successful and gene expression has been reported in the proximal tubule and even the glomerulus (Figure 8). While gene delivery with this technique has been successful, the gene expression is localized to the injection site and

widespread expression has not been observed (125, 126). The importance of widespread expression is critical for the treatment of disease.

1.6.5 Hydrodynamic Fluid Delivery

Hydrodynamic delivery is a process that uses pressure as a means to overcome internal permeability barriers to gene uptake. The force of injection leads to an increase in intravascular pressure, which causes changes in membrane permeability due to cellular stretching, which leads to gene uptake. First characterized in the 1990s, hydrodynamic delivery has been carried out in the heart, skeletal muscle, liver, diaphragm, and the kidney. The process was first carried out via the tail vein and from the tail vein followed by the limb vein. These delivery models report expression levels around 40% (127-132).

Issues with renal fluid delivery arise from the glomerular filtration barrier (GFB) and its propensity to filter compounds out in the urine leading to low efficiency of gene expression. The direct target of renal hydrodynamic delivery is the proximal tubule epithelial cell due to its capacity to readily endocytose exogenous compounds. As previously mentioned, the limitation is the GFB. To avoid the limitations of the GFB, hydrodynamic delivery in the kidney has been attempted in the renal vein, artery, and ureter (22, 133). The current model established by Dr. Peter Corridon is renal vein injection (Figure 9) (22). Studies of hydrodynamic fluid injection through the renal vein have indicated high levels of gene expression from either viral or non-viral vectors (Figure 10) (22). Our studies indicate that injection forces between 60-75 mmHg are required for tubular uptake and gene expression (Figure 11). The utilization of this

technique is the driving force for the treatment of renal injury, both before and after disease onset.

To better understand the mechanisms of hydrodynamic delivery in the kidney, we set out to study its mechanism of action following an Ischemia Reperfusion Injury (IRI) (Chapter 3). Using our proteomic data, we determined that delivering *IDH2* or *SULT1C2* by hydrodynamic delivery has the potential to prevent AKI. We next studied if gene delivery prior to IRI is protective and if so, determine the mechanism of protection (Chapter 4).

1.7 Studies of Renal Function

Hydrodynamic isotonic fluid delivery (HIFD) to the kidney has the potential to ameliorate AKI (Chapter 3). To ensure normal kidney physiology, images and injury scoring of the kidney were conducted using light microscopy, confocal or 2-photon imaging, and tissue sectioning with staining. SCr measurements were analyzed to ensure amelioration of the disease and Florescence Activated Cell Sorting (FACS) was conducted to determine changes in immune response. As mentioned previously, AKI leads to changes in renal blood flow and even changes in cellular permeability.

2-photon imaging and line scans allowed us analyze changes in permeability and blood flow. The capitulation of this data leads us to believe that HIFD has the potential to ameliorate AKI (1).

1.8 Studies of Mitochondria Function

Hydrodynamic delivery of *IDH2* or *SULT1C2* has the potential to prevent AKI mimicking IPC (Chapter 4 and 5). IDH2 localizes to and alters the activity of the mitochondria. Following hydrodynamic delivery, we imaged mitochondria to ensure normal mitochondria physiology. Once normal physiology was established, we set out to analyze respiration, ATP levels, membrane potential and reduction potential. The culmination of our *in vivo* and *in vitro* studies indicates that IDH2 has the potential to mimic late window ischemic preconditioning. Hydrodynamic delivery of SULT1C2 post-transitionally modifies the mitochondria leading to increases in membrane potential and oxidative phosphorylation protecting the cell from oxidative stress.

1.9 Hypothesis

Hydrodynamic Isotonic Fluid Delivery (HIFD) is a means to ameliorate AKI. Hydrodynamic fluid delivery following AKI increases blood flow and membrane permeability compared to sham IPC alone, allowing for small molecule uptake. This delivery is also shown to improve renal injury scoring, reduce SCr levels, and reduce inflammation and the inflammatory response within the kidney. This data demonstrates a possible mechanism for hydrodynamic isotonic fluid delivery and the ability to translate this method to the bedside.

For patients that are at increased risk for AKI, hydrodynamic delivery of candidate genes shows the potential to prevent AKI by mimicking late window ischemic preconditioning. Gene delivery of *IDH2* reduces cell death and SCr

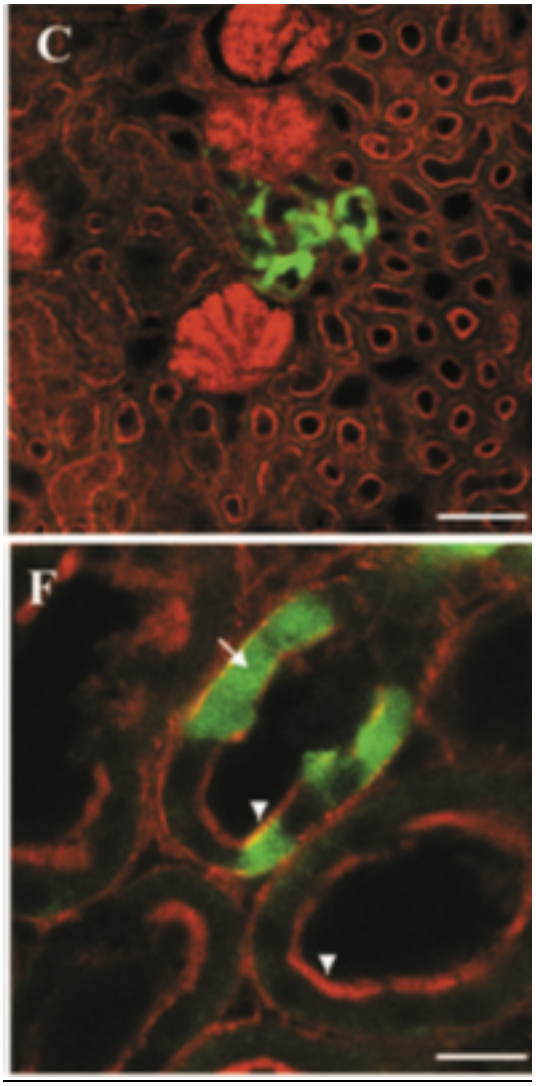

Figure 8: Micropuncture Gene Delivery to the Kidney (126). The GFP expression is located in the injected proximal tubule.

levels and leads to increases in mitochondria membrane potential, oxidative phosphorylation, and ATP levels. The mechanism by which protection occurs is to prevent a Warburg (glycolytic) shift by increasing ATP reserves, spare respiratory capacity, and Complex II activity. The combination of hydrodynamic isotonic fluid delivery and gene therapy has the potential to be used in the clinic to treat AKI. The current therapeutic models are lacking and these translatable techniques have the potential to be powerful therapeutic treatments for AKI.

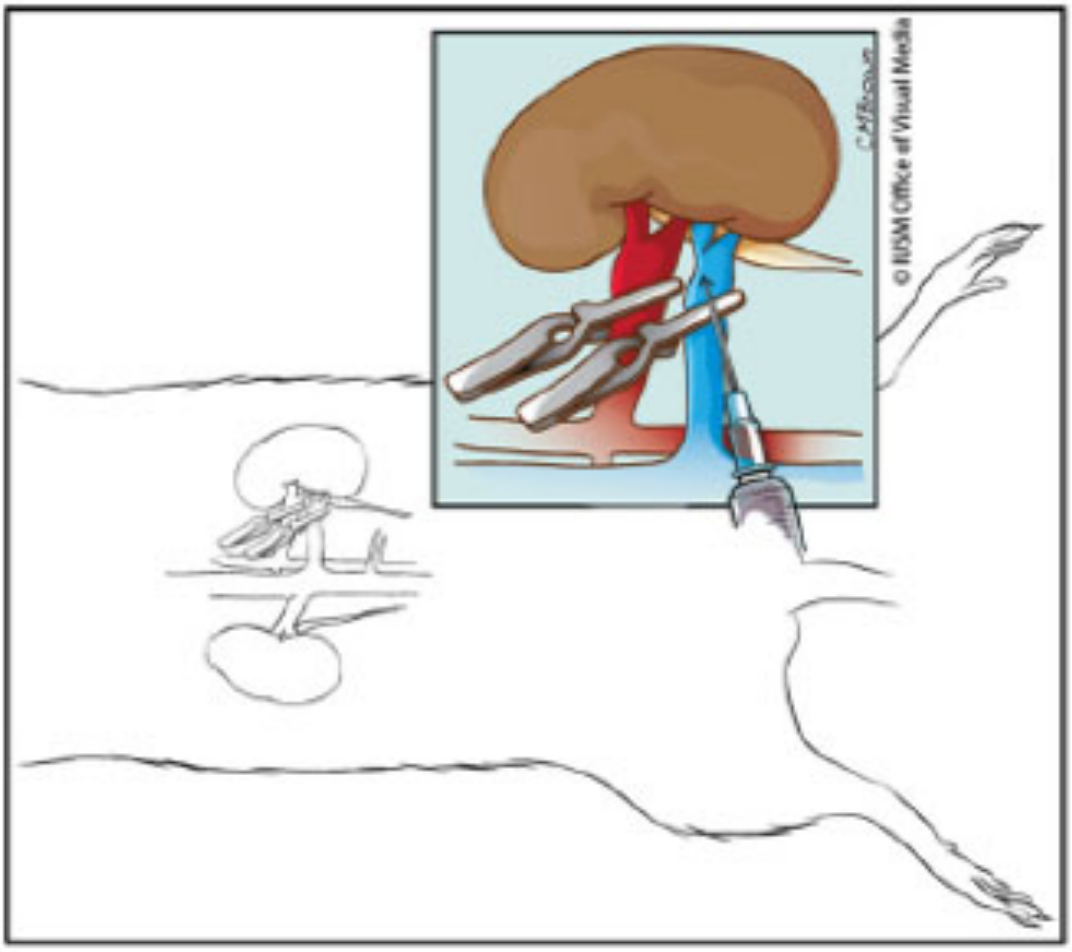

Figure 9: Renal Vein Hydrodynamic Delivery. The pressure generated by injection through the renal vein leads to gene uptake and expression in the kidney.

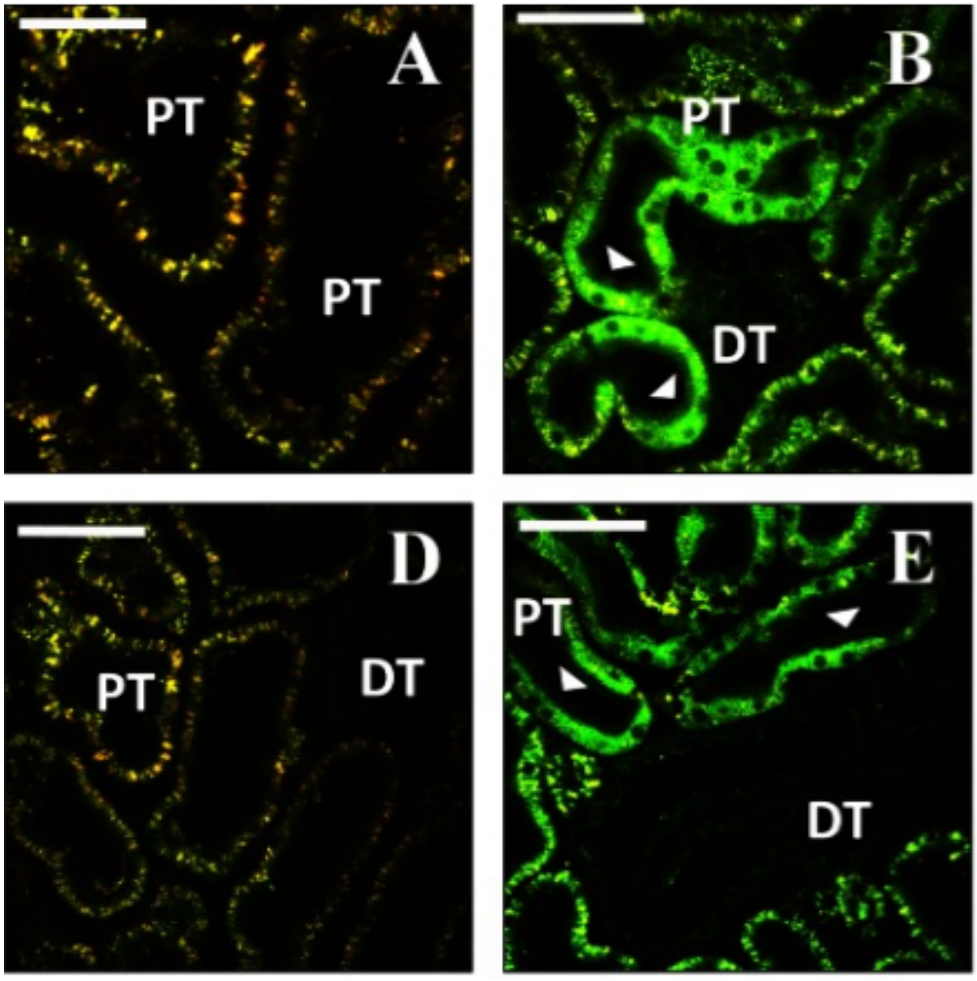

Figure 10: Hydrodynamic Fluid Delivery of EGFP from Corridon *et al* (22). Arrows indicate gene expression in proximal tubule as a result of gene delivery. Panels A/D are 2 photon images of tubular auto-fluorescence, while panels B/E show EGFP expression following gene delivery

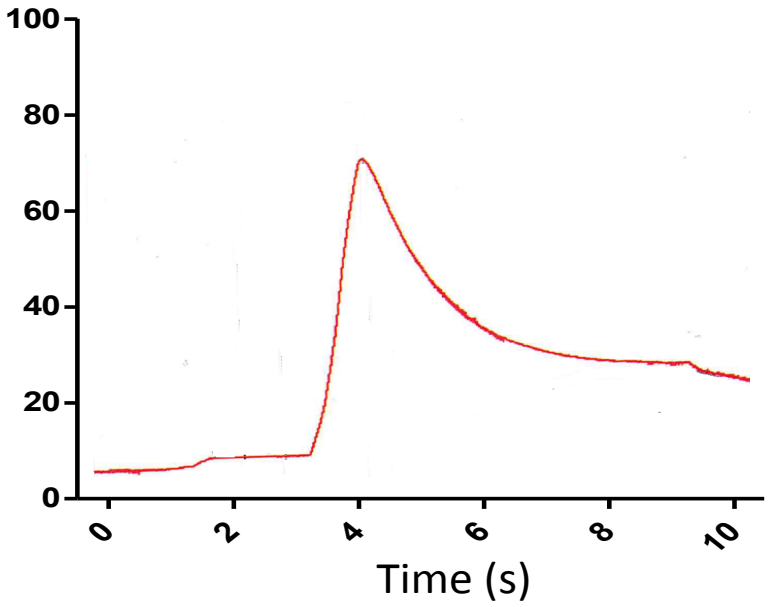

Figure 11: Hydrodynamic Injection Pressure (1). The average of three 0.5 cc saline injections studies indicated that forces of 60-75mm Hg lead to gene expression within the kidney.

CHAPTER 2: MATERIALS AND METHODS

2.1 Materials

All fluorescent probes were purchased from ThermoFisher Scientific (Waltham, MA). IDH2 antibody was purchased from Protein Tech (Chicago, IL). Sulfotyrosine antibody was purchased from MilliporeSigma (Billerica, MA). The c-MYC antibody (9e10), developed by JM Bishop at the University of California, San Francisco, was obtained from the Developmental Studies Hybridoma Bank, created by the NICHD of the NIH and maintained at The University of Iowa, Department of Biology, Iowa City, IA 52242. Beta actin was purchased from MilliporeSigma (Billerica, MA). All secondary antibodies were purchased from Jackson Laboratories (West Grove, PA). All plasmid DNA was purchased from Origene (Rockville, MD). Human recombinant SULT1C2 was purchased form Abcam (Cambridge, MA). 3' Phosphoadenosine-5' Phosophosulfate (PAPS) was purchased from MiliporeSigma (Billerica, MA). Cholesterol Sulfate was purchased from Avanti Polar Lipids, inc (Alabaster, AL). Laurdan was purchased from ThermoFisher Scientific (Waltham, MA). FIJI was obtained from the NIH website (National Institutes of Health, Bethesda, MD).(134) Transfection reagents were purchased from ThermoFisher Scientific (Waltham, MA). Seahorse reagents and kits were purchased from Agilent (Santa Clara, CA). Oroboros and Oroboros related reagents were purchased from Oroboros Instruments (Innsbruck, Austria).

2.2 Animals and Cell Culture

2.2.1 Live Rats

Male Sprague-Dawley rats (Envigo, Indianapolis, IN) (250-350 g) were used for our *in vivo* studies. Rats had access to food and water and all experiments conducted followed NIH guidelines. Rats were randomly assigned to control or experimental groups. Approval from Indiana University School of Medicine Institutional Animal Care and Use Committee (IACUC) and Richard L. Roudebush Veterans Adminstration Medical Center Animal Care and Use Committee was gained prior to all *in vivo* studies.

2.2.2 Mouse Proximal Tubule S3 Cell Culture

Murine S3 proximal tubule epithelial cells were cultured in modified essential media (50:50 HAM F-12: DMEM, with L-glutamine, HEPES, sodium selenite, sodium pyruvate, phenol red, and insulin) supplemented with 1% penicillin-streptomycin, 7% fetal bovine serum (FBS), and 4.1% sodium bicarbonate solution (Sigma-Aldrich Corporation, St. Louis, MO) and grown in a 37^{o}C, 5% CO and 38% O_2.

Validation of the cell line origin was performed by IDEXX BioResearch (Columbia, MO) and the cells have the following STR profile (MCA-4-2: 20.3; MCA-5-5: 17, 18; MCA-6-4: 14; MCA-6-7: 12, MCA-9-2: 15; MCA-12-1: 16, 17; MCA-15-3: 22.3; MCA-18-3: 17; MCA-X-1: 28)

2.2.3 Mouse Embryonic Fibroblast Cell Culture (NIH 3T3)

NIH 3T3 (135) cells were purchased from American Type Culture Collection (Manassas, VA) and maintained in culture according to ATCC recommendations. Mouse embryonic fibroblasts were cultured in Dulbecco's modified eagle minimum essential media (American Type Culture Collection, Manassas, VA) containing 10% fetal bovine serum (FBS) and 1% Penicillin-streptomycin solution (Sigma-Aldrich Corporation, St. Louis, MO) and grown in 37^{o}C, 5% CO_2 incubator.

2.3 Live Animal Surgeries

2.3.1 Hydrodynamic Fluid Delivery

Male Sprague-Dawley rats were anesthetized by inhaled isoflurane (Webster Veterinary Supplies, Inc., Devens, MA), with 2 L/O_2 per minute for the entirety of the procedure (approximately 30 minutes) and placed on a heating pad. Animal respiration, reflex response, color, and body temperature were monitored throughout the surgical procedure. Once the animal was fully anesthetized, the abdomen was shaved and sanitized with three alternating rounds of Betadine Surgical Scrub (Purdue Products L.P., Stamford, CT) and 70% ethanol treatments. An abdominal midline incision was made to locate the left renal pedicle. The renal pedicle was isolated with 3-0 silk. The pedicle was elevated with the silk to place one micro-serrefine cross clamp (Fine Science Tools, Foster City, CA) across the pedicle for a three minute period. Following clamp placement, the silk was elevated again to inject 0.5 ml of 0.9 % sterile saline, or 2-3 μg/ gram body weight of transgenes into the renal vein at a rate of 0.1 ml/s, using a 30 -gauge

needle. The needle was then removed, and a cotton swab was applied to the injection site for a minimum of 30 seconds to induce hemostasis. After the three-minute period, the clamp was removed. Once blood flow to the kidney was restored, the midline incision was closed and the animal was allowed to recover. Analgesia was given according to IACUC guidelines.

2.3.2 Hydrodynamic Fluid Delivery: Pressure Testing

Rats were anesthetized as previously described and underwent renal vein injection as previously mentioned. To measure the pressure of injection, an additional one inch 30 -gauge needle was bent 90 degrees and connected to the injection needle distal to the syringe. The additional needle was connected to a force transducer and pressure readouts were taken as the liquid exited the injection needle. The needle was then removed, and a cotton swab was applied to the injection site for a minimum of 30 seconds to induce hemostasis. After the three-minute period, the clamp was removed. Once blood flow to the kidney was restored, the midline incision was closed and the animal was allowed to recover. Analgesia was given according to IACUC guidelines.

2.3.3 Tetramethylrhodamine Methyl Ester (TMRM) Jugular Vein Infusion

Rats were anesthetized, prepared, and monitored as previously described. Following preparation, the jugular vein was exposed and isolated using 3-0 silk loops. The superior loop was tied off and clamped to elevate the jugular vein. PE-50 catheter tubing was then inserted through a minor incision made in the vein and the second silk loop was tied off to anchor the catheter in place. The catheter was connected to a 1 mL

syringe containing either saline or TMRM. The animals were then placed on an Olympus FV 1000 confocal microscope (Olympus Tokyo, Japan) as described by Dunn *et al* (136) for multiphoton imaging. Image J was used to calculate the mean TMRM intensity value for each group as described by Hall *et al* (133).

2.3.4 Tail Vein Injections

Anesthetized rats were placed on a heating pad to allow the tail vein to dilate. A 25-gauge butterfly needle, attached to a syringe with biomarkers, was then inserted into the tail vein.

2.3.5 Ischemia Reperfusion

Rats were anesthetized with an intraperitoneal injection of ketamine (100mg/kg) + xylazine (10 mg/kg) + acepromazine (2.5 mg/kg) cocktail and placed on a heating pad to maintain core body temperature. Animals were monitored throughout the surgical procedure and prepared as previously described. An abdominal midline incision was made to locate both left and right kidney pedicles. First, the right pedicle was isolated, followed by the left; micro-serrefine clamps (Fine Science Tools, Foster City, CA) were placed on both the left and right pedicle for a period of 35 minutes to induce ischemia. During ischemia, the midline incision was closed temporarily to maintain core body temperature. Following the 35-minute period, the clamps were removed from the pedicles to restore blood flow, the midline incision was closed and the animal was allowed to recover. Analgesia was given according to IACUC guidelines.

2.3.6 Ischemia Reperfusion: Unilateral Nephrectomy with 35-minute Contralateral-Cross Clamp

Rats were anesthetized with an intraperitoneal injection of ketamine (100mg/kg) + xylazine (10 mg/kg) + acepromazine (2.5 mg/kg) cocktail and placed on a heating pad to maintain core body temperature. Animals were monitored throughout the surgical procedure and prepared as previously described. An abdominal midline incision was made to locate both left and right kidney pedicles. The right pedicle was isolated and tied off using 3-0 silk. Once the pedicle was ligated, the right kidney was removed and bleeding was monitored to ensure proper ligation. The contralateral kidney pedicle was clamped for 35 minutes. Following the 35-minute period, the clamps were removed from the pedicles to restore blood flow, the midline incision was closed, and the animal was allowed to recover. Analgesia was given according to IACUC guidelines.

2.3.7 Ischemia Reperfusion Injury with 24-hour Hydrodynamic Isotonic Fluid Delivery

Rats were anesthetized with an intraperitoneal injection of ketamine (100mg/kg) + xylazine (10 mg/kg) + acepromazine (2.5 mg/kg) cocktail and placed on a heating pad to maintain core body temperature. Animals were monitored throughout the surgical procedure and prepared as previously described. An abdominal midline incision was made to locate both left and right kidney pedicles. First, the right pedicle was isolated, followed by the left; micro-serrefine clamps (Fine Science Tools, Foster City, CA) were placed on both the left and right pedicle for a period of 35 minutes to induce ischemia. During ischemia, the midline incision was closed. Following the 35-minute period, the

clamps were removed from the pedicles to restore blood flow, the midline incision was closed and the animal was allowed to recover. Analgesia was given according to IACUC guidelines.

24 hours later the following procedure was conducted. Male Sprague-Dawley rats were anesthetized by 130mg/cc thiobutabarbital (Inactin Hydrate). Animals were monitored throughout the surgical procedure and prepared as previously described. The renal pedicle was isolated with 3-0 silk. The pedicle was elevated with the silk to place one micro-serrefine cross clamp (Fine Science Tools, Foster City, CA) across the pedicle for a three-minute period. Following clamp placement, the silk was elevated again to inject 0.5 ml of 0.9 % sterile saline, or 2-3 ug/ gram body weight of transgenes into the renal vein at a rate of 0.1 ml/s, using a 30 -gauge needle. The needle was then removed, and a cotton swab was applied to the injection site for a minimum of 30 seconds to induce hemostasis. After the three-minute period, the clamp was removed. Once blood flow to the kidney was restored, the midline incision was closed. Following experimentation, animals were euthanized according to IUCAC guidelines.

2.3.8 Intravital Imaging

2.3.8.1 Surgery

Rats were anesthetized with an intraperitoneal injection of 130 mg/kg of thiobutabarbital (Inactin Hydrate). Animal respiration, reflex response, color, and body temperature were monitored throughout the surgical procedure. Once the animal was fully anesthetized, the left flank was shaved and then the animal's left kidney was

located. Following location, a small incision was made on the flank and the kidney was exposed through the incision. The animal was then transported to the imaging room for renal imaging (Figure 12).

2.3.8.2 Confocal or 2-Photon Microscopy Setup

The kidney was placed face down into a 35mm glass dish allowing the rat body weight to stabilize the interaction between the kidney and the stage to reduce motion (Figure 12). Saline was poured into the dish to ensure the kidney did not dry out. An Olympus FV 1000 MPE microscope (Olympus, Tokyo, Japan) with a Spectra Physics MaiTai Deep Sea Laser (710-990 nm) with a 20 or 60X water immersion objective was used for imaging. Intravital images were acquired using wavelengths ranging from 820-860 nm.

This system is also equipped with two external detectors for multi-photon imaging and dichroic mirrors to collect red, green, and blue light emissions. This light is collected via a three-band pass filter system. Blue light is collected between 420-460 nm, green light between 495-540 nm, and red light between 575-630 nm. For GFP studies, the pseudo green and red channel were merged to eliminate the possibility of tubule autofluorescence.

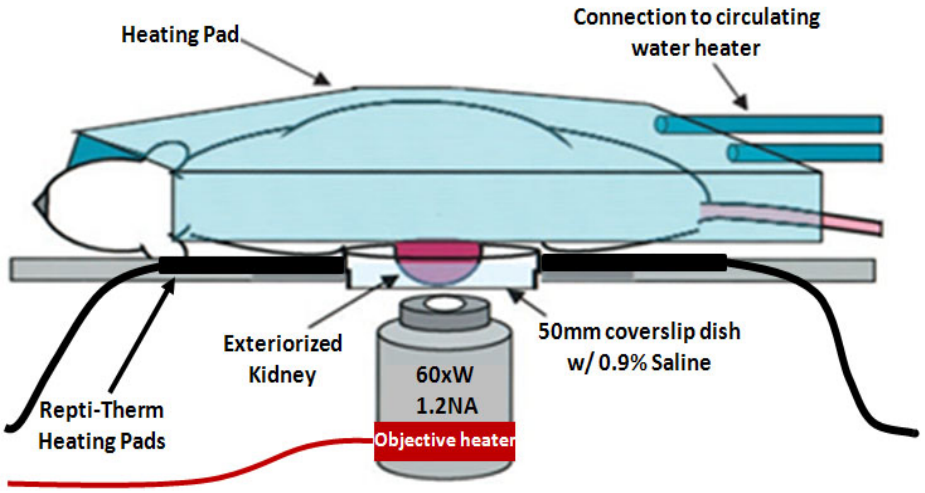

Figure 12: Intravital Imaging Preparation. (Courtesy of Ruben Sandoval)

2.3.8.3 Fluorescence Recovery After Photo-bleaching

Four days prior to imaging male Sprague-Dawley rats (250-350g) received hydrodynamic delivery of adenoviral GFP occludin or occludin 860 as previously described. Animals were prepared for intravital light microscopy as previously described. For FRAP, GFP occludin images were acquired in multi photon mode and bleaching of the occludin protein occurred in one photon mode. Our FRAP studies followed the methods established by Zheng *et al* (137).

2.3.8.3 Blood Flow Measurements

24 hours following renal IRI, isoflurane-anesthetized rats were prepared for intravital light microscopy as described above. A line scan was generated from the center of the vessel of interest continuously at a rate of two milliseconds per line for one second (1000 total lines). The scan measures flowing red blood cells, which do not take up dye and are therefore black. To analyze the scan, all channels of the line scan are merged into a single channel. This results in a vertical axis denoting time and a horizontal axis denoting the length or distance of the scan. The velocity of the blood cells was determined using the dark lines which depict the movement of the blood cell along the scan over time. The flow velocity was determined by measuring the slope as described by Dunn *et al* (136).

2.3.8.4 Vascular Permeability Studies

24 hours' post-nephrectomy with contralateral ischemia reperfusion injury, hydrodynamic isotonic fluid delivery was performed on the remnant kidney. 20 minutes after hydrodynamic fluid isotonic delivery, 150 kDa TRITC conjugated dextran and Hoechst 33342 was injected via tail vein. Intravital imaging was performed on the kidney at a rate of two milliseconds per line for a total of five minutes. Vascular permeability was determined by measuring the change in red channel fluorescence along a line perpendicular to a capillary wall.

Sequential changes in fluorescence intensity over time were used to determine the rate of high molecular weight dextran entry into the interstitial compartment. Ten fields were studied for each animal and statistical significance was determined at a p value less than 0.05 using Student's t test.

To evaluate changes in Hoechst 33342 signal, 512 x 512 image scans were collected with simultaneous acquisition of 420nm and 514nm wavelengths at one scan per second using 800nm excitation light in two-photon mode. Thirty scans were acquired from each animal with random field selection. Images were acquired 24 hours post-IRI and 20 minutes after hydrodynamic isotonic fluid delivery in post-IRI rats. Images were also collected from sham-operated rats. Image intensity values were obtained by defining a circular region of interest (ROI). Average intensity values were obtained by placing the ROI over nuclei in all cells in the field using FIJI (134).

2.4 Freeze Substitution and Embedding

All samples were freeze substituted using a Leica Automatic Freeze Substitution (AFS) Unit (Leica Microsystems, Vienna, Austria). Samples were freeze substituted in 0.01% OsO_4, 0.1% GA, 0.25% uranyl acetate in acetone and embedded in LR Gold (Electron Microscopy Services, Hatfield, PA). The freeze substitution schedule was as follows: held at -90^o C for three days, warmed to -25^o C at 5^o C per hour, then held at -25^o C for six hours. Some of the samples were warmed to 0^o C over a 2.5 hour period, rinsed with 100% acetone, warmed to room temperature, infiltrated in 1:2 resin:acetone for two hours and then followed by 2:1 resin:acetone overnight. Samples were embedded and then polymerized at -20^{o}C. Sections were cut with a Leica Ultracut UCT Ultramicrotome (Leica Microsystems, Vienna, Austria). Sections were imaged with a FEI electron microscope equipped with an AMT CCD camera.

2.5 Evaluation of Renal Tubular Damage and RBC Congestion

Renal tubular damage was evaluated from formalin-fixed paraffin embedded samples stained using hematoxylin and eosin (H&E). Six random images (three cortex, three outer medulla) were obtained using a Leica DMLB microscope (Scientific Instruments, Columbus, OH) using a 20x objective. For each kidney, an average of 60 tubules were scored from images by an observer who was blinded to the treatments using a modified 1-4 scoring system described previously (138). Data presented are based on the average score per tubule corresponding to each animal. RBC congestion was analyzed using ImageJ software, whereby regions of interest were identified visually and used to calculate percent surface area (to determine vascular congestion).

2.6 Assessment of Renal Infiltrating Cells

Harvested kidneys were minced and digested with liberase (2μg/ml; Roche, Basel, Switzerland) for 15 minutes at 37°C using Gentle MACs (Miltenyi, San Diego, CA). Digested tissue was filtered through a 100-μm filter mesh and washed with medium. Mononuclear cells were separated by Percoll (Sigma-Aldrich, St. Louis, MO) and counted by hemocytometer. To evaluate T lymphocytes, the cells were stained with antibodies against rat CD4 (PE-Cy7), CD8a (Alexa 647) and CD161 (PE-Cy7). To evaluate the T helper subtype, the cells were permeabilized and stained with antibodies against cytokines such as IFN-gamma (FITC; Th1), IL-4 (PE; Th2) and IL-17 (FITC; Th17). To evaluate regulatory T-cells, mononuclear cells were stained with either CD4 or CD4 along with Foxp3 (PE). To evaluate B cells and Mac/DC, mononuclear cells were stained with antibodies against RTIB (FITC) and Cd11b/c (PE) respectively. Fluorescence was measured using flow cytometry (FACSCalibur, BD Biosciences, San Jose, CA) and dot plots were analyzed using Flowjo software (Tree Star, Ashland, OR). Lymphocyte gating strategy was identical to that shown previously (139). The data is expressed as a total number of cells per gram of kidney.

2.7 Serum Creatinine Measurements

To determine the effectiveness of our plasmid in protecting renal mitochondria, serum creatinine measurements were collected prior to injury and 24-hours post injury. Animals were briefly anesthetized under isoflurane, and blood was collected via tail vein incision. Blood was collected in a heparin treated 1 mL Eppendorf tube.

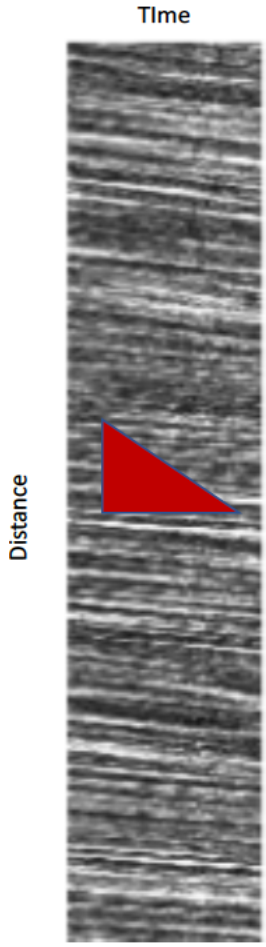

Figure 13: Line Scan(1). Line scan info:24 hours following renal IRI, isoflurane-anesthetized rats were prepared for intravital light microscopy as described above. A line scan was generated from the center of the vessel of interest continuously at a rate of 2 msec per line for 1 sec (1000 total lines). The scan measures flowing red blood cells, which do not take up dye, and are therefore black. To analyze the scan, all channels of the line scan are merged into a single channel. This results in a vertical axis denoting time and a horizontal axis denoting the length of the scan, or distance. The velocity of the blood cells was determined using the dark lines which depict the movement of the blood cell along the scan over time.

The tubes were then centrifuged at 10,000 x g for 10 minutes and the serum was stored at 4^{o}C. A Point Scientific QT 180 analyzer and creatinine reagent kit (Point Scientific, inc, Canton, MI) were used to analyze serum creatinine according to Point Scientific protocol.

2.8 Proteomics

Male Sprague-Dawley rats were subjected to an ischemia reperfusion injury as previously described. The animals were allowed to recover for two weeks. Following recovery, the renal mitochondria were isolated as previously described and frozen at -80^{o}C until proteomic analysis. Proteomic analysis was conducted as described by Molloy *et al* (140, 141).

2.9 Plasmid Vectors

All plasmids were prepared using Qiagen Maxi prep systems (Qiagen, Chatsworth, CA, USA). These plasmids were suspended in saline for gene delivery and 2-3 μg of DNA per gram body weight was delivered through the renal vein. The following plasmids were used: Mitochondria Isocitrate Dehydrogenase II (NADP+) (Origene Technologies, Inc., Rockville, MD), enhanced Green Fluorescent Protein (eGFP) Actin (eGFP-actin) and Tubulin (EGFP tubulin) (Clonetech Laboratories, Inc., Mountain View, CA). The mitochondria *IDH2* is a nuclear encoded gene and an Open Reading Frame (ORF) clone of the *Homo sapiens* Isocitrate Dehydrogenase II.

2.10 DNA Gel Electrophoresis

The E-Gel® with SYBR Safe 1.2% agarose gel (Invitrogen, G521801) was inserted into the E-Gel® PowerBaseTMv.4. Each well of the gel was loaded with 500ng plasmid DNA. The electrophoresis time was set at 30 min.

2.11 Cellular Transfection

2.0×10^5 cells were plated into each well of a six well plate the day before transfection (alternatively cells were plated and grown on a 35- mm glass bottom, No. 1.5 coverslip dish with standard thickness of 0.17 mm (Corning Inc., Corning, NY)). 24 hours later cells were transfected with either *IDH2* or myc-*IDH2* using Lipofectamine 3000 kit, following the Lipofectamine 3000 transfection protocol (ThermoFisher, Waltham, Ma) and were collected for mitochondria respiration analysis, IHC, or confocal imaging 24-48 hours after transfection.

2.12 Confocal or 2-photon Imaging of Fluorescent Cells

Confocal imaging studies were conducted on an Olympus FV 1000-MPE Microscope (Olympus, Tokyo, Japan). Cell cultures were grown in 35mm glass bottom, No. 1.5 coverslip dishes with standard thickness of 0.17 millimeters (Corning Inc., Corning, NY) The dishes were placed above the objective and the microscope was set to acquire 512x512 pixels in blue, green, and red-pseudocolor images. To minimize both photoxicity and photobleaching, we reduced both the energy level of the excitation light and the duration of excitation.

2.13 Immunohistochemical Staining and Colocalization

Immunohistochemical staining was conducted on myc-*IDH2* and mock transfected NIH 3T3 using myc 9e10 antibody (1:100) and FITC donkey anti-rabbit as previously described (142). The cells were allowed to grow to 80% confluency on glass cover slips following transfection (48 hours). The cells were then fixed with 4% PFA for 10 minutes and then washed with PBS three times. After fixation, the cells were permeabilized with 0.1% Triton X-100 (ThermoFisher Scientific, Waltham, MA) for 10 minutes and then washed with PBS three times. After rinsing with PBS, the cells were blocked with 1% normal goat serum (ThermoFisher Scientific, Waltham, MA) in PBS for one hour at room temperature. Following blocking, the primary antibody solution was placed on the cells for 30 minutes at room temperature followed by two ten minute washes in PBS. Following the washing, a secondary antibody solution containing a 1:20,000 dilution of Hoechst 33342, 100 nM Mitotracker Red, and secondary antibody was placed on the cells for 30 minutes. The cells were then washed in PBS as previously described. After the final rinse, the cells were mounted onto a slide using Fluorsave reagent (MilliporeSigma Billerica, MA) and allowed to dry overnight. Cells were imaged using an Olympus FV 1000 confocal microscope at 820 nm. Red to green colocalization indicated myc-tagged *IDH2* localized to mitochondria. Manders colocalization tests were conducted as described by Dunn *et al* 2011 (143).

2.14 Propidium Iodide

Transfected, mock transfected, and control S3 cells underwent PI treatment to determine the efficiency of IDH2 in preventing cell death as previously described (144).

These S3 cells were subjected to 90 minutes of hypoxia in a hypoxia incubator chamber. Following hypoxia, the growth media was changed and cells were stained with 0.1 ug/ml Hoechst 33342 and 1.0 mg/ml PI for 20 minutes. These cells were then fixed using 4 % PFA for 25 minutes. Following fixation, PI positive cells were counted under a Nikon Livecell microscope with the 10x objective equipped for epifluorescence microscopy.

2.15 In vivo Mitochondria Analysis

2.15.1 Extracting the Kidney

The rats were anesthetized with inactin hydrate. A midline incision was made and the kidney pedicle ligated and the kidney removed. Following isolation of the kidney, the kidney was placed onto an 0^{o} C petri dish. Once placed onto the petri dish five mL of sterile saline was poured over the kidney. Following the washing of the kidney, the capsule was removed. Once the capsule was removed, the kidney was longitudinally bisected, using a razor blade to expose the cortex and medulla. Once exposed, the cortex was isolated, minced into fine pieces, and then weighed. Following the procedure, the animal was euthanized.

2.15.2 Electron Microscopy: Mitochondria Structure Analysis

The specimens were fixed in 2% Paraformaldehyde 2% Glutaraldehyde in 0.1M phosphate buffer. After fixation, the specimens are rinsed with phosphate buffered saline (PBS) followed by post fixation with 1% osmium tetroxide in phosphate buffer for one hour. After rinsing again with PBS, the tissue specimens are dehydrated through a series

of graded ethyl alcohols from 70 to 100% concentration. After dehydration, the specimens were infiltrated with two changes of 100% acetone and a 50:50 mixture of acetone and the embedding resin (Embed 812, Electron Microscopy Sciences, Hatfield, PA) overnight. The next day the specimens are transferred to fresh aliquot of 100% embedding media for a minimum of two hours, then embedded in a fresh aliquot of 100% embedding media. Following polymerization overnight at 60°C the blocks are then ready to section. Thin sections were cut (70-80nm), stained with uranyl acetate and lead citrate, then viewed on a Tecnai BioTwin electron microscope (FEI, Hillsboro, OR) with digital images taken with an AMT (Advanced Microscope Techniques, Danvers, MA) CCD camera.

2.15.3 PBI SG3 Shredder Mitochondria Homogenization

The minced cortex was weighed and separated into groups of 300mg. Next, 300 mg of cortex was positioned into the ram side of the pulse tube; the section was then capped closed and 700 microliters of mitochondria isolation buffer (250 mM Sucrose, 20 mM HEPES ph 7.9, 10 mM KCl, 1.5 mM $MgCl_2$, and 1.0 mM EDTA) was added to the cap side of the pulse tube; this section was capped closed. Next the tube was placed into the PBI Shredder and locked into position two. The shredder was run for 30 seconds and the supernatant was removed and placed into microcentrifuge tubes.

2.15.4 Mitochondria Purification

The mitochondria homogenate was centrifuged at 800x g for 10 minutes; after 10 minutes the supernatant was transferred to a new set of microcentrifuge tubes and the

pellet was discarded. Next, the supernatant from the first centrifugation was centrifuged at 14,000x g for 10 minutes; after 10 minutes the supernatant was discarded and the pellet was resuspended in one mL of mitochondria isolation buffer. For the final spin, the pellet from round two was centrifuged at 14,000x g for 10 minutes; after 10 minutes the supernatant was discarded and the pellet is resuspended in 0.5 mL of mitochondria isolation buffer.

2.15.5 Mitochondria Protein Measurement

Following resuspension, the mitochondria lysate tubes were placed on ice for mitochondria respiration analysis using an Oroboros and three μL of each sample was removed for Bio-Rad Bradford Protein Assay (Bio-Tek Instruments, Inc) to determine mitochondria protein concentration.

2.15.6 Mitochondria Respiration Analysis: Oroboros Oxygraph-2k

Mitochondria respiration analysis was conducted in an Oroboros Oxygraph-2k (Oroboros Instruments, Innsbruck, Austria) as previously described (145, 146). Equivalent amounts of mitochondria protein were loaded into a final volume of 2.0 mL miRO5 (110 nm sucrose, 20mM HEPES 20, 20mM taurine, 60 mM K-lactobionate, 3 mM $MgCl_2$, 10 mM KH_2PO_4, 0.5 mM EGTA 0.5 and 1 g l^{-1} bovine serum albumin, pH 7.1) respiration buffer with constant stirring (750 rpm). Following mitochondria lysate addition, flux was allowed to stabilize before addition of substrates or ADP. Substrates were added in the following order and diluted to the following concentrations: 10 uM

Isocitrate, 2.5 uM Malate, 20 nM ADP, 7.5 uM Pyruvate, 20 nM ADP 10 uM Succinate, and 20 nM ADP. Flux was allowed to stabilize prior to addition of the next substrate or ADP. Data was collected using Oroboros Datlab version six and all calibration prior to experimentation was conducted according to Oroboros protocols (Figure 14).

2.15.7 Mitochondria Membrane Potential Measurements: Tetramethylrhodamine Methyl Ester (TMRM)

To determine changes in mitochondria membrane potential in response to HIFD, TMRM was infused via the tail vein in sham, pre-HIFD, and post HIFD rats. Ten fields were studied for each animal and statistical significance was determined at a p value less than 0.05 using Student's t test.

To evaluate changes in TMRM signal, 512x512 image scans were collected with simultaneous acquisition of 420nm and 514nm wavelengths at one scan per second using 830nm excitation light in two-photon mode. 30 scans were acquired from each animal with random field selection. Images were acquired 20 (up but not exceeding 60 minutes) minutes post TMRM infusion in pre-HIFD rats 20 minutes and between 20-60 minutes post HIFD after HIFD. Images were also collected from sham-operated rats. Image intensity values were obtained by defining a circular region of interest (ROI). Average intensity values were obtained by placing the ROI over nuclei in all cells in a field using FIJI (134).

2.15.8 Mitochondria ATP Determination: High Performance Liquid Chromatography (HPLC)

In vivo samples were isolated from animals that had undergone renal vein hydrodynamic fluid delivery, ischemic preconditioning, or control operations as previously described. One week later kidneys were immediately isolated and snap frozen and prepared for HPLC as previously described (147). The following steps were performed on ice at 4^{o} C. Frozen whole kidneys were homogenized using a hand held mechanical tissue homogenizer in six mLs of pre-chilled 3% $HClO_4$. Once the tissue was homogenized, the homogenate sat on ice for 10 minutes. After 10 minutes, the homogenate was centrifuged at 13,000 x g at 4^{o} C for 10 minutes. The supernatant was transferred to a clean tube and one-third (300 µL) the volume of 3 M K_2CO_3 was added. The tubes were vortexed and placed on ice for 10 minutes. Following the incubation period, the samples were centrifuged at 13,000 x g at 4^{o} C for 10 minutes and the supernatant was transferred to a clean microcentrifuge tube.

2.16 *In vitro* Mitochondria Analysis

2.16.1 Mitochondria Stress Test: Seahorse

Mitochondria respiration analysis was conducted using a Seahorse XF 96 extracellular flux analyzer as previously described (148). 5,000 MPTC S3 cells were plated in Seahorse XF 96 cell culture microplate 24 hours prior to analysis. Analysis was performed with the appropriate growth media containing 10 mM glucose, 100 mM sodium pyruvate and 1M glutamine.

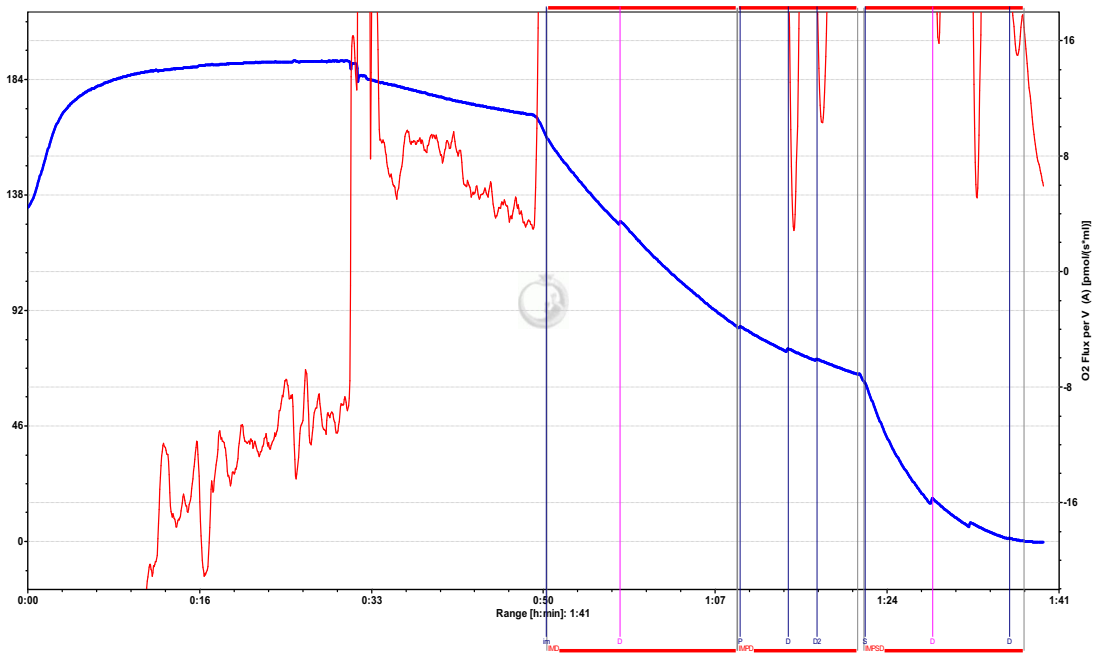

Figure 14: Oroboros Oxygraph-O2k. The figure depicts mitochondria respiration analysis in an Oroboros. The blue line represents oxygen concentration, while the red line indicates represents oxygen flux. Substrates added include: Isocitrate (I), Malate (M), Pyruvate (P), Succinate (S), and ADP (D).

Cells were allowed to acclimate for one hour prior to analysis. Baseline measurements were conducted for transfected and mock transfected cells prior to compound addition. Respiration measurements were conducted following injections of 7 μM FCCP and 6 μM Rotenone/Antimycin A. All flux data is expressed in OCR, in pmol/min/cell (Figure 15).

2.16.2 Mitochondria Membrane Potential Analysis

MPTC S3 cells were transfected as previously described. Two days following transfection cells were plated onto a 96 well plate. One day later the JC-1 assay was performed as follows. 5 μM of JC-1 was added to depleted cell media and cells were placed in a hypoxia incubator chamber for 30 minutes. Following hypoxia, cell luminescence was measured using a spectrophotometer with an excitation wavelength of 490 nm. Emission was measured at both 527 nm and 590 nm. Mitochondria membrane polarization was measured by ratioing 527nm to 590nm. Higher ratio values are indicative of higher membrane potential.

2.16.3 Fluorescence Lifetime Imaging Microscopy: Determination of Cellular NAD(P)H Levels

MPTC S3 cells were prepared and transfected as previously described. Following transfection, cells underwent fluorescence lifetime imaging microscopy (FLIM) as described by Gratton *et al* (149) and phasor plots were established and analyzed according to Winfree *et al* (150) and Digman *et al* (151).

Mitochondria lysates were isolated as previously described. 30 nM of Human Recombinant SULT1C2 protein, 20 μM PAPS, and 10 μM Laurdan were added to the sample and 50 μL were placed mounted on a slide and underwent FLIM a previously described.

2.17 Western Blot Analysis

Following isolation, the kidney was placed onto an 0^{o} C petri dish. Once placed onto the petri dish 5 mL of sterile saline was poured over the kidney. Following the washing of the kidney, the capsule was removed. Once the capsule was removed, the kidney was longitudinally bisected, using a razor blade to expose cortex and medulla. Once exposed the cortex was isolated and minced into fine pieces and then weighed. The cortex was then homogenized, on ice in the cold room, using a dounce homogenizer and 300 uL of RIPA buffer (150 mM NaCl, 50 mM Tris-Cl PH 8.0, 1% Triton X-100, 0.5% Sodium Deoxycholate, and 1% SDS) (ThermoFisher Scientific, Waltham, MA). Once homogenized, the lysate was transferred to a microcentrifuge tube. The lysate was centrifuged at 13,000 rpm for 15 minutes at 4^{o}C. After this cycle, the supernatant was transferred to a clean microcentrifuge tube and sonicated. Following sonication, the tubes were centrifuged as previously described, and the supernatant was transferred to a clean tube. Protein concentration was determined using either BCA assay (ThermoFisher, Waltham, MA) or Bradford assay (Bio-Rad, Hercules, CA). 3 μg of protein was mixed with 2x Laemmli Sample Buffer and placed in a warming tray (70 ^{o}C for 10 minutes). Protein samples were then loaded into a 10% SDS Page Gel (Life Technologies, Carlsbad, CA) along with 8 μL of molecular weight standards

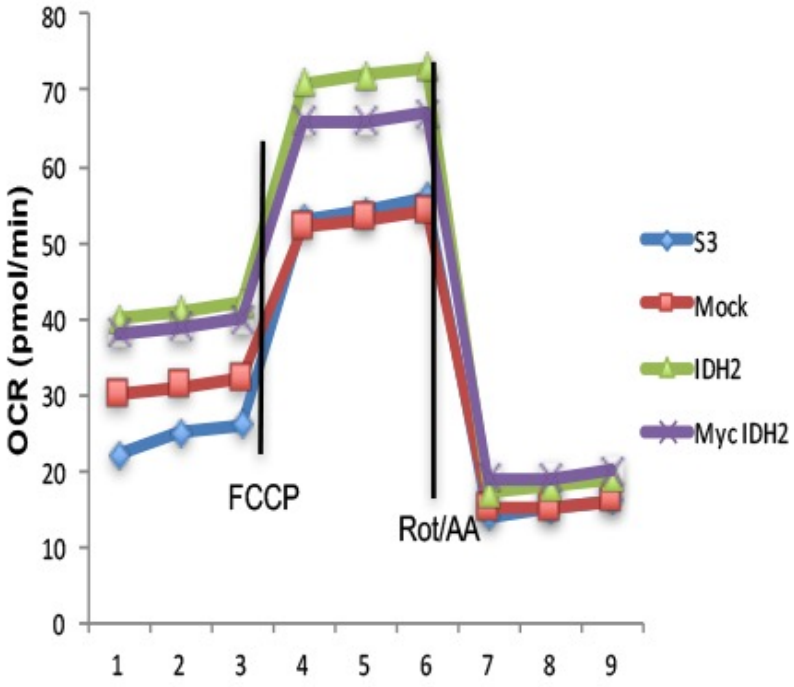

Figure 15: Seahorse Mitochondria Stress Test Graph. Graph detail changes in S3 cell oxygen consumption. Addition of FCCP indicates maximal respiration, while the Rotenone/Antimycin A addition indicates complex II respiration.

The gel ran for 56 minutes at 200 V and was then electroblotted onto either nitrocellulose or PVDF membranes, depending on antibody recommendations, for 36 minutes at 24 V.

These membranes were then blocked in TBS with 3% FBS or TBS with 5% dry milk overnight at 4^{o}C. Membranes were incubated in primary antibody in antibody dilution buffer (either 0.3% FBS in TBS or 5% dry milk in TBS) for one hour at room temperature. Membranes were then washed with TBST (TBS with Tween-20) and then incubated in secondary antibody in antibody dilution buffer for one hour at room temperature. After three more washes with TBST, the protein bands were visualized by chemiluminescence using SuperSignal^{TM} West Pico Chemiluminescent Substrate (ThermoFisher, Waltham, MA). After a five-minute incubation period, the SuperSignal was removed and the membrane was wrapped in Polyvinyl Chloride wrap (ThermoFisher, Waltham, MA). Images were acquired using x-ray film in a darkroom.

2.18 Statistical Analysis

All statistical analyses were conducted using a two-tailed unpaired Student's t-test. Colocalization was determined using Mander's localization analysis (143). All bar graphs are expressed as means ± s.d.

CHAPTER 3: REVERSAL OF ACUTE KIDNEY INJURY

Paper: Collett JA, Corridon PR, Mehrotra P, **Kolb AL**, Rhodes GJ, Miller CA, Molitoris BA, Pennington JG, Sandoval RM, Atkinson SJ, et al. Hydrodynamic Isotonic Fluid Delivery Ameliorates Moderate-to-Severe Ischemia-Reperfusion Injury in Rat Kidneys. *Journal of the American Society of Nephrology: JASN.* 2017 (1).

3.1 Photographic Analysis of Renal Vasculature following IRI

Ischemic injuries can be broken down into two phases. The first phase is lack of blood flow to the kidney. The major effect of a reduction in blood flow is the loss of oxygen. The direct implication of oxygen loss is alteration in oxidative phosphorylation, specifically a Warburg Shift leading to heavy glycolytic metabolism. The second phase and probably the most detrimental is the reperfusion phase (45, 152). The reperfusion of blood into the kidney results in immune cell infiltration and red blood cell aggregation culminating in changes to renal vasculature. Ischemia reperfusion injury leads to changes in both epithelial and endothelial cell adhesion (8, 9, 42, 153, 154). To determine if our model of IRI caused changes in cell adhesion leading to the formation of red blood cell aggregates, termed rouleaux, typically seen with ischemic injury, we used correlative light and electron microscopy. Kidney sections were analyzed by light microscopy and then particular regions of interest were fixed for electron microscopy (Figure 16). In figure 16A, light microscopy indicates the aggregation of rouleaux (arrows) in the capillary lumen while 16B shows the same region at ultrahigh resolution. To compare ischemic and control kidneys, electron micrographs of uninjured kidneys were analyzed and non-aggregated red blood cells were observed, indicating lack of ischemic injury.

Figure 16 indicates the effect of reperfusion on the renal vasculature was similar to what has been reported in the literature (155, 156).

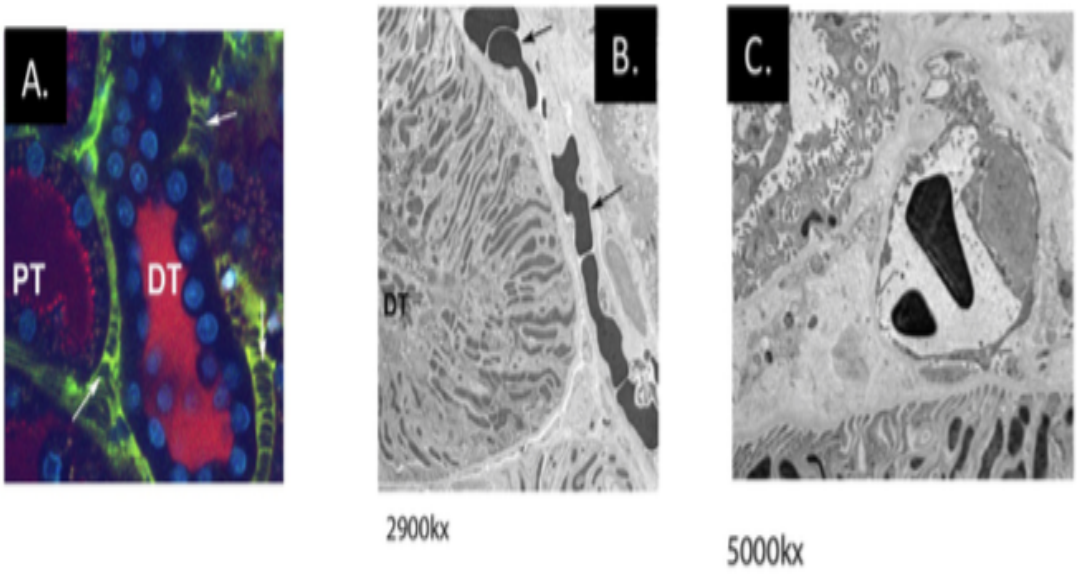

Figure 16: Microscopic Analysis of Kidneys Following Ischemic Injury. A) Multiphoton image of the renal vasculature. 150kD FITC dextran in green is taken up by the plasma, while red blood cells and rouleaux do not take up the dye. The images indicate formation of rouleaux (arrows) in the vascular space. B) Electron micrograph of A taken following fixation to depict renal structure following injury. C) Electron micrograph of uninjured renal vasculature.

3.2 The Amelioration of AKI by Hydrodynamic Isotonic Fluid Delivery

The current clinical model for the treatment of AKI is to restore glomerular filtration rate and blood flow through the kidney. Our interest with hydrodynamic isotonic fluid delivery was to determine whether it would be translatable to the clinic. This technique has proven useful in the delivery of macromolecules to the kidney (22). We set out to determine if hydrodynamic isotonic fluid delivery could be used to change the prognosis and course of AKI. We hypothesized that this highly pressurized injection, ranging from 60-to-75 mmHG (Figure 11) and characterized by streaks of saline and blanching in the kidney (Figure 18), would alter the course of AKI by reducing vascular congestion.

To study the effects of hydrodynamic isotonic fluid delivery on AKI, rats were subjected to IRI followed 24 hours later by renal vein hydrodynamic isotonic fluid delivery or injection in the vena cava. The animals were allowed to recover for four days and serum creatinine levels were analyzed to follow the course of injury. Figure 17 A-C indicate that animals that received hydrodynamic isotonic fluid delivery through the renal vein had reductions in SCr levels not seen in animals injected through the vena cava. The change in SCr, as indicated by figure 17 C was 1.65± 0.34 mg/dL. These findings were correlated with changes in renal morphology (Figure 19) and tissue injury scoring (Figure 20). The images indicate acceleration in recovery and improved survival from IRI as a result of hydrodynamic isotonic fluid delivery that were not seen in animals that received vena cava injections (Figure 21). The culmination of the SCr data and morphological analysis indicate hydrodynamic isotonic fluid delivery can potentially alter the path of AKI.

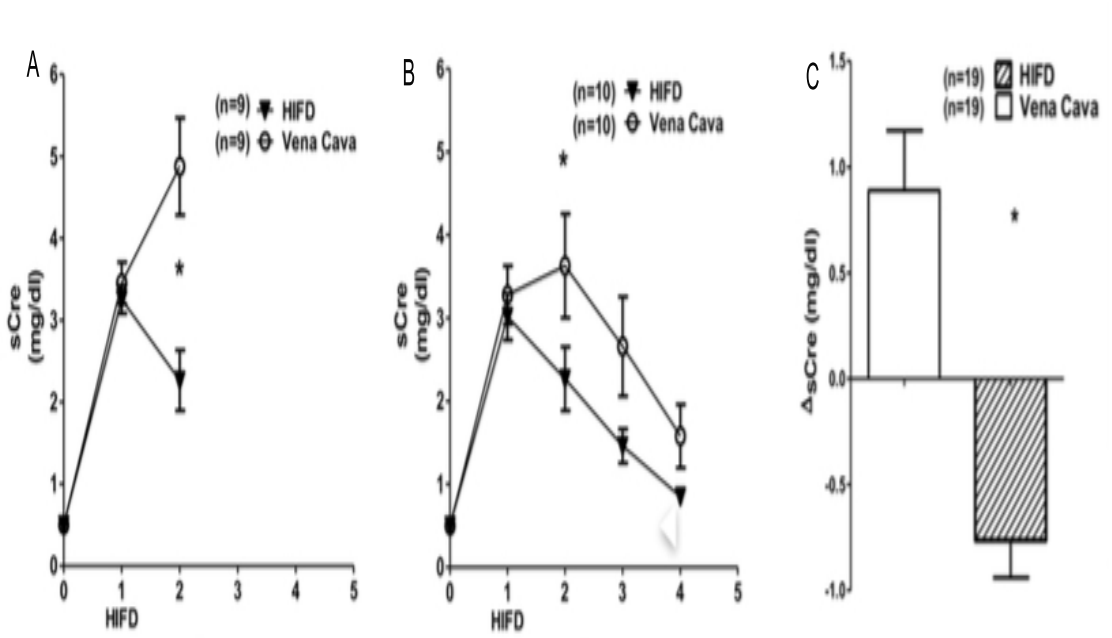

Figure 17: Serum Creatinine Levels following Hydrodynamic Isotonic Fluid Delivery in Either Renal Vein or Vena Cava. SCr changes following IRI in animals treated with HIFD through the renal vein or vena cava control. A) SCr values 48 hours following injury and 24 hours' post HIFD. B) SCr values four days post IRI and 72-hours post HIFD. C) The change in SCr 24 hours' post HIFD includes values from two and four day groups. *P value <0.05 in HIFD versus vena cava. Statistics determined by unpaired student's t-test.

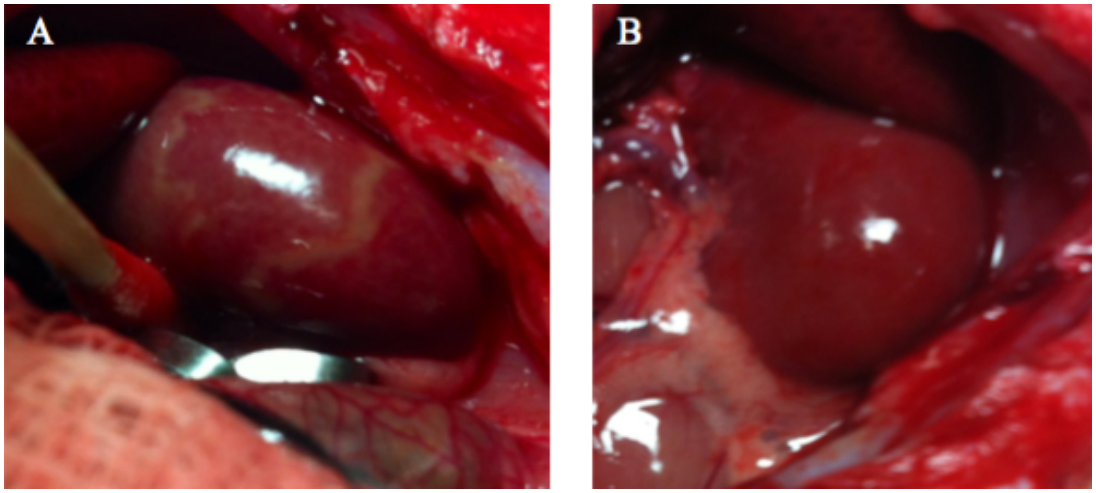

Figure 18: Characteristics of Renal Physiology Prior to and Following Hydrodynamic Isotonic Fluid Delivery. Following HIFD, blanching and streaking is observed in the kidney (A) compared to three-minutes prior to injection (B).

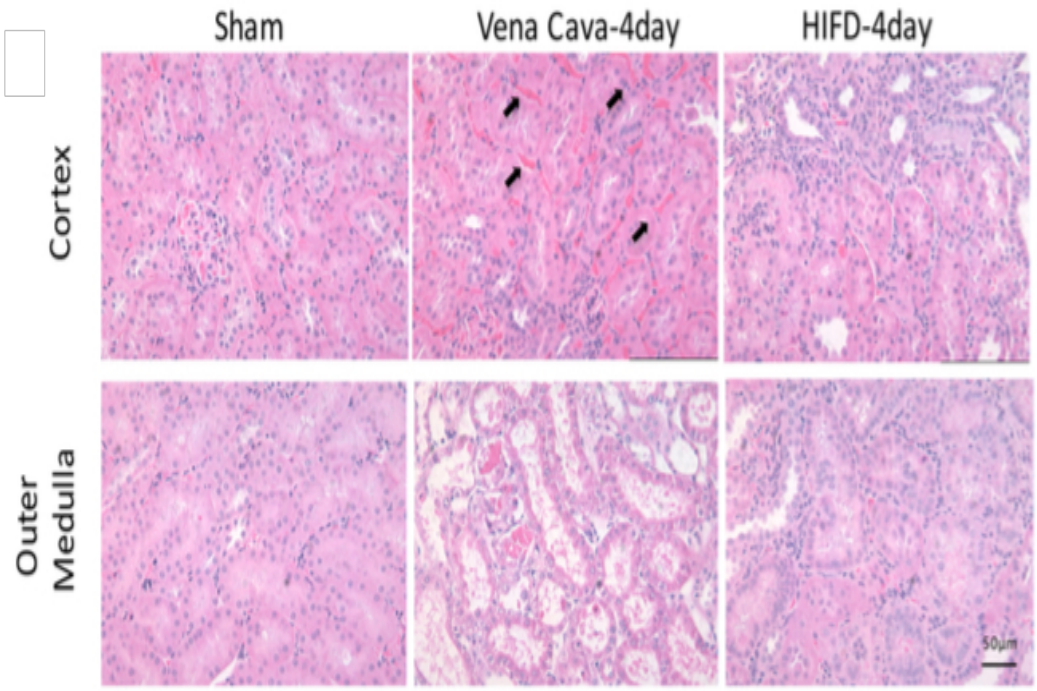

Figure 19: Renal Histology 4-days post IRI. Hematoxylin and Eosin staining of cross-sections of the cortex and outer medulla. The renal histology indicates decreases in rouleaux (arrows) and vascular congestion in animals that received Hydrodynamic Isotonic Fluid Delivery.

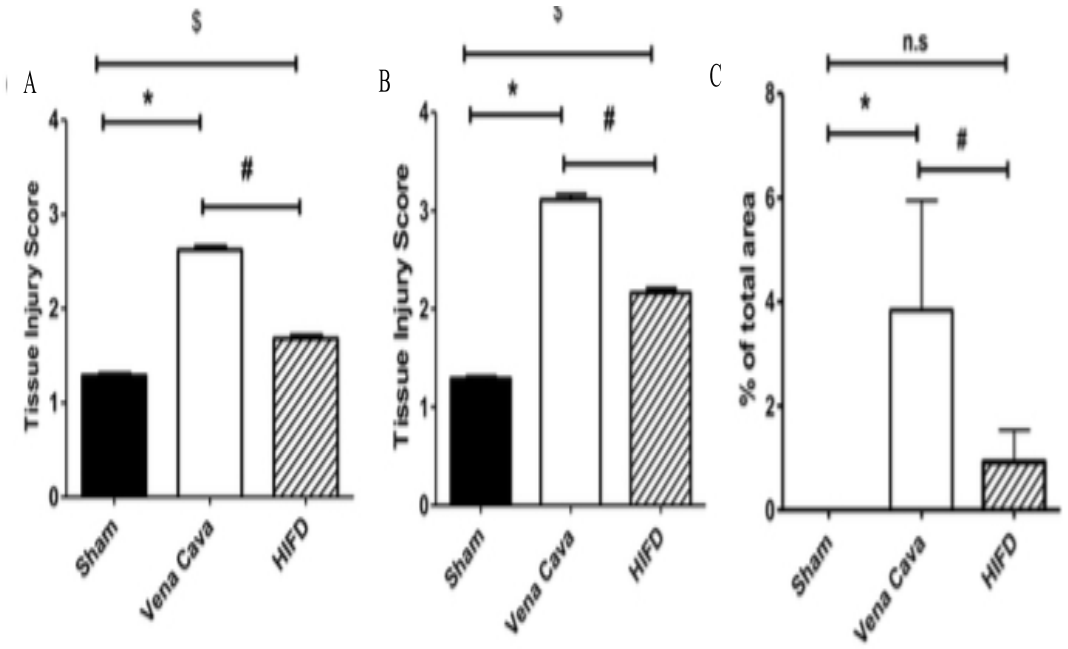

Figure 20: Tissue Injury Scoring. Renal histology was used as a basis for tissue injury scoring of the cortex (A) and outer medulla (B). (C) Represents the total area of vascular congestion in renal cortex. *,$,# p value <0.05 for sham versus vena cava (*), HIFD versus vena cava (#), or sham versus HIFD ($).

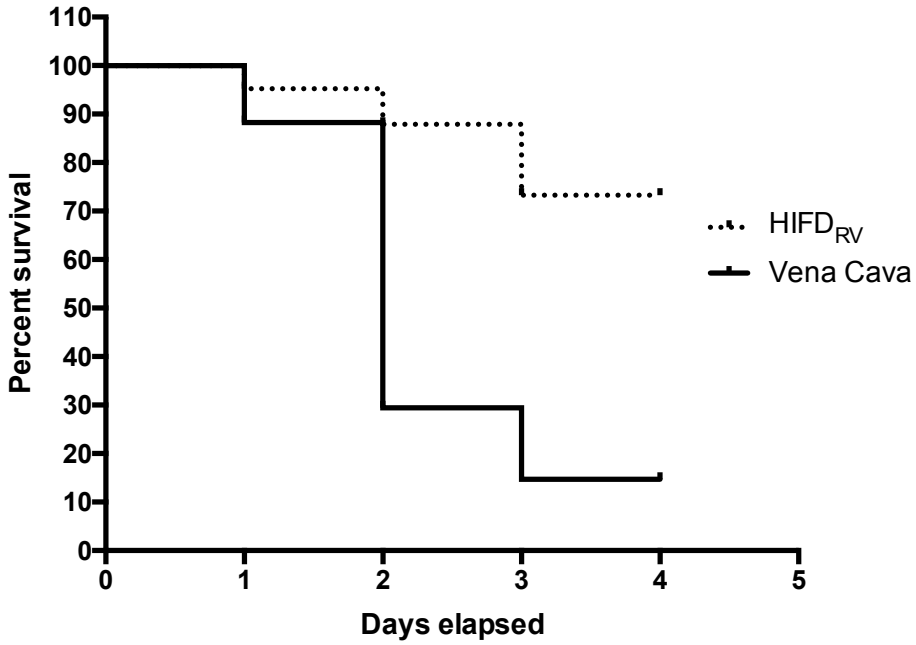

Figure 21: Survival Graph. Hydrodynamic Isotonic Fluid Delivery improves survival in animals following an IRI by 70%.

3.3 Restoring Capillary Perfusion with Hydrodynamic Isotonic Fluid Delivery

The histology shown in Figure 19 indicated decreased RBC accumulation in the vasculature following hydrodynamic isotonic fluid delivery. To test for changes in capillary perfusion, animals were subjected to IRI followed 24 hours later by hydrodynamic isotonic fluid delivery and intravital imaging of renal blood flow. Prior to hydrodynamic isotonic fluid delivery, I was able to identify areas in renal vasculature congested with rouleaux and hypoperfused (Figure 22 A). Following hydrodynamic isotonic fluid delivery, renal perfusion increased and rouleaux aggregation decreased leading to increased blood flow (Figure 22B; arrows). Blood flow analysis following IRI indicated an 81% reduction in blood flow velocity compared to sham treated animals. Following hydrodynamic isotonic fluid delivery, blood flow velocity increased 2.3-fold within 30 minutes of hydrodynamic isotonic fluid delivery compared to pre-hydrodynamic isotonic fluid delivery groups (Figure 23). While still lower than sham animals, hydrodynamic isotonic fluid delivery increased blood flow rates significantly compared to animals that did not receive hydrodynamic isotonic fluid delivery.

In addition to changes in perfusion in the kidneys, I also identified changes in cell membrane permeability. Hoechst 33342, which labels cell nuclei, has a molecular weight of 452g/mol, and due to its cell permanent properties is able to easily label cell nuclei. Its molecular weight is consistent with that of small therapeutic compounds generally used to treat kidney disease. 24 hours after IRI, Hoechst 33342 was injected via the tail vein and analyzed by intravital light microscopy. The fluorescence intensity signal was low in animals following IRI compared to sham treated animals (Figure 22 A-C). The average fluorescent intensity was 20.12±2.8 (au). Following hydrodynamic isotonic fluid

delivery, the intensity increased approximately 3.5-fold to 73.2±1.1 (au) (Figure 24). It is important to point out that during the hydrodynamic isotonic fluid delivery procedure no additional Hoechst 33342 was given indicating that increases in average fluorescence intensity are likely due to increased perfusion. To ensure that hydrodynamic isotonic fluid delivery was not detrimental to the vasculature, 150 kDa TRITC dextran was also injected through the tail vein. Figure 25 indicates that fluorescent intensity of interstitial space does not change as a result of hydrodynamic isotonic fluid delivery. Intravital imaging of renal vasculature before and after hydrodynamic isotonic fluid delivery indicates that hydrodynamic isotonic fluid delivery following IRI increases renal blood flow and cell permeability while decreasing rouleaux congestion.

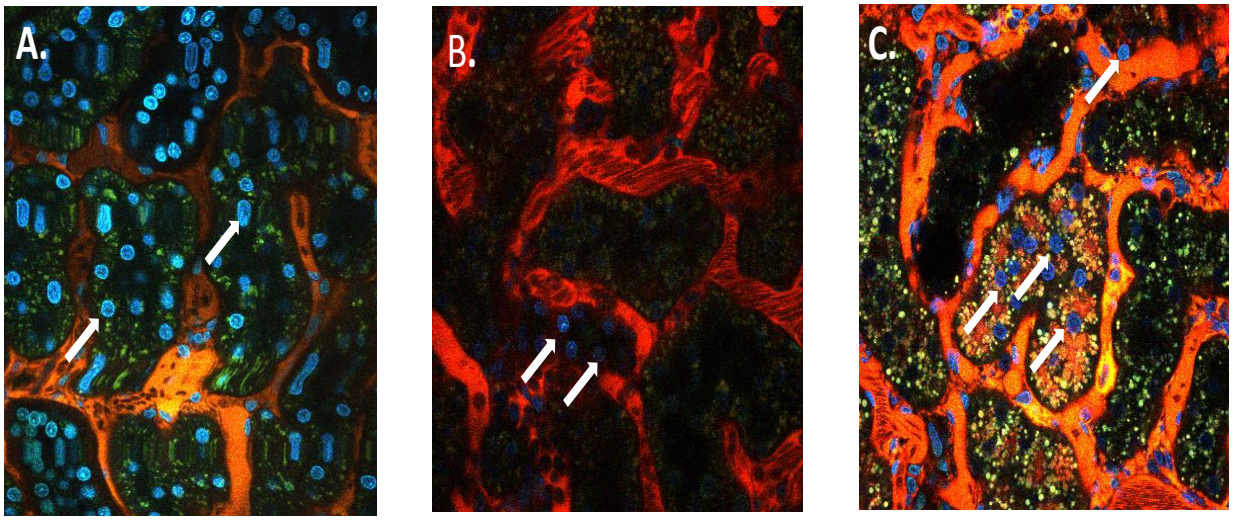

Figure 22: Renal Blood Flow and Vascular Permeability. Multiphoton imaging of sham kidney(A), 24-hours post-IRI and pre-HIFD (B) and 24-hours post-IRI 20 minutes post-HIFD (C). Blue color is Hoechst 3342 staining of cell nuclei, red/orange is 150 kDa TRITC dextran.

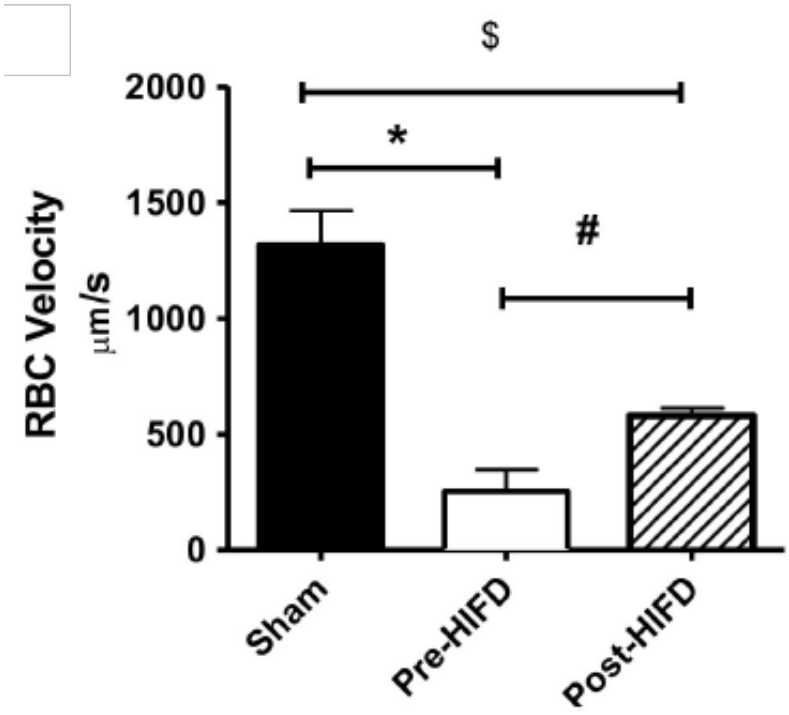

Figure 23: Changes in RBC Velocity due to IRI and Hydrodynamic Isotonic Fluid Delivery. RBC velocity was calculated by conducting line scan analysis (Figure 13) according to Dunn *et al* and Lin *et al* (136, 157). The calculation of the slope of the line gives the overall velocity. ,#,$ p value <0.05 for sham versus post-HIFD ($), sham versus pre-HIFD(*), and pre-HIFD versus post-HIFD (#).

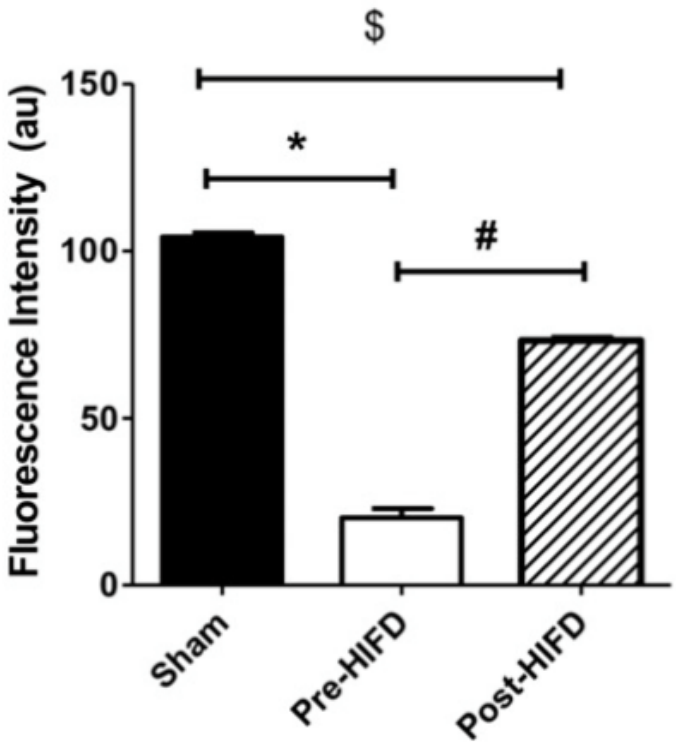

Figure 24: Permeability Changes in Response to Hydrodynamic Isotonic Fluid Delivery. The average mean fluorescence intensity was calculated from 10 ROI from three separate experiments for sham, pre-HIFD and post-HIFD. *,#,$ p value <0.05 for sham versus post-HIFD ($), sham versus pre-HIFD(*), and pre-HIFD versus post-HIFD (#).

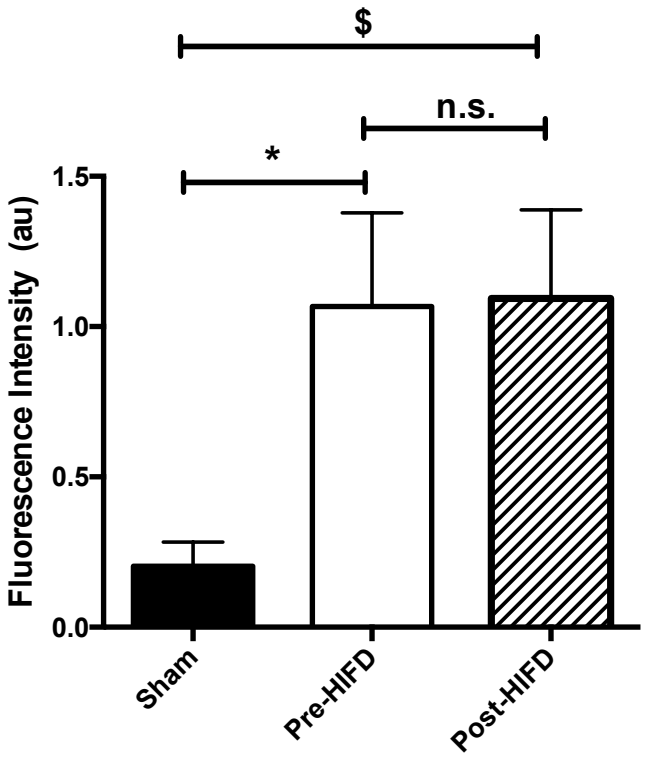

Figure 25: Analysis of Interstitial Vascular Leakage. Analysis of permeability changes in interstitial space as a percentage of tubular fluorescence in response to Hydrodynamic Isotonic Fluid Delivery. 10 ROI from three separate experiments for sham, pre-HIFD and post-HIFD were analyzed. *,#,$ p value <0.05 for sham versus post-HIFD ($), sham versus pre-HIFD(*).

3.4 The Effects of Hydrodynamic Isotonic Fluid Delivery on Infiltrating Mononuclear Cells

To better understand the role of inflammatory cells in IRI, we analyzed mononuclear cell populations 48 hours following injury by fluorescence activated cell sorting (FACS). Following injury, we noticed increases in CD4+, CD8+, B, CD4+17+, CD8+17+, and DC/Macrophage populations compared to control uninjured animals. The effects of hydrodynamic isotonic fluid delivery on mononuclear cells was astounding as we noticed significant reductions on all previously mentioned cell populations compared to vena cava control injections (Figure 26). hydrodynamic isotonic fluid delivery following IRI reduces the number of infiltrating mononuclear cells thereby preventing increases in vascular congestion and inflammation associated with IRI (Figure 27) (Table 5).

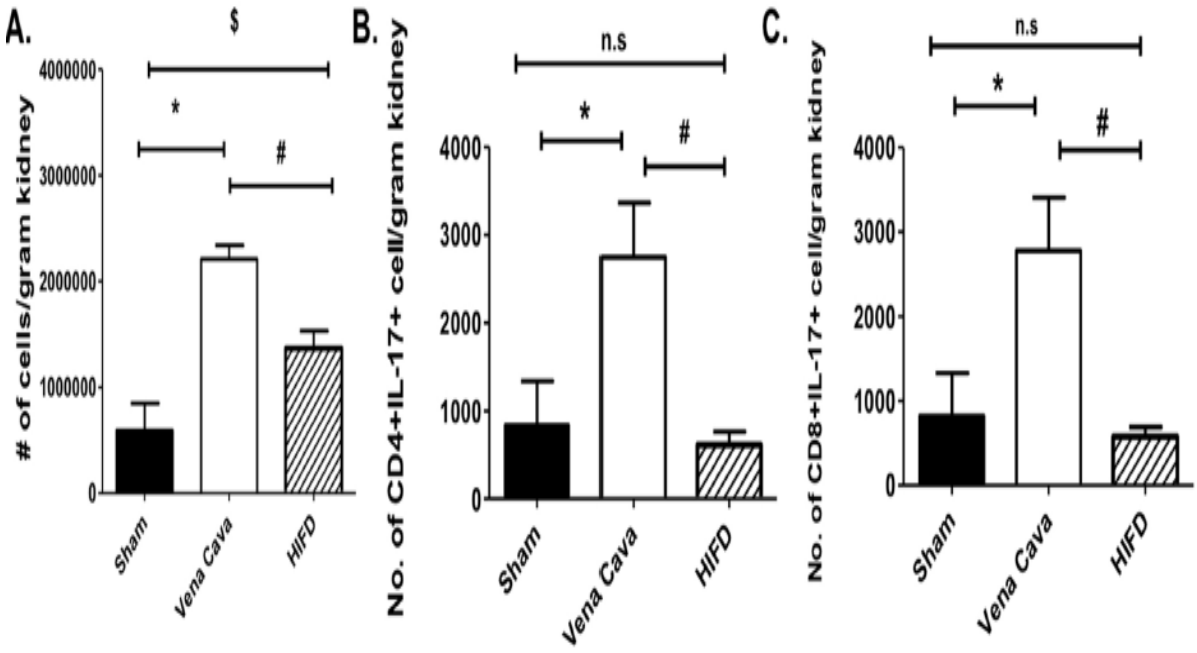

Figure 26: Effects of Hydrodynamic Isotonic Fluid Delivery on Infiltrating Mononuclear Cells. To determine if Hydrodynamic Isotonic Fluid Delivery reduced the number of infiltrating mononuclear cells, kidneys from sham, IRI plus vena cava injection, and IRI plus Hydrodynamic Isotonic Fluid Delivery were isolated for FACS analysis. (A) The total number of infiltrating cells in the kidney. (B) IL $17^{+}CD4^{+}$, (C) $IL17^{+}CD8^{+}$. Data depicts the mean number of cells per gram kidney. *,#,$ p value <0.05 for sham versus post-HIFD ($), sham versus pre-HIFD(*), and pre-HIFD versus post-HIFD (#).

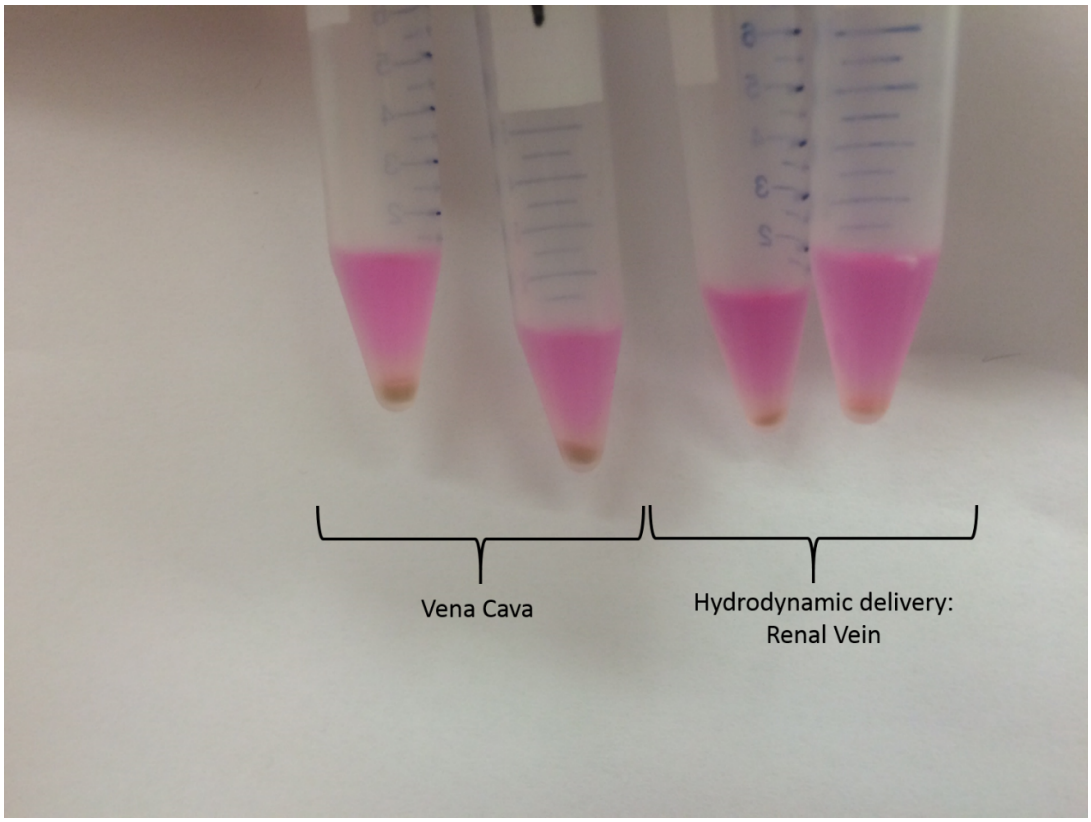

Figure 27: Renal Vein Hydrodynamic Isotonic Fluid Delivery Reduces Total Infiltrating Cell Number. Hydrodynamic Isotonic Fluid Delivery reduces the size of the cell pellet (from whole kidney) compared to vena cava injections.

Table 5: The Effect of Hydrodynamic Isotonic Fluid Delivery on Infiltrating Mononuclear Cells.

Cell Type	Treatment		
	Sham	Vena Cava	HIFD
CD4+	6272±3839	21,101±4198[a]	9987±2964[b]
CD8+	5097±4506	15,444±2637[a]	8474±1468[b]
B cells	2351±1510	5743±1609	2868±880[b]
DC/Macs	12,695±5433	34,684±7758	21,495±3880[b]
CD4+IL-4+ (Th1)	161±58	280±52.8	200±50
CD4+IFN-γ+ (Th2)	277±82	1301±667	399±113
% CD4+Foxp3+	0.7±0.01	0.405±0.04	0.72±0.08[b]
% CD8+Foxp3	0.35±0.1	0.15±0.02[a]	0.29±0.06

[a]p< 0.05 sham versus IRI + a vena cava. [b]p<0.05 in IRI + vena cava versus IRI +HIFD

3.5 Hydrodynamic Isotonic Fluid Delivery: From Bench to Bedside

A critique of hydrodynamic isotonic fluid delivery is the presence of an arterial clamp. In a clinical setting, clamping the renal artery is not ideal and unlikely to be practiced. To determine if hydrodynamic isotonic fluid delivery is translatable to the clinic, we repeated our experiments in the absence of an arterial clamp, leaving only the renal vein clamped. We observed similar reductions in SCr following hydrodynamic isotonic fluid delivery compared to vena cava injected animals (28A). In addition to reductions in SCr, we also observed similar decreases in CD4+, CD8+, B, CD4+17+, CD8+17+, and DC/Macrophage populations compared to vena cava injected controls (28B-F). Finally, our blood flow analysis indicated increases in RBC velocity similar to the increases seen when the arterial clamp was applied (28G). In its entirety, Figure 28 indicates that the arterial clamp has no measurable effect on the hydrodynamic isotonic fluid delivery process and that hydrodynamic isotonic fluid delivery has the potential to reduce vascular congestion, increase RBC velocity following IRI, and reduce the inflammatory effect typically seen following injury.

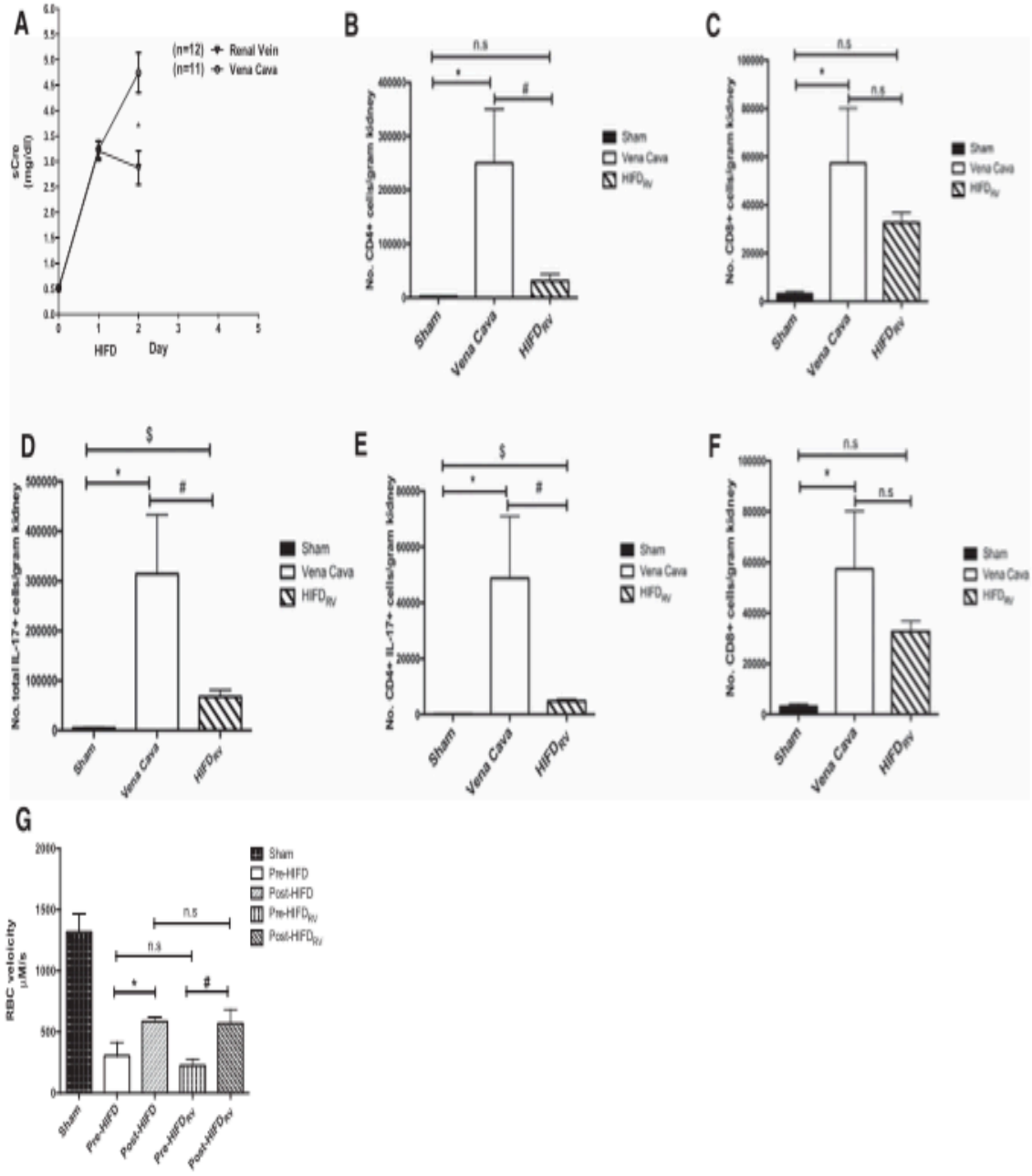

Figure 28: Hydrodynamic Isotonic Fluid Delivery Improves Renal Function Regardless of Arterial Clamping. This figure illustrates Hydrodynamic Isotonic Fluid Delivery is translatable to the clinic. $HIFD_{RV}$ only sees similar reductions in SCr at two-days post IRI compared to vena cava injected animals (A). There are also decreases in infiltrating mononuclear cells compared to vena cava injected animals (B-E), and decreases in total number of infiltrating cells compared to vena cava injected animals (F). Finally, $HIFD_{RV}$ improves RBC velocity similar to the results from figure 22. *,#,$ p value <0.05 for sham versus post-HIFD ($), sham versus pre-HIFD(*), and pre-HIFD versus post-HIFD (#).

3.6 The Effects of Hydrodynamic Isotonic Fluid Delivery on Mitochondria

The effects of hydrodynamic isotonic fluid delivery as a potential therapeutic for AKI cannot be ignored. We have demonstrated that hydrodynamic isotonic fluid delivery following IRI has the potential to increase GFR and urine output leading to reductions in SCr. We were able to demonstrate that the potential mechanism of these reductions was related to decreases in vascular congestion and mononuclear cell infiltration allowing increases in renal blood flow. As a next step, I decided to analyze the effect of hydrodynamic isotonic fluid delivery on mitochondria membrane potential. Following injury, mitochondria activity changes leading to a reduction in oxidative phosphorylation and membrane potential allowing increases in reactive oxygen species and potential activation of apoptotic pathways. To determine if hydrodynamic isotonic fluid delivery has the potential to increase mitochondria activity and promote cell survival following injury, TMRM was injected via the tail vein 24 hours after IRI and intravital imaging of renal mitochondria occurred pre-and post-HIFD. 24 hours after injury, mitochondria membrane potential was low indicating low levels of mitochondria activity. Following hydrodynamic isotonic fluid delivery, mitochondria membrane potential improves suggesting increases in mitochondria activity (Figure 29). Fluorescent quantification of mitochondria membrane potential indicated that hydrodynamic isotonic fluid delivery leads to a three-fold increase in mitochondria activity (Figure 30). Increases in mitochondria membrane potential following hydrodynamic isotonic fluid delivery indicate another mechanism in disease reversal. As previously mentioned, the increase in potential was linked to an increase in oxidative phosphorylation, alleviation of ROS typically seen following ischemia, and prevention of cell death cascades (62)-(67).

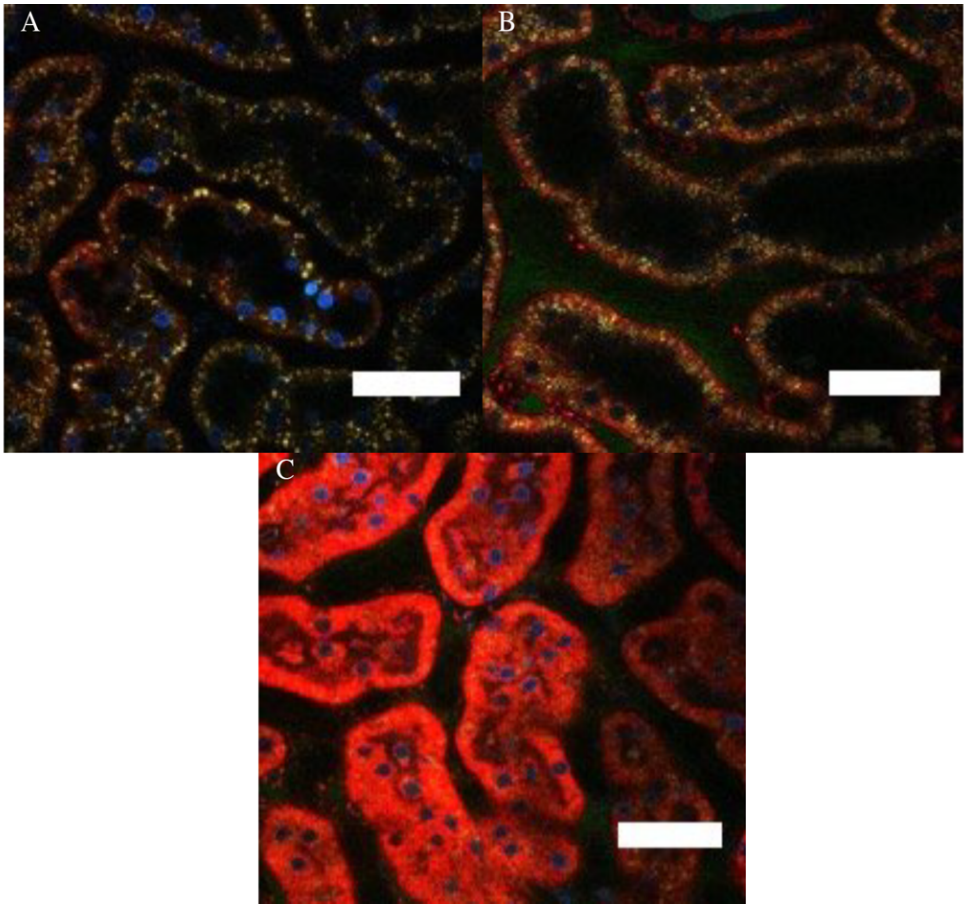

Figure 29: The Effects of Hydrodynamic Isotonic Fluid Delivery on Mitochondria Membrane Potential. To analyze mitochondria membrane potential following AKI, animals were subjected to an ischemic injury. A) Membrane potential in a sham animal, B) 24-hours post-injury and pre-HIFD, and C) 24-hour post-injury and 30 minutes post-HIFD.

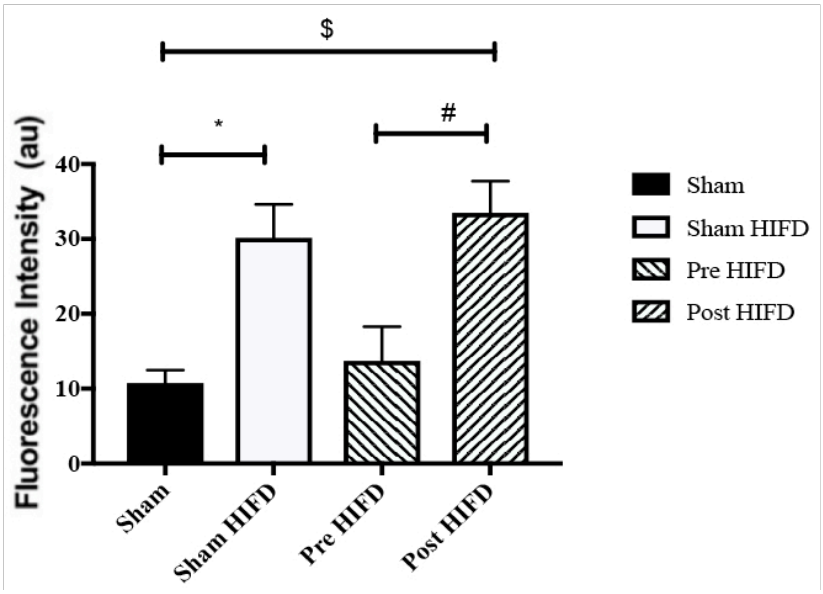

Figure 30: Quantification of the Effects of Hydrodynamic Isotonic Fluid Delivery on Mitochondria Membrane Potential. N of three animals per group. Hydrodynamic Isotonic Fluid Delivery increases mitochondria membrane potential 24 hours following injury. The average mean TMRM fluorescence intensity was calculated from 10 ROI from three separate experiments for each group. *,#,$ p value <0.05 for sham versus post-HIFD ($), sham versus sham-HIFD(*), and pre-HIFD versus post-HIFD (#).

CHAPTER 4: PREVENTION OF AKI BY MIMICKING ISCHEMIC PRECONDITIONING

Paper: **Kolb** *et al.,* Exogenous Gene Transmission of Isocitrate Dehydrogenase-II Mimics Late Window Ischemic Preconditioning Protection

4.1 Hydrodynamic Delivery does not Damage Renal Mitochondria

Hydrodynamic delivery is a useful tool in the reversal of AKI (Chapter 3). Collett *et al* were able to demonstrate that hydrodynamic isotonic fluid delivery increased vascular perfusion and blood flow by reducing vascular congestion and number of infiltrating mononuclear cells (1). Corridon *et al* have also shown that hydrodynamic delivery is capable of delivering macromolecules to the kidney (22). As mentioned previously, mitochondria are a target of AKI. We set out to determine if gene delivery to mitochondria was possible employing this technique, and if so, how this protection is established.

Prior to conducting gene delivery experiments, we analyzed effects of the high-pressure forces of hydrodynamic delivery on mitochondria using electron microscopy. Normal mitochondria physiology includes: ovular shape, dense matrix and parallel cristae (158). Figure 31 and 32 depict renal mitochondria from a sham animal that did not receive an injection and from a hydrodynamic isotonic fluid delivery animal. The figures indicate that the pressure forces generated by the injection did not change morphology of mitochondria (Figure 31 and 32).

Figure 31: Electron Micrograph of Sham Animals That Did Not Receive Renal Vein Injections have normal appearing mitochondria (arrows).

Figure 32: EM Image of Renal Mitochondria Following Hydrodynamic Delivery. Mitochondria (arrows) physiology appears normal.

4.2 Proteomic Analysis of IPC

IPC was induced by subjecting rats to bilateral renal IRI for 30 minutes followed by recovery for 14 days, resulting in the resolution of serum creatinine back to levels in sham-operated controls. As expected, this maneuver significantly attenuated the elevation in serum creatinine in rats 24-hours following a second ischemic insult (Figure 33). Renal cortical mitochondria were isolated from IPC or sham IPC rats at 14 days and used for a proteomic screen. Table four shows the proteins that are significantly altered in IPC rat kidney versus sham IPC rat kidney. 12 proteins were significantly altered, (six increased, six decreased compared to sham IPC animals) by the 14 day IPC protocol (Table 4). Of these, IDH2 was chosen for further analysis due to its function in the TCA cycle and as a branch point enzyme for lipid and protein synthesis. To confirm these findings, we repeated the IPC protocol and conducted immune blots for IDH2 on mitochondria isolated from renal cortex, demonstrating an approximate 10-fold increase in IDH2 when compared to control rats (Figure 34).

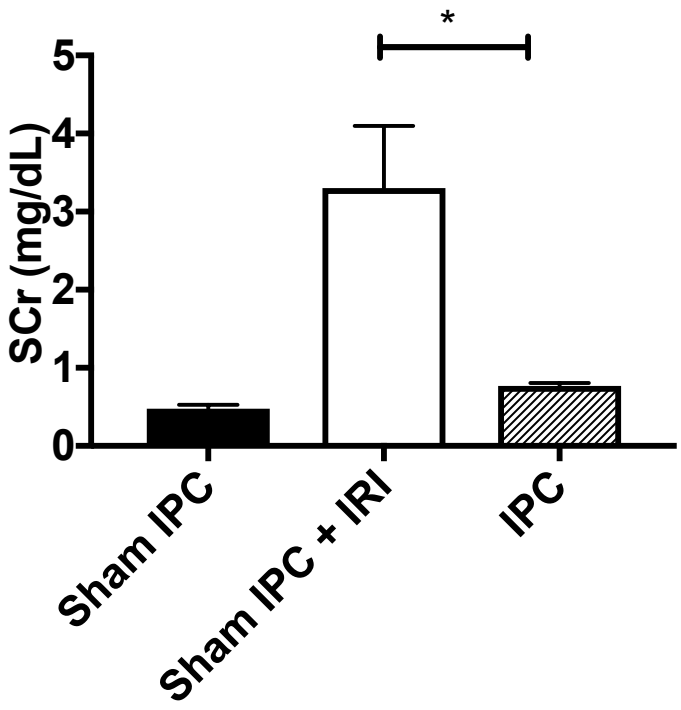

Figure 33: Analysis of the Effects of IPC on SCr. Rats were subjected to sham, sham-IPC, and IPC surgeries and subsequent IRI evaluated by SCr after 24 hours. ($p < 0.05$ Sham IPC versus IPC).

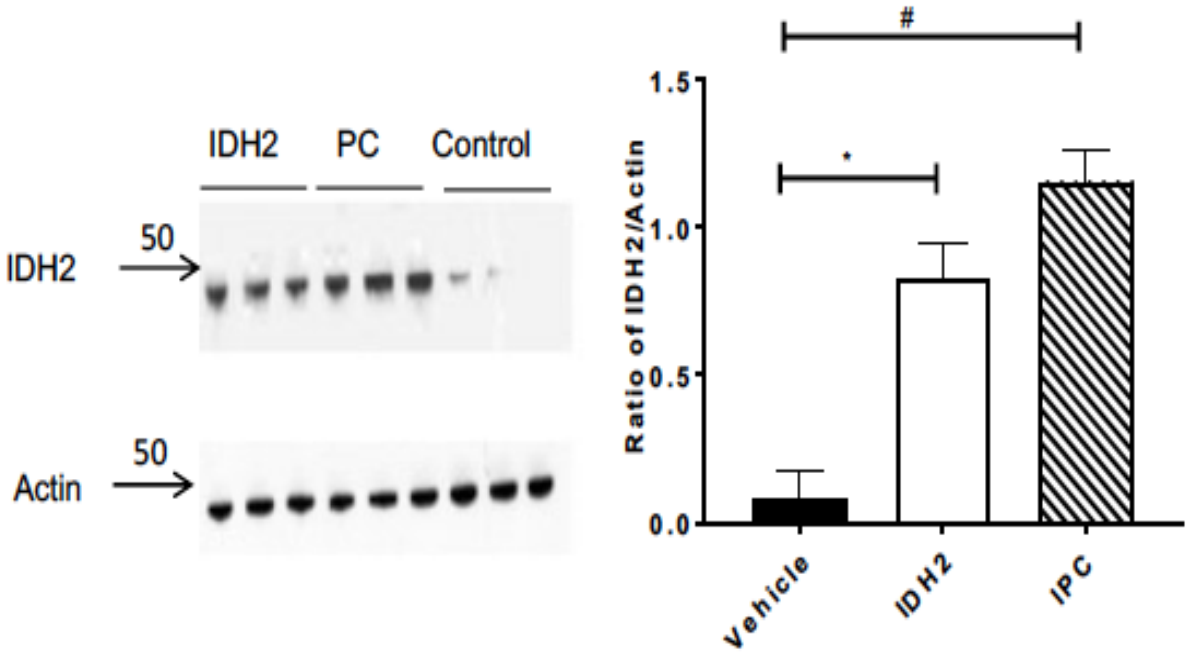

Figure 34: Gene Delivery of *IDH2* Shows Similar Levels of IDH2 as IPC. Immune blot of IDH2 in animals injected with saline, *IDH2*, or following IPC. Side panel illustrates the ratio of IDH2 to Actin using FIJI (*p <0.05 IDH2 versus vehicle; # p<0.05 IPC versus vehicle).

4.3 IDH2 Protection Against Hypoxia Injury

Initial screening of IDH2 activity utilized immortalized murine renal proximal tubule S3 cells (MPTC), which were derived from a large T antigen mouse through direct microscopic dissection and have been used in studies of acute ischemic injury and nephrotoxic kidney injury (159, 160). To confirm that exogenous *IDH2* targets mitochondria, *in vitro* transfection was performed using a N-terminal myc-tagged *IDH2*. Multi-photon imaging revealed that myc-tagged IDH2 clearly localized in mitochondria stained with Mitotracker red (Figure 35 a-e). The Manders coefficient for colocalization was 0.8, indicating a high degree of mitochondria colocalization (143). S3 cells transfected with plasmids bearing *IDH2* were resistant to necrosis following hypoxia as compared to mock transfected cells (9%±7.8% versus 42%±27.6%; $p<0.05$; Figure 36). Cells transfected with *IDH2* maintained higher intracellular ATP/AMP ratios even in response to hypoxia (Figure 37) and have elevated mitochondria membrane potential (Figure 38). These increases in membrane potential were also linked with improved cell health and survival (Figure 36; $p<0.05$; and 38).

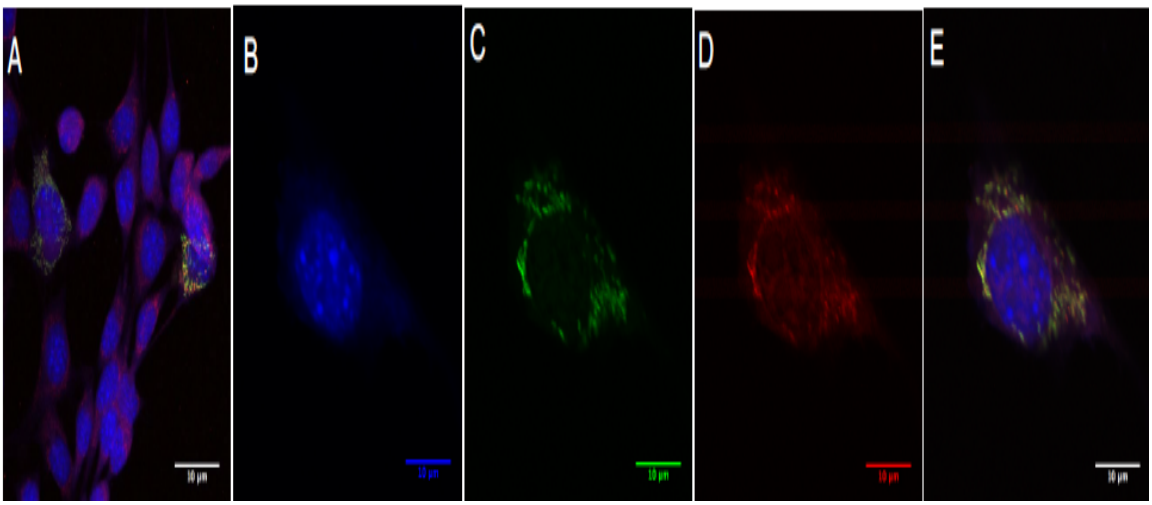

Figure 35: IDH2 Localization to the Mitochondria. IDH2 myc localization in NIH 3T3 cells. NIH 3T3 cells were transfected with N terminal myc-tagged *IDH2* (**e**) or cells not transfected (**a**). The blue channel shows Hoechest labeling (**b**), the green channel shows myc IDH2 (**c**), and the red channel shows Mitochondria (**d**).

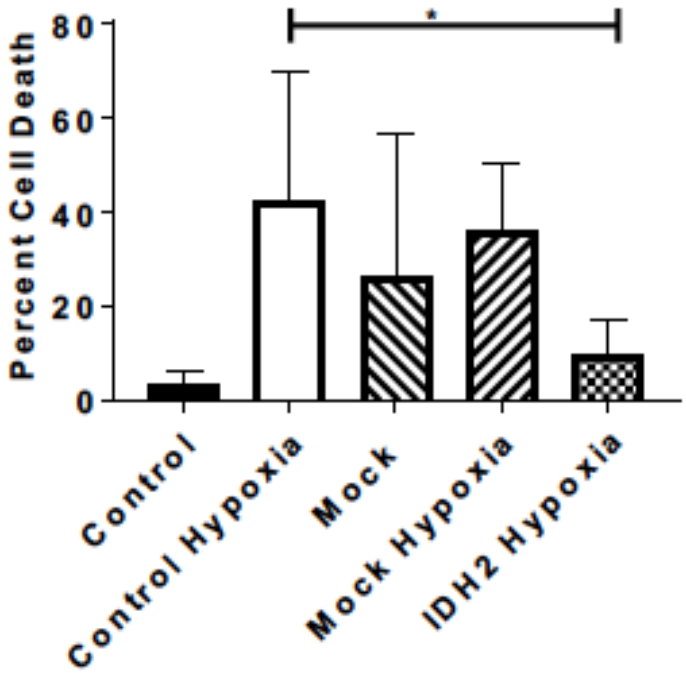

Figure 36: IDH2 Reduces Cell Death. Quantitative analysis of propidium iodide cells. Following transfection, S3 cells were subjected to 90 minutes of hypoxia in a hypoxia incubator chamber. Following hypoxia, the growth media was changed and cells were stained with 0.1 ug/ml Hoechst 33342 and 1.0 mg/ml PI for 20 minutes. IDH2 reduces cell death relative to control (*p <0.05 Hypoxic IDH2 versus Hypoxic control).

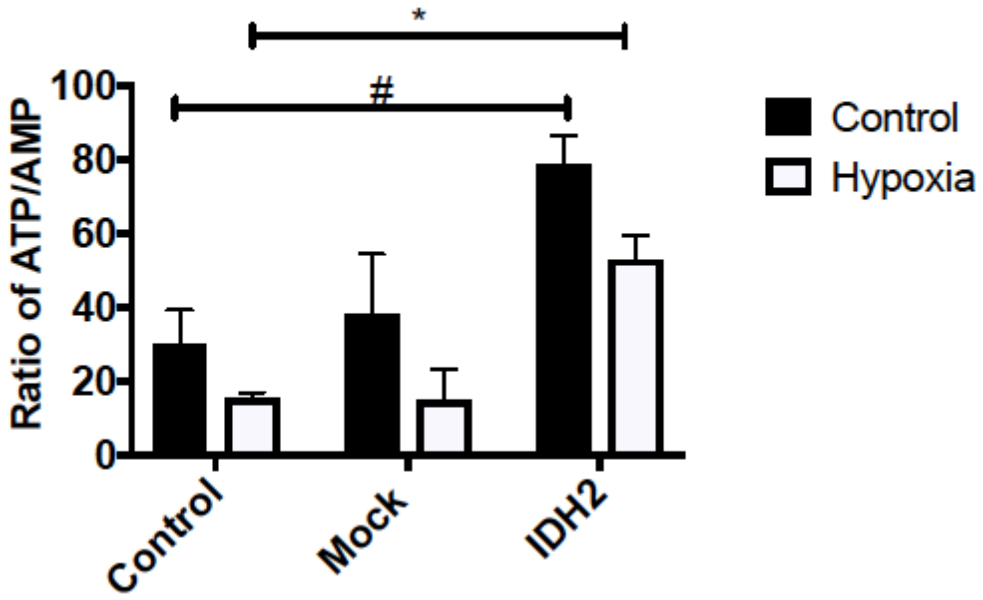

Figure 37: IDH2 Increases ATP/AMP Ratios *in vitro*. ATP/AMP ratios in MPTC S3 with or without IDH2 and hypoxia (* denotes $p<0.05$ hypoxic IDH2 versus hypoxic control; # $p<0.05$ IDH2 versus control).

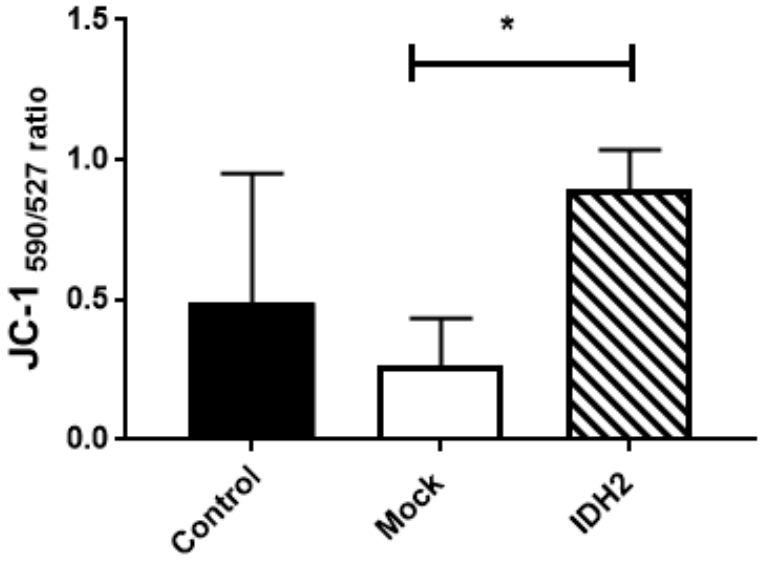

Figure 38: IDH2 Alters Mitochondria Membrane Potential. JC-1 fluorescence intensity ratios in MPTC S3 with or without *IDH2* following hypoxia increases following *IDH2* transfection (*p<0.05 Mock versus IDH2).

Figure 39 depicts the effects of *IDH2* transfection on mitochondria respiration in S3 cells. Baseline oxygen consumption rate (OCR) of MPTC S3 cells was 29.4±6.8 pmol/min/cell, while transfection with *IDH2* significantly increased the OCR to 41±2 pmol/min/cell (Figure 40). Maximal uncoupled respiratory capacity following addition of FCCP was also enhanced by *IDH2* transfection (Figure 41). Complex II OCR, evaluated following the addition of Rotenone and Antimycin A (inhibitors of Complex I and III), was also significantly increased by *IDH2* transfection (Figure 42). Our final *in vitro* analysis was to test if *IDH2* over expression affected reserve or spare respiratory capacity (SRC). This is measured as the difference between maximal respiration and baseline respiration. Normal S3 cell SRC was 23.5±8.4 pmol/min/cell. In cells transfected with *IDH2*, SRC was 31.9±11 pmol/min/cell indicating the addition of *IDH2* increased MPTC SRC (Figure 43).

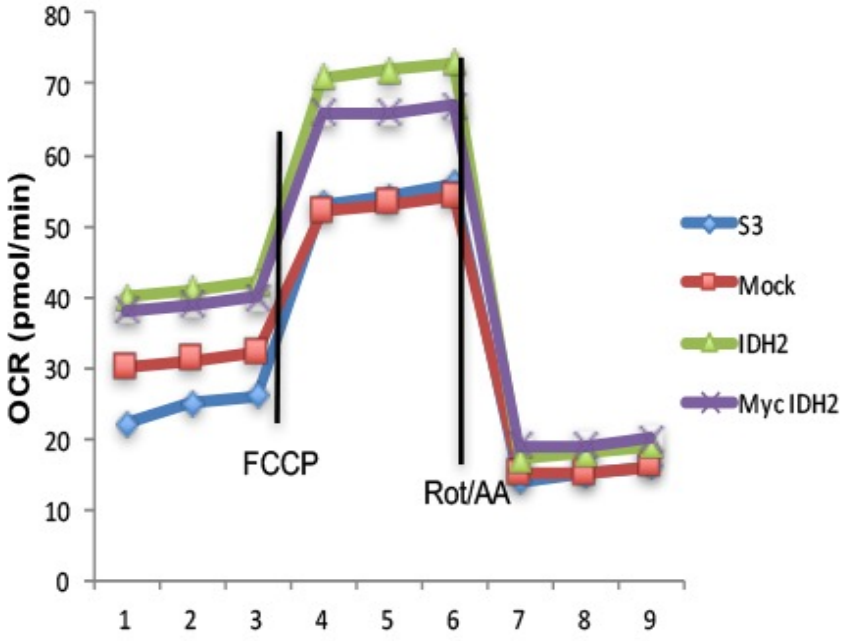

Figure 39: *In vitro* Mitochondria Respiration Analysis. Respiration was analyzed using a Seahorse. 7 µM FCCP and 6 µM Rotenone and Antimycin A were added to determine the effects of IDH2 on different respiratory states.

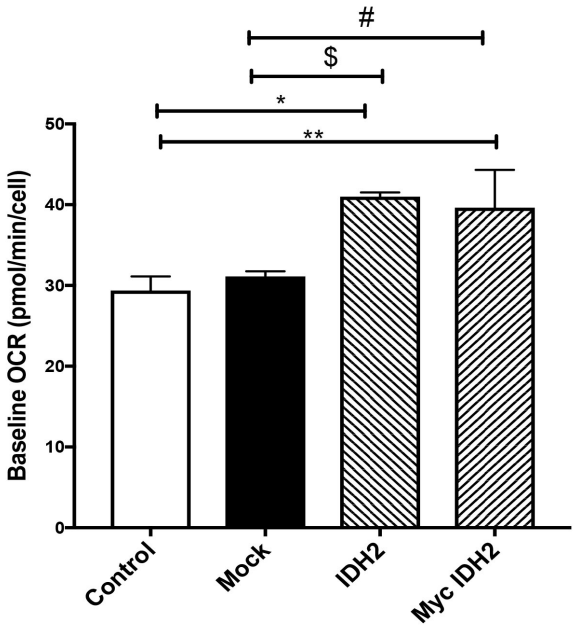

Figure 40: Baseline OCR in MPTC S3 Cells. *IDH2* transfection increases baseline OCR. (* denotes p<0.05 IDH2 versus control; # denotes p<0.05 myc IDH2 versus control; $ denotes p <0.05 myc IDH2 to mock; ** denotes p<0.05 IDH2 versus mock).

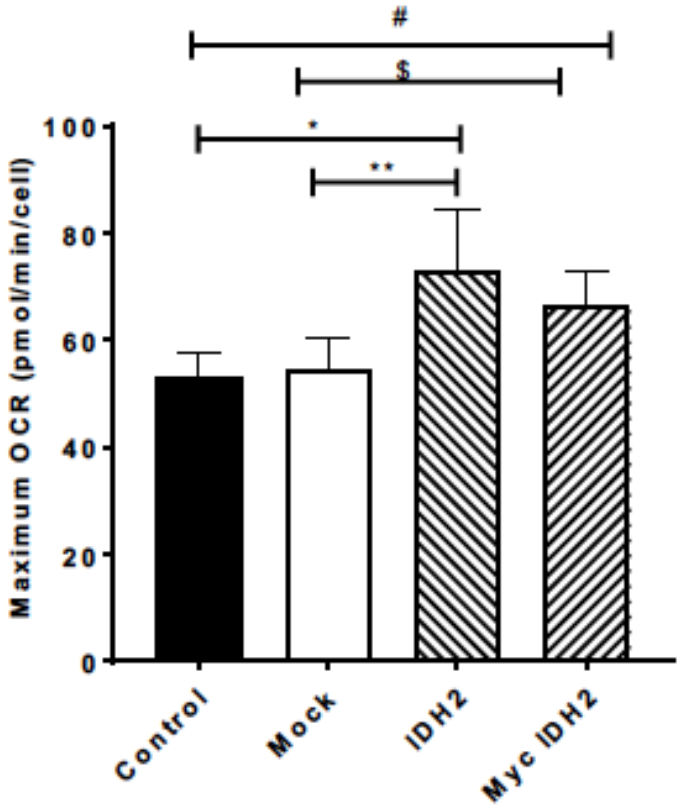

Figure 41: Maximal OCR in MPTC S3 Cells. *IDH2* transfection increases maximum OCR. (* denotes p<0.05 IDH2 versus control; # denotes p<0.05 myc IDH2 versus control; $ denotes p <0.05 myc IDH2 to mock; ** denotes p<0.05 IDH2 versus mock).

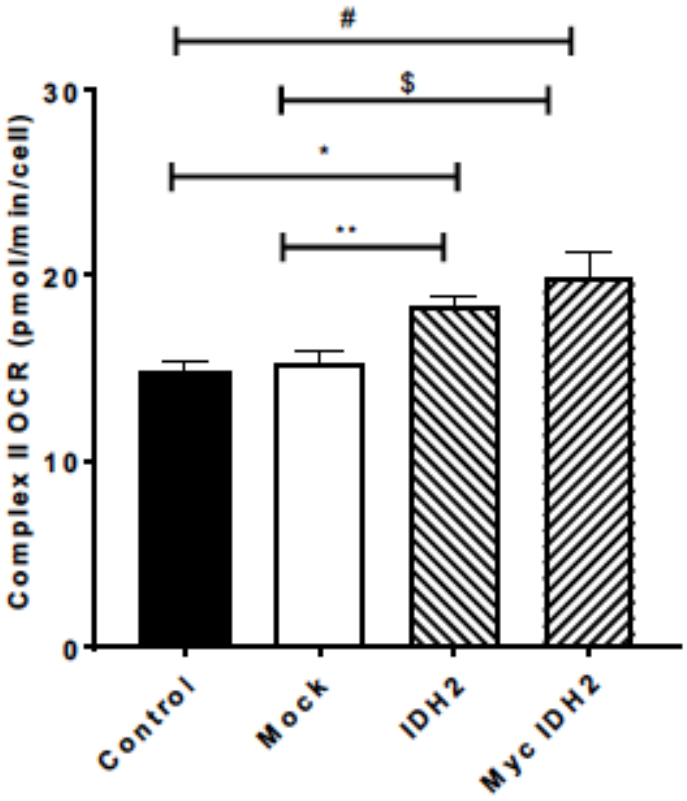

Figure 42: Complex II OCR in MPTC S3 Cells. *IDH2* transfection increases Complex II OCR. (* denotes p<0.05 IDH2 versus control; # denotes p<0.05 myc IDH2 versus control; $ denotes p <0.05 myc IDH2 to mock; ** denotes p<0.05 IDH2 versus mock).

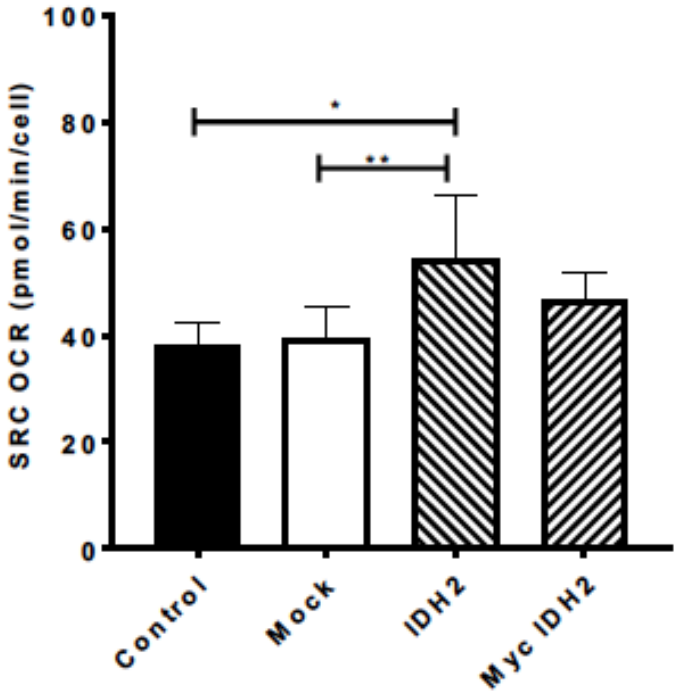

Figure 43: SRC OCR in MPTC S3 Cells. Maximal respiration minus baseline respiration was used to calculate SRC. *IDH2* transfection increases SRC OCR. (* denotes $p<0.05$ IDH2 versus control; ** denotes $p<0.05$ IDH2 versus mock).

4.4 Gene Delivered *IDH2* Targets to Mitochondria

Retrograde hydrodynamic injection of plasmid cDNA through the renal vein has been shown to be an effective means of facilitating exogenous gene expression in the rat kidney (22). To evaluate the effects of *IDH2* up-regulation in the kidney, N-terminal myc-tagged *IDH2* or saline was delivered by hydrodynamic injection. After seven days of recovery, isolated renal cortical mitochondria contained approximately three-fold higher levels of IDH2 versus animals injected with saline alone, as indicated by immune blots (Figure 44). These data indicate that hydrodynamic delivery of *IDH2* results in sustained expression of protein in proximal tubule mitochondria to levels comparable to that observed during resistance to IRI following IPC.

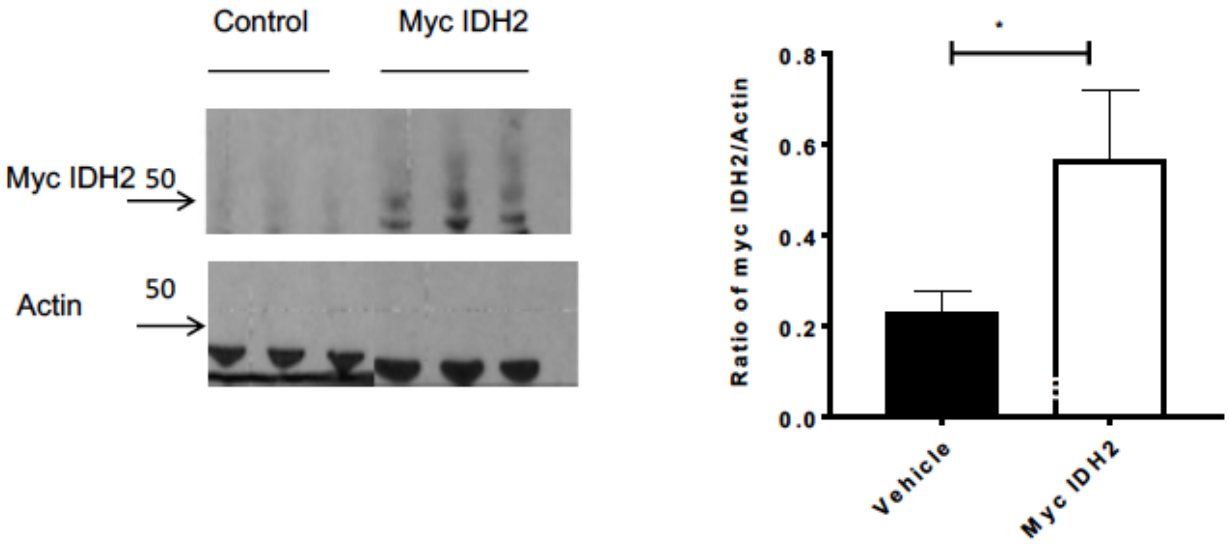

Figure 44: Myc-tagged IDH2 Localizes to the Mitochondria. Representative immune blot of protein (5 μg) from mitochondria extracts. Lanes 1-3 are saline only and lanes 4-6 are myc-tagged IDH2. Band densitometry (right panel) of ratio of myc-tagged IDH2/Actin is shown (*$p<0.05$ myc IDH2 versus vehicle).

4.5 IDH2 Mimics IPC in changing Mitochondria Membrane Potential

Since IDH2 was found to localize to mitochondria, we analyzed changes in mitochondria function in response to IRI. Mitochondria polarization was evaluated with TMRM and intravital imaging. Following two weeks of IPC (i.e. 14 days following recovery from 35 minutes of IRI), the TMRM signal from rat kidney tubules was significantly elevated relative to that observed in sham-IPC control rats (Figure 45a and d). Similarly, rats subjected to *IDH2* delivery have significantly increased TMRM signal relative to saline injected control animals (Figure 45b-c and Figure 46). To evaluate whether *IDH2* delivery *in vivo* influenced mitochondria respiration, renal cortical mitochondria were isolated and analyzed using oximetry. Respiration was measured in response to isocitrate, pyruvate, and succinate to evaluate complex I and II activity. Mitochondria isolated from *IDH2* treated animals showed increased state II and state III respiration relative to saline injected animals, regardless of the substrate utilized (Figure 47). A potential mechanism for increased membrane potential was increases in reduction potential and reduction potential stores. We analyzed NAD(P)H levels using FLIM and found minimal changes in these reduction potential stores (Figure 48 and 49). Indicating the importance of maintaining cellular reduction pool ratios.

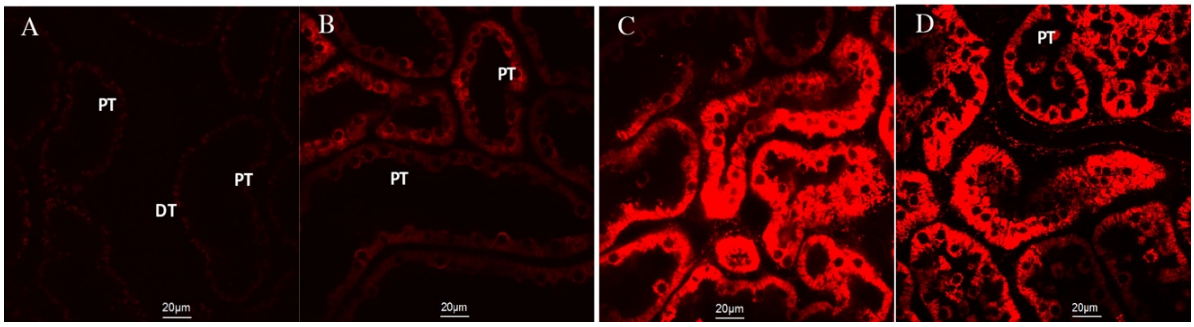

Figure 45: Mitochondria Membrane Potential Following Gene Delivery and IPC. TMRM labeled mitochondria by intravital microscopy in sham rats (**a**), rats after injection of saline(**b**), *IDH2* (**c**) or following IPC (**d**).

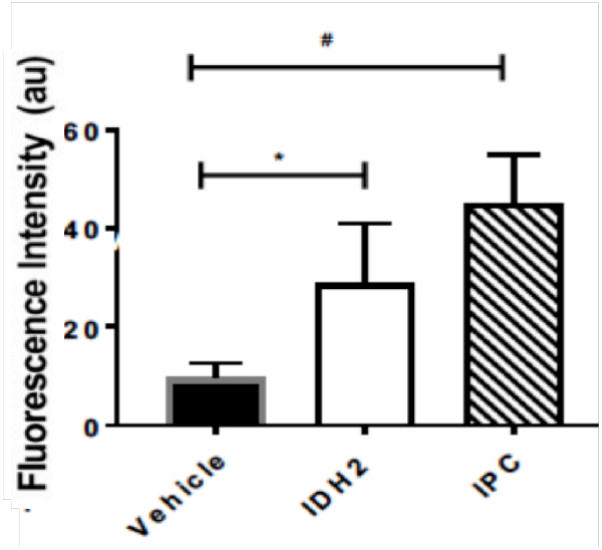

Figure 46: Quantification of TMRM Intensities. Intensities from Figure 44 a-d were averaged giving a mean TMRM intensity value (n=50 tubules per rat; three rats per group; *p <0.05 IDH2 versus vehicle # p <0.05 IPC versus vehicle).

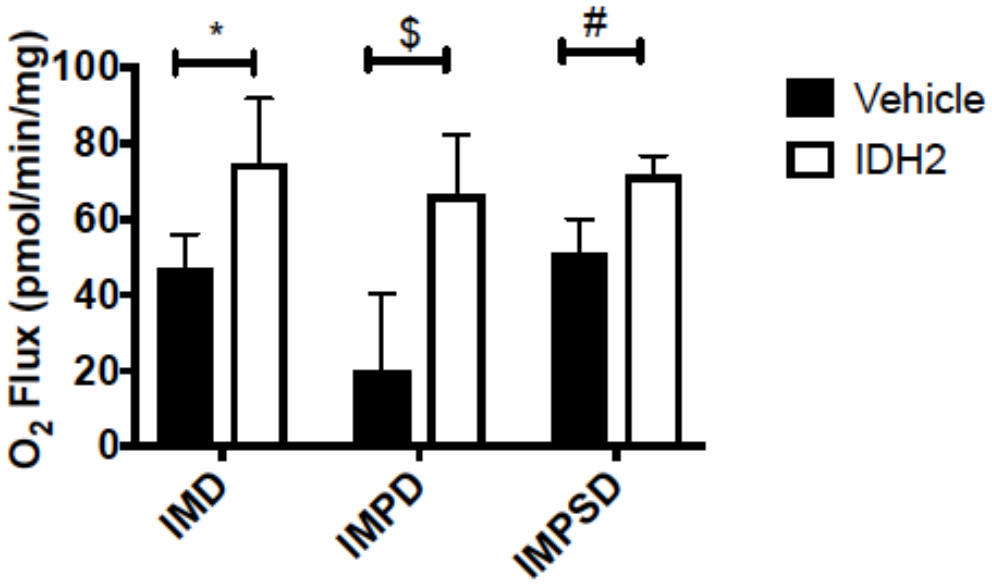

Figure 47: Mitochondrial oximetry from Isolated Renal Mitochondria. Respiration of isolated renal mitochondria one week after saline or *IDH2* injections. Oxygen flux was assayed following addition of: Isocitrate (I), Malate (M), Pyruvate (P), Succinate (S), and ADP (D)(n=3/group). (IMD- Isocitrate, Malate and ADP; * p <0.05 IDH2 versus vehicle) (IMPD-Isocitrate, Malate, Pyruvate and ADP; # p <0.05 IDH2 versus vehicle) (IMPSD-Isocitrate, Malate, Pyruvate, Succinate and ADP; $ p <0.05 IDH2 versus vehicle).

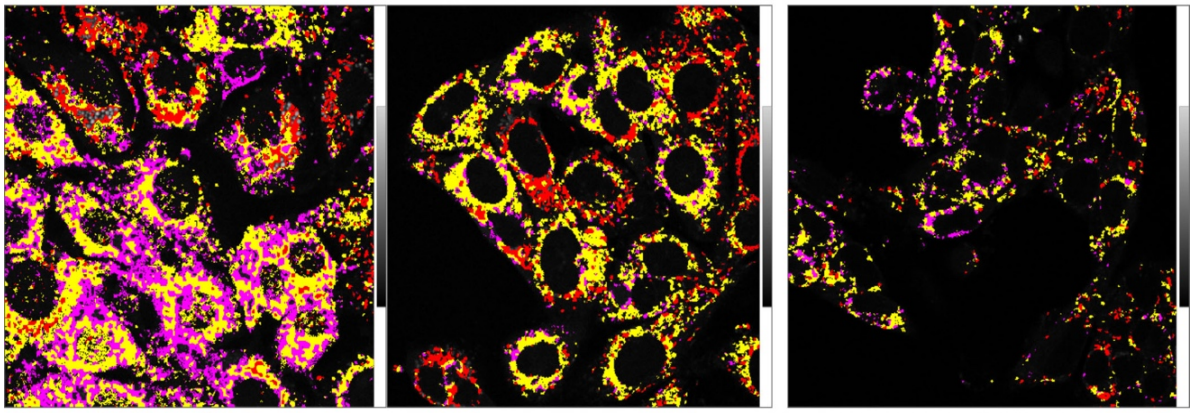

Figure 48: FLIM of NAD(P)H. Transfection with *IDH2* causes minimal change in the reduction potential. Colors indicate different regions of interest on the phasor plot in Figure 49.

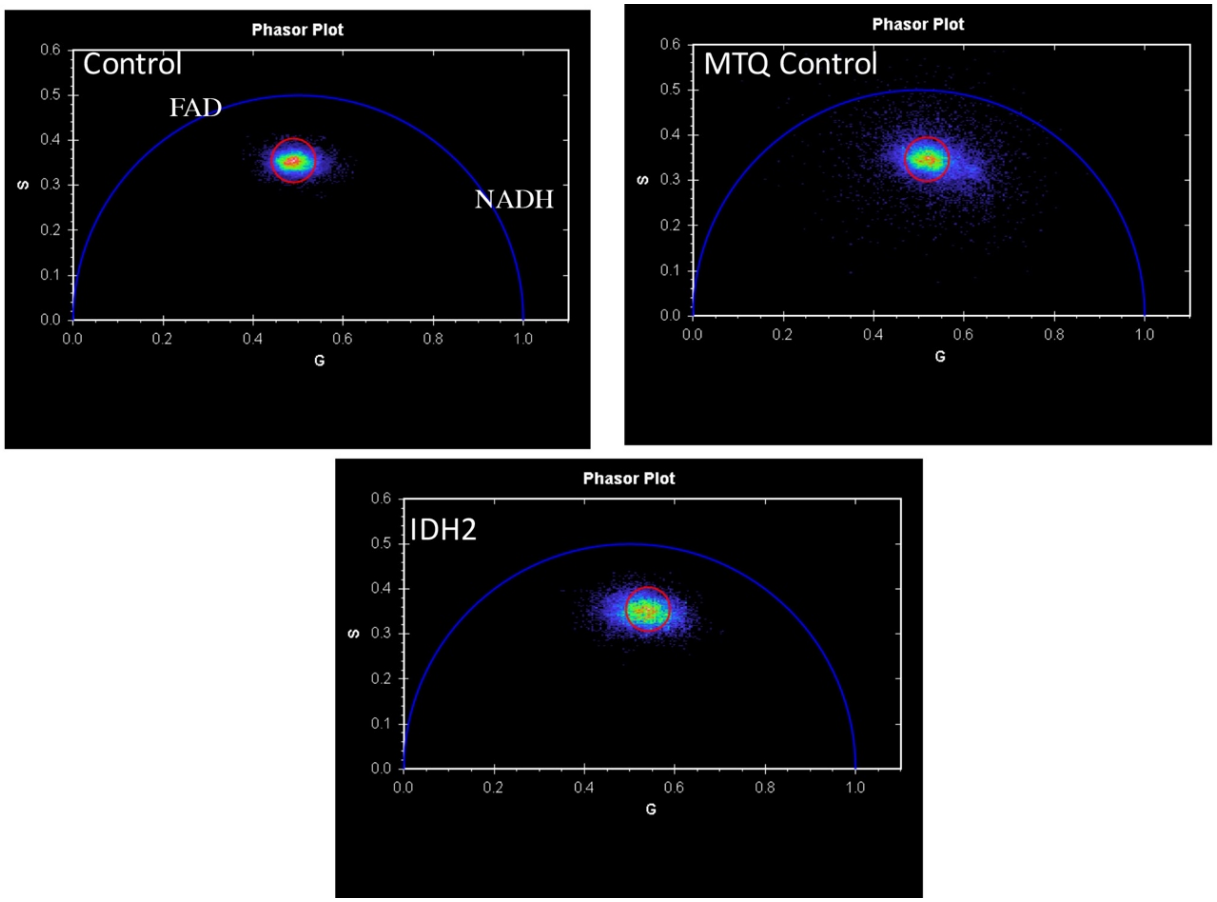

Figure 49: FLIM Phasor Plot. Plot shows minimal changes in reduction potential stores. Shifts toward zero indicate increased FAD, while shifts toward one indicate increased NADH. Gene transfection does not increase reduction potential and there is no statistical difference between groups.

4.6 IDH2 Increases Oxidative Phosphorylation and Prevents Tissue Injury

To determine if *IDH2* delivery mimics IPC, we subjected rats to either IPC or *IDH2* delivery and allowed them to recover. As expected, IPC treated rats were resistant to IRI as indicated by reduced serum creatinine 24 hours following IRI, relative to sham IPC. Interestingly, *IDH2* resulted in a similar reduction in SCr (Figure 50) and improved tissue histology in response to IRI (Figure 51 and 52). Analysis of mitochondria 60 minutes following reperfusion demonstrated that IDH2 preserved respiratory capacity relative to vehicle controls (Figure 53). Finally, IPC and *IDH2* delivery both increased ATP levels versus sham and saline injected control animals indicating IDH2 enhances ATP stores, thereby protecting against IRI (Figure 54).

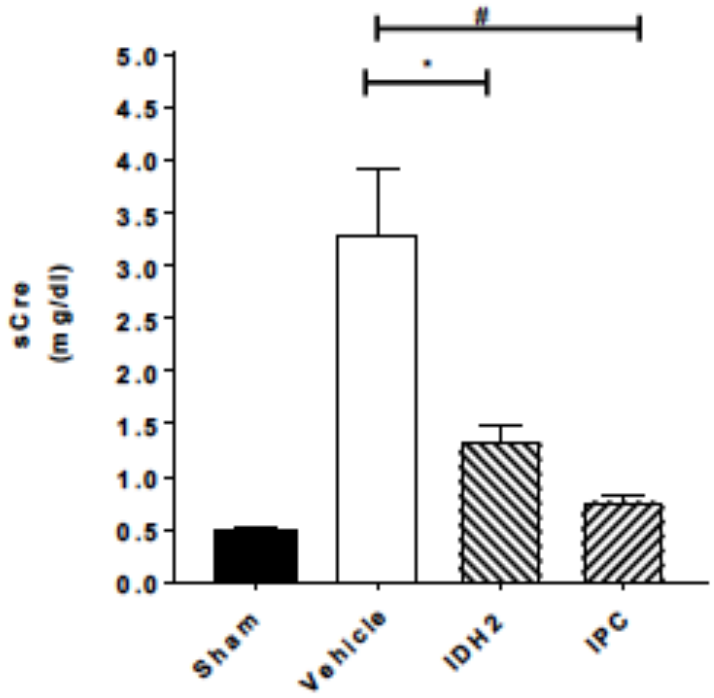

Figure 50: IDH2 Mimics IPC and Blunts SCr Increase. Comparison of SCr following IPC or *IDH2* delivery 24 hours following IRI (*p < 0.05 IDH2 versus vehicle; #p < 0.05 IPC versus vehicle).

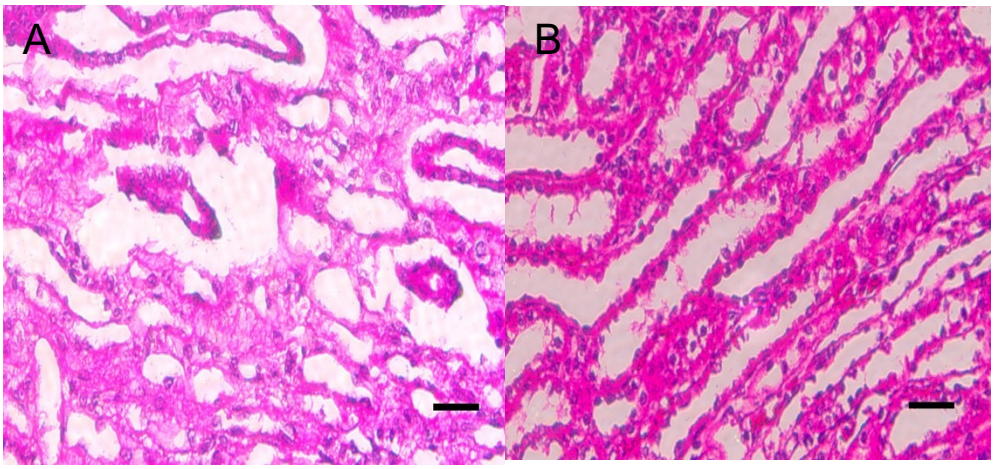

Figure 51: Tissue Histology Detailing the Effects of IDH2 on Injury Prevention. Hematoxylin and Eosin stained section of renal outer medulla following IRI in rats treated with saline **(a)** or *IDH2* injection **(b)** is shown.

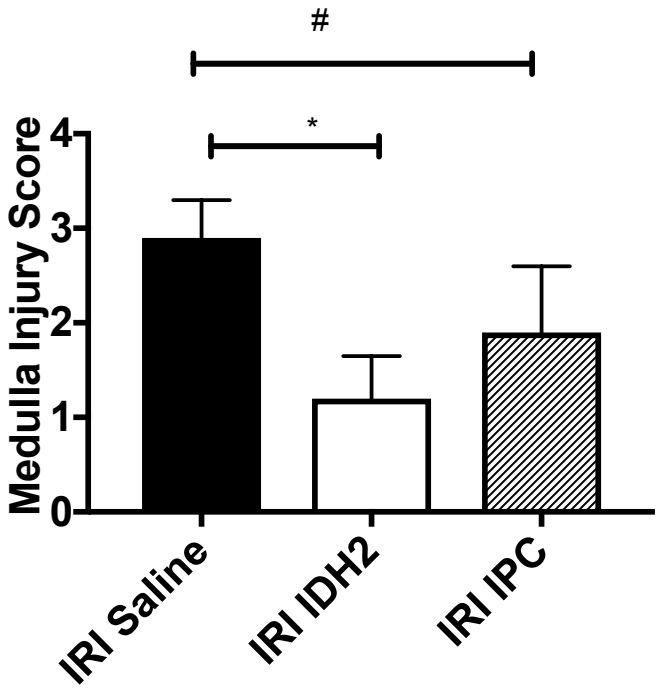

Figure 52: Quantitation of Tissue Histology. Corresponding injury scoring for Figure 48 (# p<0.05 IRI IPC versus IRI Saline; *p<0.05 IRI IDH2 versus IRI saline).

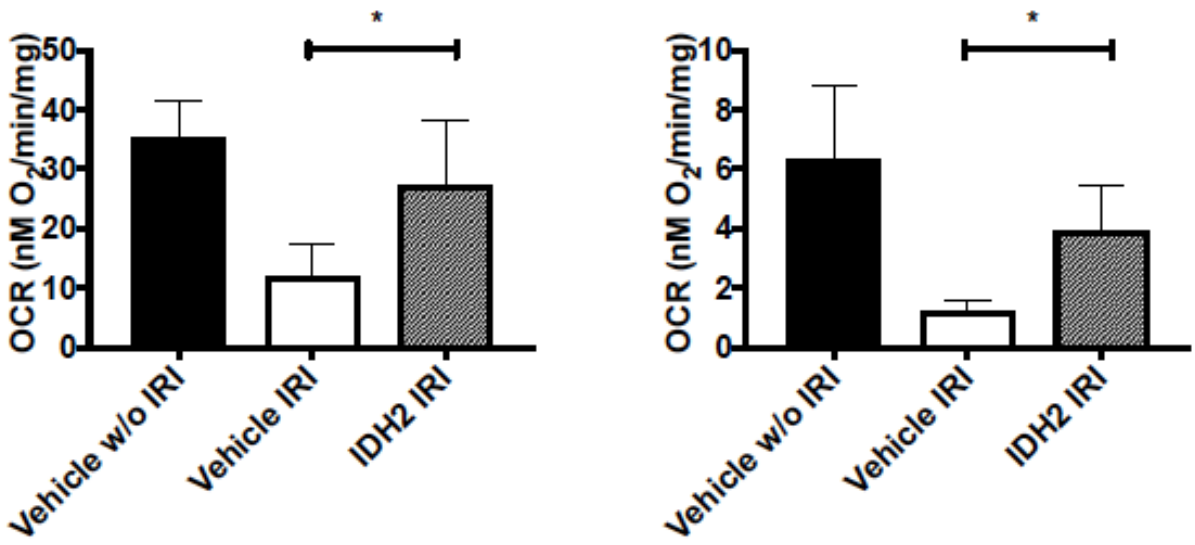

Figure 53: The Protective Effects of IDH2 on Mitochondria Oximetry. Mitochondria respiration one hour following IRI in vehicle or *IDH2* treated rats is shown with pyruvate (A) or succinate (**B**) as a substrate (A-B; n=4 per group; * $p<0.05$ IDH2 IRI versus vehicle IRI).

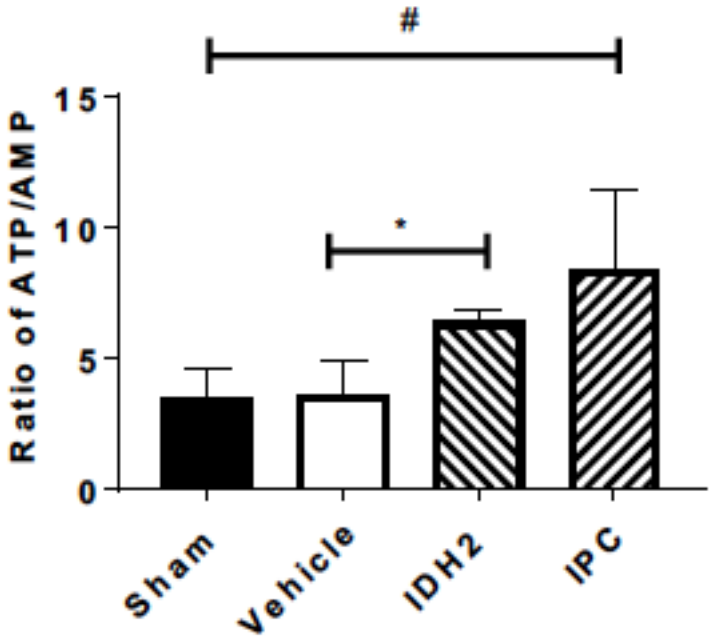

Figure 54: Analysis of IDH2 on ATP/AMP Ratio *in vivo.* Renal ATP/AMP ratio is shown in sham, vehicle, IDH2, and IPC treated rats. (*$p < 0.05$ IDH2 versus vehicle; #$p < 0.05$ IPC versus sham).

CHAPTER 5: ADDITIONAL STUDIES

5.1 Analysis of Epithelial Tight Junction Proteins Following Ischemia

5.1.1 Abstract

Tight junction proteins are critical regulators of cell leak and membrane polarity. Ischemic injuries to tight junctions decrease the cells' ability to maintain this control, leading to increases in the leak state and decreases in membrane polarity. However, our *in vivo* data indicates ischemia increases the rate of tight junction turnover compared to pre-ischemic tight junctions. To test the mobility of tight junctions, adenoviral GFP occludin was hydrodynamically delivered through the renal vein. Four days later the kidney was exposed for intravital microscopy and labeled tight junctions were selected for FRAP. FRAP was conducted on both pre-and post-ischemic tight junctions and on control regions. Cells were treated with 0 μM H_2O_2, 55 μM H_2O_2 or 110 μM H_2O_2 for 2 hours at 37^o C before FRAP. Control cells treated with 0 μM H_2O_2 have an immobility of 43% ± 14% with a half-life of 68.2 ±17.3 seconds. Cells treated with 55 μM H_2O_2 have an immobility of 32% ±16% with a half-life of 88.5 ±23.7 seconds. Cells treated with 110 μM H_2O_2 have an immobility of 37% ±15% with a half-life of 82.3 ±21.03 seconds. For our animal model, tight junction or non-tight junction regions of the apical membrane were selected for FRAP. The immobility of pre-ischemic tight junctions is 93% ±9%. The immobility of ischemic tight junctions is 34% ±24%. The average half-life recovery of ischemic tight junctions is 23.13 ±1.07 seconds. The pre-ischemic tight junctions show

minimal recovery at 180 seconds following FRAP. Results are statistically significant with a p value <0.05.

5.1.2 Background

Tight junctions are located on apical surfaces of adjoining cells. They are composed of various proteins such as occludin, claudin, and cingulin. The primary responsibility of these junctions is to regulate the movement of ions, solutes, and other molecules around the cell, establishing a paracellular permeability layer. Construction of this permeability layer by tight junctions establishes two diffusion pathways: the pore and leak pathway. The pore pathway allows the diffusion of small solutes at high capacity, while the leak pathway allows the diffusion of large solutes at low capacity (161). The role of paracellular permeability has been well characterized in disease, including kidney disease (162). It is believed that occludin is a regulator of paracellular permeability and thus a target of renal disease triggered by ischemic injuries. Ischemic injury to tight junctions increases paracellular leak and degradation of tight junctions. To study the importance of tight junction proteins *in vitro,* we used increasing concentrations of H_2O_2, seen to increase during ischemia contributing to decreased paraceullular permeability and enhanced ischemic injury, to induce ischemia (163, 164). We used FRAP, or fluorescence recovery after photobleaching, to analyze the movement of occludin (labeled with GFP) into tight junctions. To study these effects *in vivo,* animals were injected with the same occludin constructs through the renal vein and FRAP was used to analyze occludin movement before and after ischemia.

5.1.3 FRAP Analysis of MDCK Tight Junctions

To determine occludin mobility *in vitro,* MDCK cells were transfected with GFP occludin, occludin 840 truncation GFP, and occludin ZO-1 binding domain deletion GFP. These cells were then exposed to increasing concentrations of H_2O_2 and underwent FRAP. Cells transfected with occludin GFP have increased immobility compared to cells transfected with the other constructs and decreased immobility with increasing H_2O_2 concentrations (Figure 55). Analysis of half-life indicated that increasing concentrations of H_2O_2 decrease the time it takes for these proteins to move into tight junctions (Figure 56). These data point to ischemia slowing the movement of the occludin proteins into tight junctions.

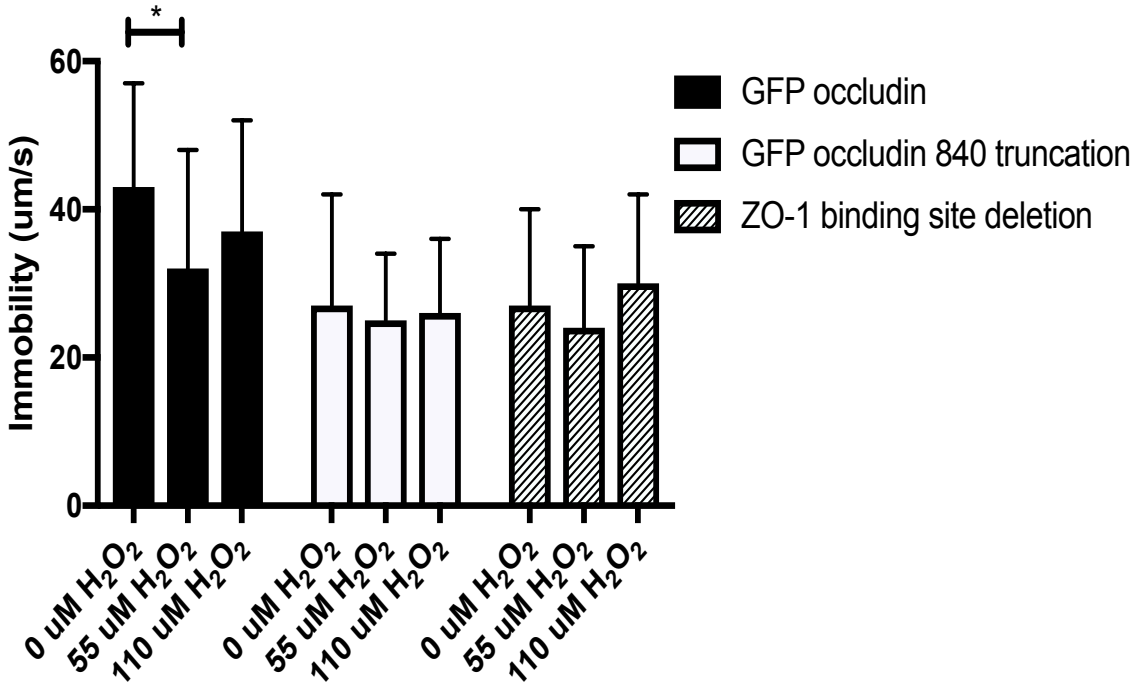

Figure 55: Analysis of Immobility of Occludin in MDCK Cells in Response to Injury. Cells were transfected with either GFP occludin, occludin 840 truncation, or ZO-1 binding site deletion and exposed to increasing concentrations of H_2O_2 (* $p<0.05$ 0 uM versus 55uM GFP occludin).

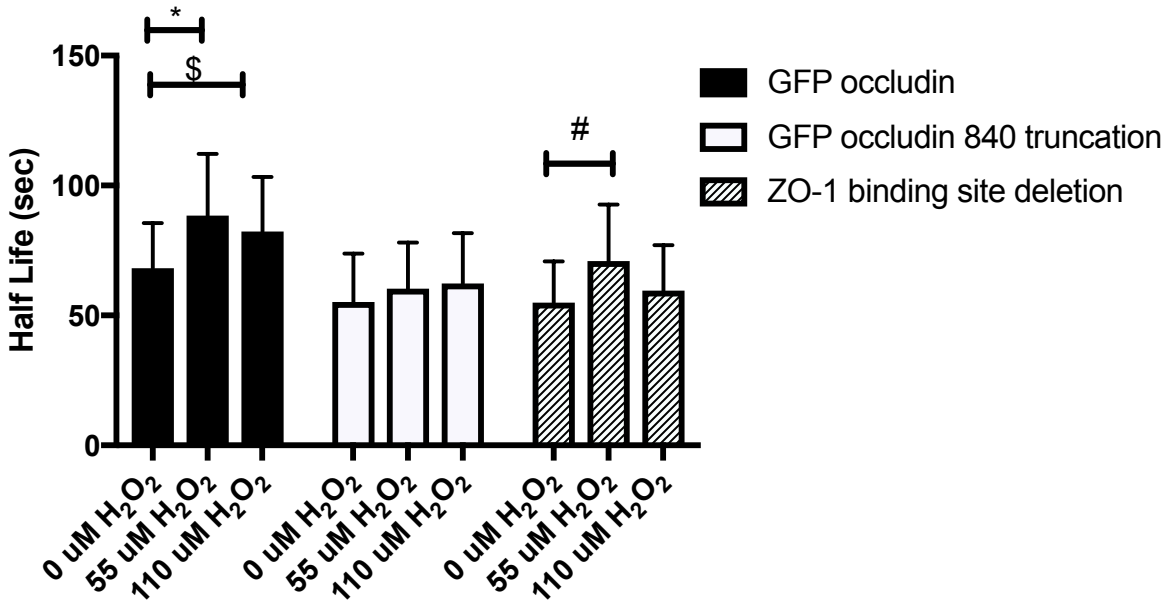

Figure 56: Analysis of Occludin Half-Life in Response to Injury. Cells were transfected with either GFP occludin, occludin 840 truncation, or ZO-1 binding site deletion and exposed to increasing concentrations of H_2O_2 (* $p<0.05$ 0 uM versus 55uM GFP occludin; $ $p<0.05$ 05 0 uM versus 110 uM GFP occludin; #, $p<0.05$ 05 0 uM versus 55uM ZO-1 deletion).

5.1.4 FRAP Analysis of Tight Junction Proteins *In vivo*

To determine if tight junction mobility decreases *in vivo,* we used hydrodynamic delivery to inject animals with the same occludin constructs used in our *in vitro* models. Figure 57 indicated high immobility of occludin prior to ischemia, but a significant decrease in immobility following ischemia contrary to our *in vitro* data. Analysis of half-life also indicated increased occludin turnover following ischemia compared to control and *in vitro* models (Figure 58). Our *in vivo* data indicates that rather than increasing occludin immobility, ischemia decreases immobility aiding in tight junction recovery following injury.

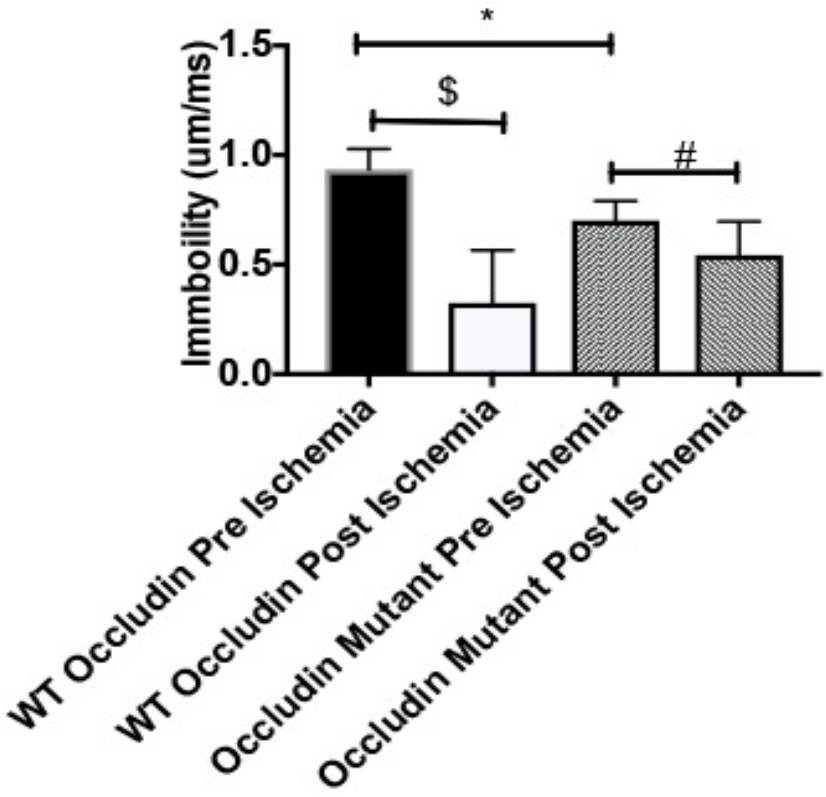

Figure 57: Analysis of Tight Junction Immobility *in vivo.* Rats received hydrodynamic delivery of adenoviral GFP occludin or occludin 860 truncation and four days later underwent FRAP before and after ischemia (n=4 per group; *$p<0.05$ WT pre- ischemia versus occludin mutant pre-ischemia; $ $p<0.05$ WT pre-ischemia versus WT post-ischemia; # $p<0.05$ occludin mutant pre-ischemia versus occludin mutant post-ischemia).

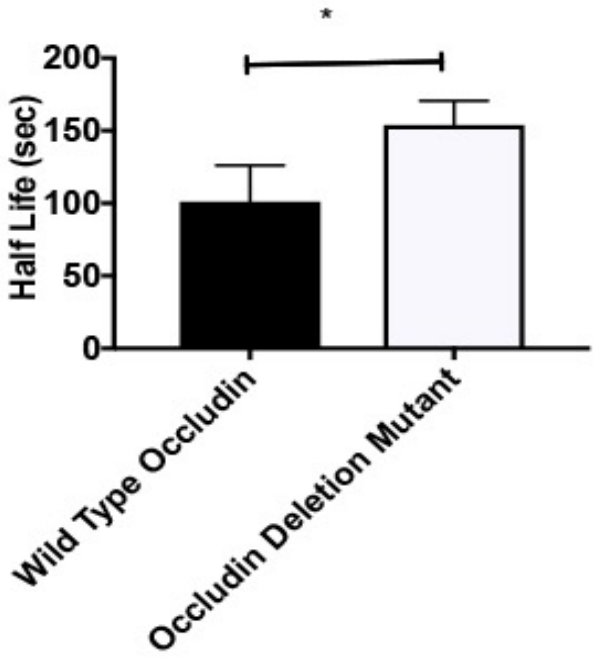

Figure 58: Analysis of Occludin Half-Life Following Ischemia. Rats received hydrodynamic delivery of adenoviral GFP occludin or occludin 860 truncation and four days later underwent FRAP before and after ischemia. Graph shows half-life of fluorescent recovery following photobleaching (n=4 per group; *$p<0.05$ WT versus mutant).

5.1.5 Conclusion

Paracellular leak is a potential mechanism for renal epithelial cell death. While the main cause remains unclear, what we know is that ischemic injuries target tight junction proteins such as occludin and increases in H_2O_2 exacerbate this injury (161, 163). Our data indicate that occludin turnover is slow following injury and that this may contribute to an increased leak state. Using this information, we analyzed the leak pathway in our animal model. Using hydrodynamic gene delivery, we imaged occludin *in vivo,* both before and after ischemia. Contrary to our cellular model, we found that ischemia increases tight junction mobility and recovery (Figure 57 and 58) thus decreasing the cellular leak state. The importance of occludin in our model cannot be understated. The introduction of occludin mutants in our data shows decreased mobility and recovery of fluorescence. To continue to analyze the role of occludin and other tight junction proteins in recovery, we plan to deliver other occludin mutants such as a ZO-1 binding site deletion and assay mobility and half-life *in vivo.* In the future, we plan to hydrodynamicly deliver other proteins such as claudin to determine the effects on claudin on tight junctions.

5.2 Gene Delivery of Sulfotransferase 1C2 (SULT1C2)

5.2.1 SULT1C2 Post-Translationally Increases Mitochondria Respiration.

Sulfotransferases are enzymes responsible for xenobiotic detoxification. Mechanistically, these enzymes add a sulfate group to xenobiotics which increases their water solubility and urinary excretion. We identified SULT1C2 in a proteomic screen of mitochondria isolated from ischemic preconditioned kidneys. Using hydrodynamic gene delivery, we show that SULT1C2 protects against subsequent ischemia one week after gene delivery. To determine SULT1C2's mechanism of action, we assayed mitochondria function with and without human recombinant SULT1C2 and its substrate, 3' Phosophoadenosine-5'-phosophosulfate (PAPS). Mitochondria respiration was assayed using an Oroboros Oxygraph O2K. We found that that PAPS and SULT1C2 incubated with mitochondria increase mitochondria state III respiration (from 139.4 ±36 to 370.7 ±32 pmol/min/mg), following succinate and rotenone addition, 2.7-fold compared to mitochondria ($P<0.05$). The increase in SULT1C2/PAPS dependent respiration was inhibitable with antimycin A but not rotenone. In conclusion, SULT1C2 and PAPS increase the efficiency of complex II respiration indicating a potential change in the movement of electrons through the complex culminating in increased oxidative phosphorylation. This is a novel function for an enzyme that heretofore was considered to be solely involved in detoxifying xenobiotics.

5.2.2 SULT1C2 Mimics IPC Similar to IDH2

SULT1C2 was identified in the same proteomic screen that detected IDH2. SULT1C2 was upregulated 2.4-fold compared to sham IPC animals, which is 0.2-fold higher then IDH2 (Table 4). To determine if *SULT1C2* delivery mimics IPC, we subjected rats to either IPC or *SULT1C2* delivery and allowed them to recover. As expected, IPC treated rats were resistant to IRI as indicated by reduced serum creatinine 24 hours following IRI, relative to sham IPC. Interestingly, *SULT1C2* resulted in a similar reduction in SCr (Figure 59), and improved tissue histology scoring in response to IRI (Figure 60 and 61). Analysis of mitochondria 60 minutes following reperfusion, demonstrated SULT1C2 preserved respiratory capacity relative to vehicle controls (Figure 62). In a similar fashion to IDH2 and IPC, SULT1C2 was also found to increase mitochondria membrane potential indicating both *in vitro* and *in vivo* a potential mechanism for study (Figure 63 -64).

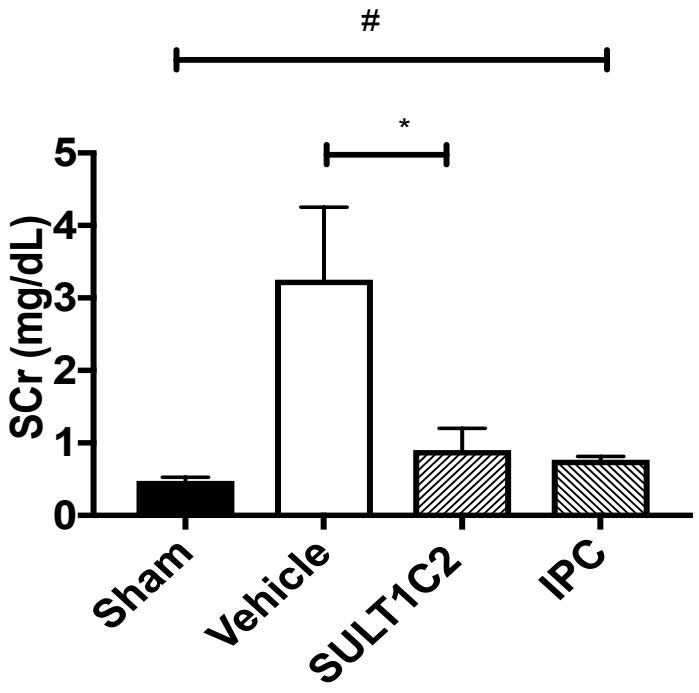

Figure 59: SULT1C2 Mimics IPC and Blunts SCr increase. Comparison of SCr following IPC or SULT1C2 delivery 24 hours following IRI (*p < 0.05 IDH2 versus vehicle; #p < 0.05 IPC versus vehicle).

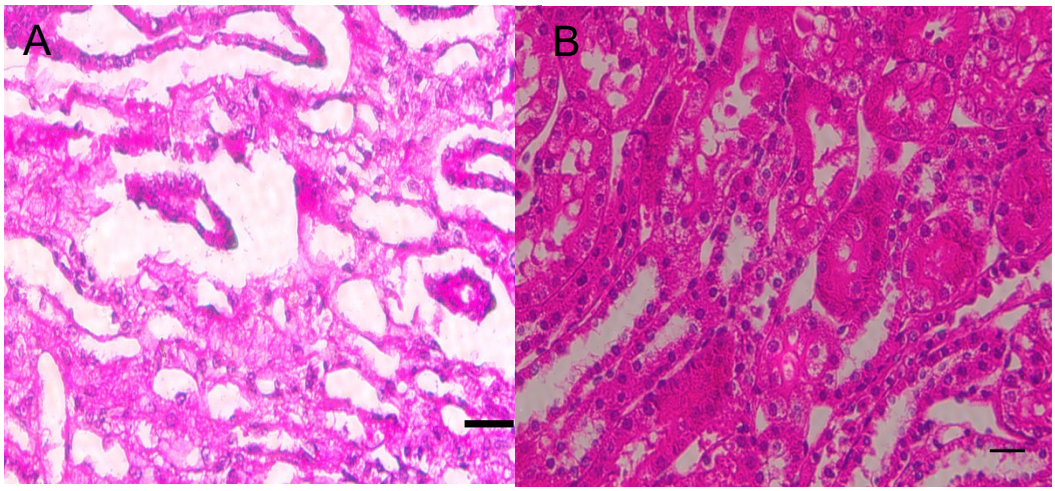

Figure 60: Tissue Histology Detailing the effects of SULT1C2 on Injury Prevention. Hematoxylin and Eosin stained section of renal outer medulla following IRI in rats treated with saline (a) or SULT1C2 injection (b).

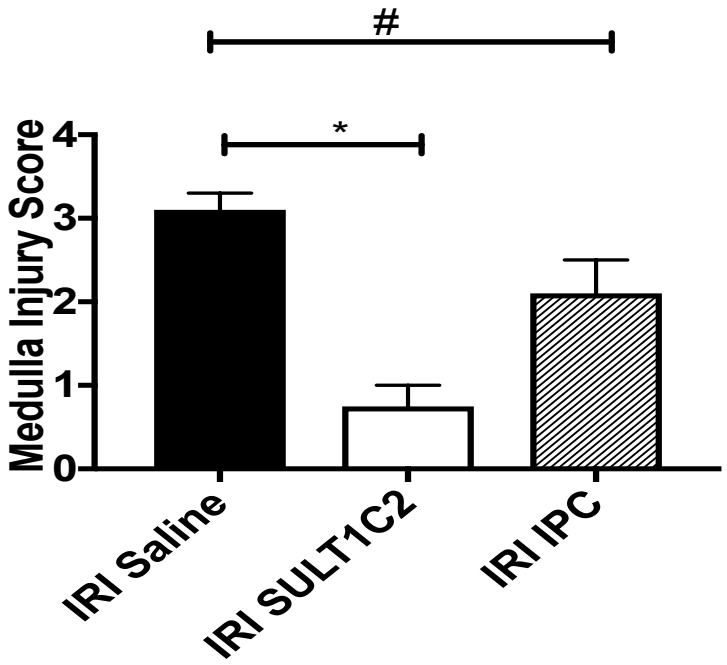

Figure 61: Quantitation of Tissue Histology. Corresponding injury scoring for Figure 60 (# $p<0.05$ IRI IPC versus IRI Saline; *$p<0.05$ IRI SULT1C2 versus IRI saline).

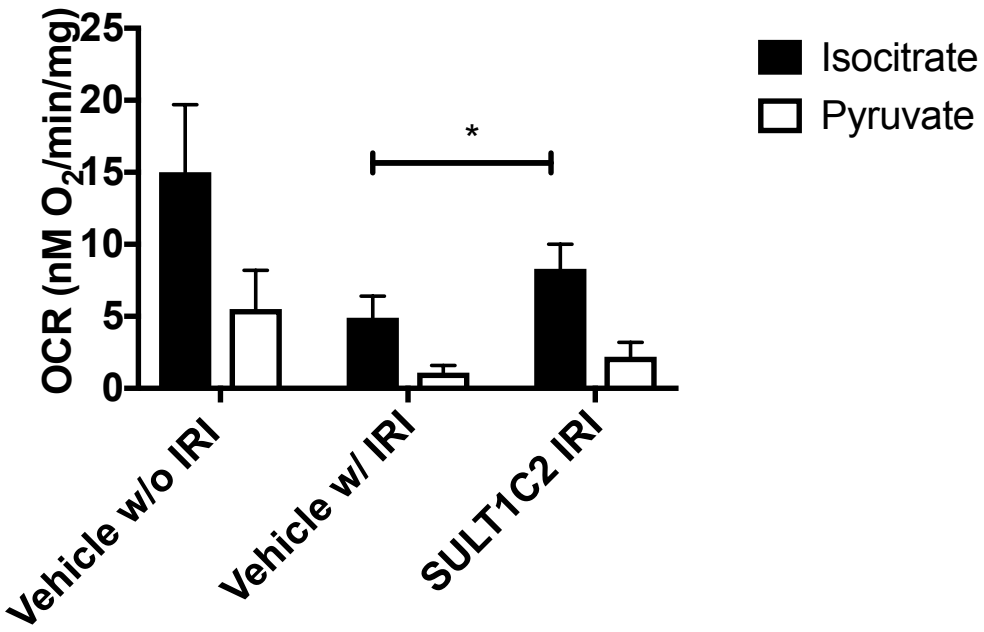

Figure 62: The Protective Effects of SULT1C2 on Mitochondria Oximetry. Mitochondria respiration one hour following IRI in vehicle or SULT1C2 treated rats is shown with pyruvate (white) or isocitrate (black) as a substrate (n=4 per group; * $p<0.05$ SULT1C2 IRI versus vehicle IRI.

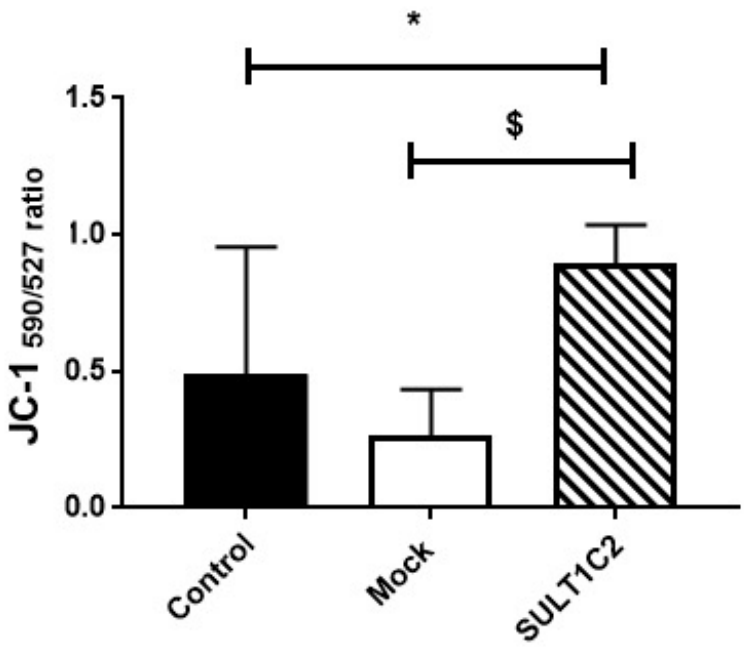

Figure 63: SULT1C2 Increases Mitochondria Membrane Potential *in vitro.* JC-1 fluorescent intensity ratios in MPTC S3 with or without SULT1C2 following hypoxia.

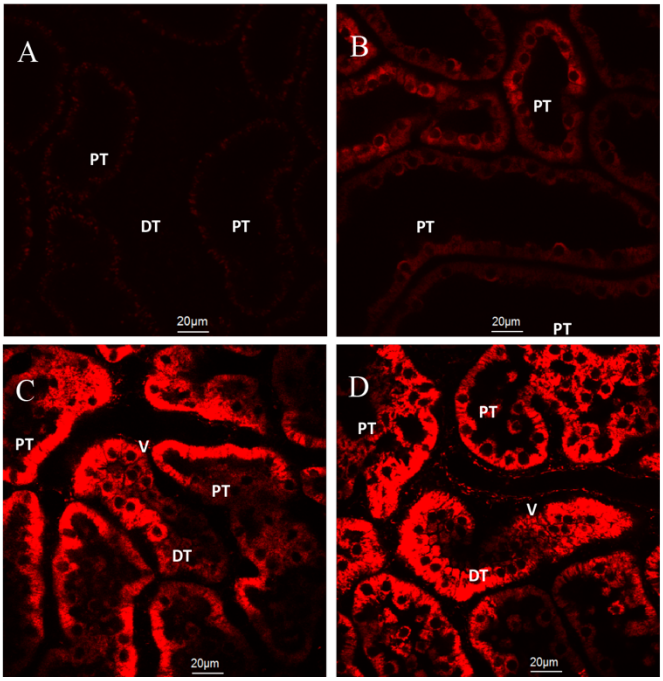

Figure 64: Mitochondria Membrane Analysis Following Gene Delivery and IPC. TMRM labeled mitochondria by intravital microscopy in sham rats (A), rats following injection of saline (B), SULT1C2 (C) or following IPC (D).

5.2.3 Characterizing the Mechanism of SULT1C2

To determine the mechanism of protection of Sulfotransferase 1C2, human recombinant SULT1C2 and its substrate PAPS were added to isolated mitochondria. Analysis of mitochondria respiration indicated that mitochondria treated with both SULT1C2 and PAPS had a 2.7-fold increase in state III respiration following Succinate addition compared to control mitochondria (Figure 65). This increase in SULT1C2/PAPS dependent respiration was inhibitable with antimycin A but not rotenone. As a potential mechanism for this increase in respiration we analyzed changes in mitochondria membrane fluidity using Laurdan and Fluorescence Lifetime Imaging Microscopy (FLIM). The addition of Laurdan to the SULT1C2/PAPS sample shows a decrease in the Fluorescent Lifetime of Laurdan compared to control mitochondria (Figure 66). This indicates a potential decrease in mitochondria membrane fluidity and a potential increase in the efficiency of electron movement through mitochondria complexes. This decrease in fluidity was the result of the addition of a sulfate group to either proteins or lipids on the mitochondria surface. We eliminated the possibility of protein sulfation by immune blot. Our data indicates that mitochondria with SULT1C2/PAPS contained membrane proteins with 4-fold lower sulfate levels then control mitochondria (Figure 67). To determine the possibility of lipid sulfation we measured mitochondria respiration in the presence of cholesterol sulfate. Our data indicates the addition of cholesterol sulfate increases mitochondria state three respiration to levels similar to that of Sult1C2 and PAPS (Figure 68).

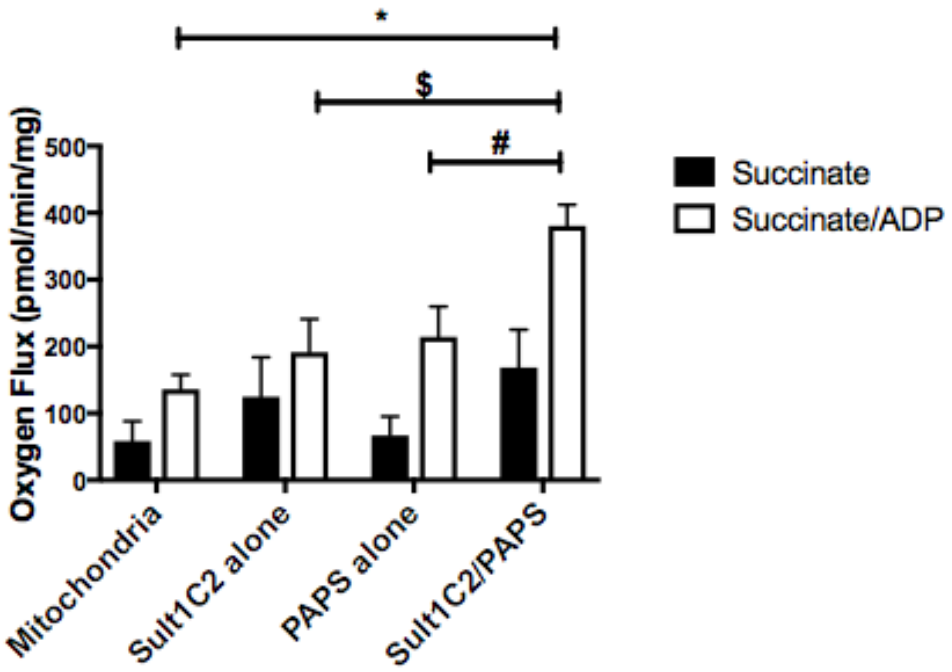

Figure 65: Post-Translational Modification of Mitochondria Respiration by SULT1C2. Mitochondria states II and III respiration were analyzed with 500 ng of mitochondria in the presence of PAPS, SULT1C2, and SULT1C2/PAPS. (n=4 in all groups; * $p<0.05$ Mitochondria alone versus SULT1C2 and PAPS; \$$p<0.05$ PAPS alone versus SULT1C2 and PAPS; # $p<0.05$ SULT1C2 alone versus SULT1C2 and PAPS.

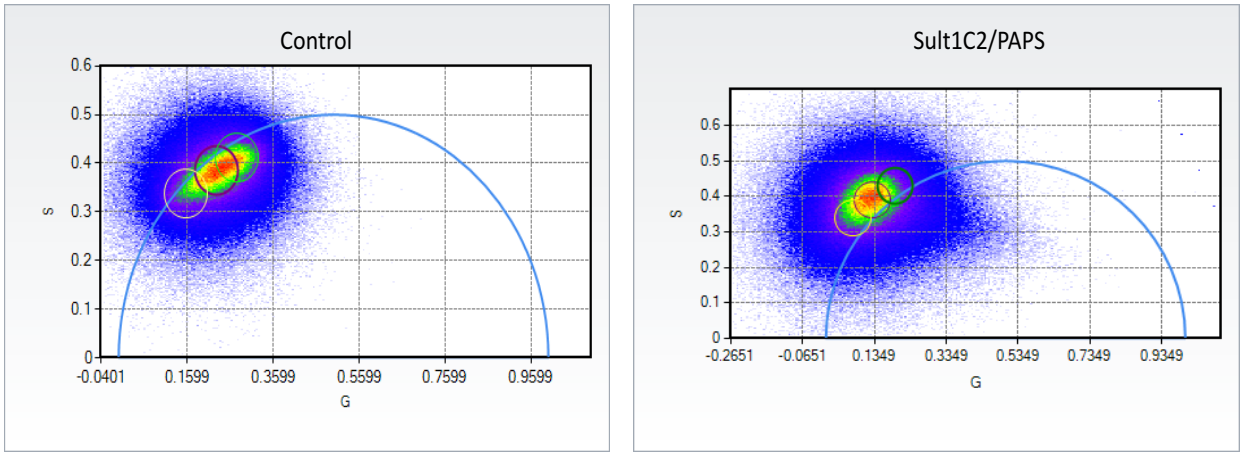

Figure 66: FLIM Analysis of Sult1C2 and PAPS on Mitochondria Membrane Fluidity. Mitochondria lysates were analyzed by FLIM following the addition of Laurdan, Mitotracker Red, Sult1C2, and PAPS. Phasor plot indicates the addition of SULT1C2 and PAPs decrease Laurdan lifetime indicating potential changes in mitochondria membrane packaging.

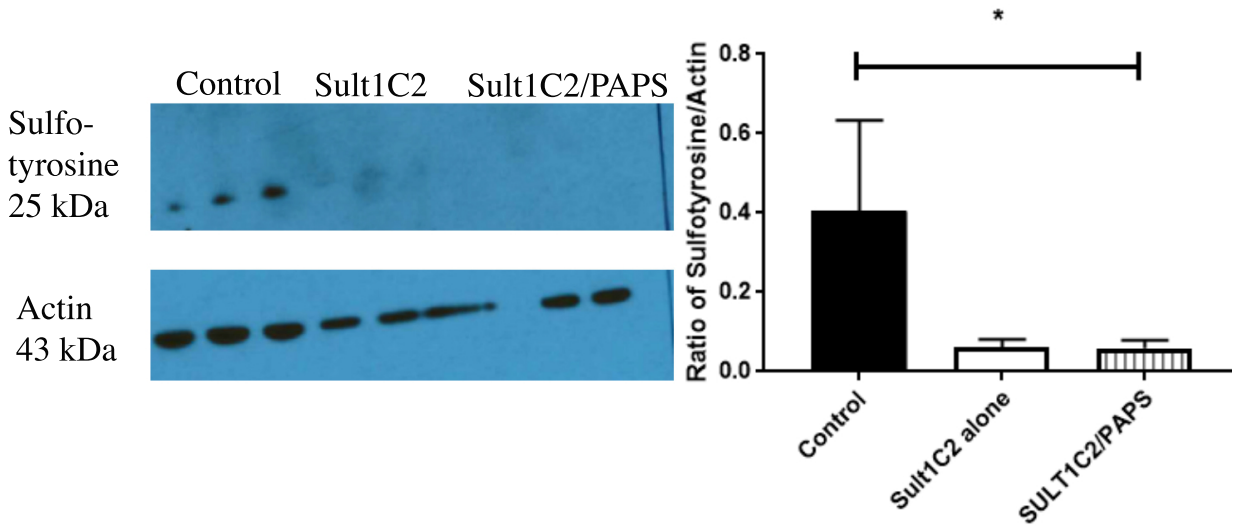

Figure 67: Sulfotyrosine Immune Blot. Mitochondria sulfotyrosine levels were analyzed in the presence of Sult1C2 alone or with Sult1C2/PAPS. Addition of SULT1C2/PAPS decreased the presence of sulfated tyrosine (n=4; *$p<0.05$ Mitochondria alone versus SULT1C2/PAPS).

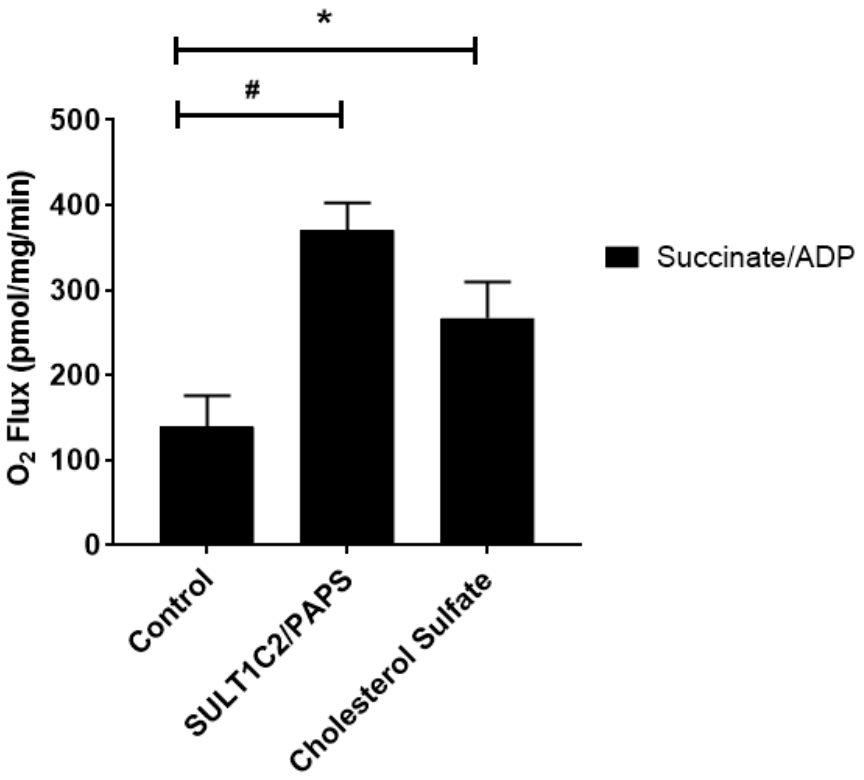

Figure 68: Lipid Sulfation Increases Mitochondria Respiration Similar to Sult1C2. Mitochondria respiration analyzed in the presence of cholesterol sulfate. Data indicates the addition of the cholesterol sulfate increases mitochondria respiration similar to Sult1C2 and PAPS (* $p < 0.05$ Control versus Cholesterol Sulfate; # $p < 0.05$ Control versus Sult1C2/PAPS).

5.2.4 SULT1C2 Conclusion

The identification of Sult1C2 in our proteomic analysis clearly indicated its importance in protecting the kidney from AKI. In addition, we demonstrate for the first time that the action of this protein occurs post-translationally (Figure 65). To determine if this post-translational modification occurred to proteins we performed an immune blot. Our immune blot indicated a decrease in mitochondria membrane protein sulfation following the addition of Sult1C2 and PAPS compared to control mitochondria (Figure 66). The lack of sulfate addition to mitochondria membrane proteins following the addition of Sult1C2 and PAPS reduced the likelihood of proteins contributing to the membrane and respiration changes (Figure 67). Next, we analyzed if this post-translational sulfation occurred to cholesterol. Mitochondria state three respiration was analyzed in the presence of cholesterol sulfate. Our data indicated that the addition of cholesterol sulfate increased mitochondria state three respiration similar to that of Sult1C2 and PAPS (Figure 68). Collectively our data indicated that Sult1C2 sulfated cholesterol found in the mitochondria membrane. This sulfation reduced membrane fluidity leading to potential increases in electron flow through the ETC culminating in increased state three respiration.

CHAPTER 6: DISCUSSION

Acute kidney injury is a complex disease to study. Treatment is limited; progression to irreversible forms of kidney injury is likely; and mortality rates continue to rise despite advances in modern medicine. A common misconception with renal disease is that dialysis is the cure. In reality, once a patient is placed on dialysis the likelihood of eliminating the need for dialysis is slim and quality of life is poor. Aside from time spent in the hospital, cost of renal treatment increases annually while the technology remains the same. Our goal was to develop a means to eliminate need for continued dialysis treatment and to reduce cost. We believe hydrodynamic fluid delivery through the renal vein provides a mechanism for treatment.

AKI targets the kidney on both a cell and organelle level. On the cellular level, AKI targets both the renal epithelium (specifically tubular epithelial cells) and the endothelium. Damage to these cell types includes vascular congestion caused by red and white blood cell aggregation, necrotic tissue, and mononuclear cell infiltration leading to inflammation (9, 19, 20, 42, 43). This damage is associated with poor capillary blood flow culminating in decreased filtration and urine output. On an organelle level, AKI targets renal mitochondria leading to bioenergetic changes resulting in decreased glycolytic and oxidative output. These changes in energetic output cause alterations in mitochondria structure and function, activating signaling pathways which initiate cell death cascades (165, 166). In order to treat AKI, both aspects of injury must be addressed.

Treatments for AKI fall into one of two groups. First, we considered patients suffering from AKI and aimed to develop a means to reverse disease progression by reducing vascular congestion and immune cell infiltration culminating in normal blood flow. The second group consists of patients at risk for AKI, but who have not yet developed the disease. We used our understanding of ischemic preconditioning (IPC) to study proteins responsible for the preconditioned state and proposed potential mechanisms for renal gene therapy. The goal for our type of gene delivery is to mimic IPC. The commonality between each group was the tool used for treatment. We used hydrodynamic fluid delivery of saline or mitochondrial genes to reverse or prevent AKI.

Our model of AKI consists of a 35-minute ischemic injury followed by 24 hours of reperfusion at which point we analyze our injury with serum creatinine measurements and tissue histology (Figures 17 and 19). Following injury, we used hydrodynamic isotonic fluid delivery through renal vein or control injections in the vena cava to study injury reversal. Following hydrodynamic isotonic fluid delivery, we see reductions in SCr, vascular congestion, and medullary tissue injury not seen in control vena cava injections (Figure 17, 19, and 20). In addition to these reductions, we also see reductions in mononuclear cell infiltration not seen in our control injections (Figures 25-27). Since congestion and inflammation are leading causes in reduction of renal blood flow, we decided to analyze renal blood flow before and after hydrodynamic isotonic fluid delivery. We found that following injury there was an 81% reduction in blood flow compared to our control animals. 30 minutes following hydrodynamic isotonic fluid delivery we see a two-fold increase in renal blood flow compared to pre-HIFD values (Figure 22). A major finding from our blood flow study came when we analyzed Hoechst

33342 (nuclear stain) which has a molecular weight of 452 g/mol. This weight is similar to medications, such as steroids or ionotropes, currently used for treating kidney injury. Following injury, Hoechst 33342 levels were low, indicating potential decreases in cellular permeability. However, following hydrodynamic isotonic fluid delivery, there was a four-fold increase in fluorescence intensity (Figures 22 and 23). This suggests that hydrodynamic isotonic fluid delivery allows movement of compounds through the cell membrane regardless of decreased membrane permeability, without damage to the epithelium (Figure 25). In Chapter 3 we are able to demonstrate a mechanism by which we can ameliorate AKI, by reducing congestion and immune cell infiltration, and propose a technique that is translatable to the clinic.

Despite the ability to reverse AKI, the kidney remains susceptible to future injury (Figure 32). Prevention of AKI by IPC was discovered in work by Zager *et al* (57) and Joo *et al* (58). Zager *et al* demonstrated that ischemic preconditioning is possible in the kidney, and Joo *et al* demonstrated in murine models that non-lethal doses of ischemia can protect the kidney from future IRI. Using this information, we analyzed the proteome of rat kidneys that were subjected to IPC. We found 12 potential candidate proteins (six upregulated, six downregulated) that promote recovery from injury. We chose to analyze Isocitrate Dehydrogenase II (IDH2), a mitochondria protein involved in the TCA cycle and reactive oxygen species reduction. Using hydrodynamic delivery, we delivered *IDH2* through the renal vein seven days prior to IRI. Delivery of *IDH2* prior to IRI protects the kidney from injury, prevents renal cell death, and maintains mitochondria respiration and ATP levels (Figures 48-52). Our findings are similar to Han *et al*, who demonstrate that IDH2 knockdown leads to impaired mitochondria and thus disease, stressing the

importance of IDH2 in maintaining normal renal function (86). Using this information, we next analyzed the potential mechanism of IDH2 protection. Using TMRM and JC-1, mitochondrial membrane dyes that are sensitive to changes in membrane potential, we found that IDH2 increases membrane potential in a similar fashion to IPC (Figure 37; Figures 44-45). This increase in membrane potential is associated with prevention of cell death pathways, coupled with increase in mitochondria bioenergetic pathway activity (62). Analysis of mitochondria respiration revealed that transfection or delivery of IDH2 increased states I, II, and III respiration (Figure 38-42; Figure 46). Interestingly, *IDH2* transfection also increased SRC, spare respiratory capacity, which has been linked to survival of cells prone to oxidative stress (167-170). *IDH2* transfection increases SRC indicating that prior to injury onset, cells are primed to handle oxidative stress and allocate additional energy to aid in cellular recovery. As we mentioned earlier, IDH2 generates NAD(P)H which can be used either in the electron transport chain or in the oxidation of H_2O_2. We hypothesized that gene delivery of *IDH2* would increase the levels of NAD(P)H in the cell. We analyzed the levels of NAD(P)H using FLIM. Our data indicates that transfection of *IDH2* does not change the levels of NAD(P)H in the cell (Figure 48-49). While our hypothesis was not correct, the results were not surprising. A major driving force of normal mitochondria metabolism is the separation and maintenance of reduction pools. For example, it is critical that cells maintain the proper ratio of NAD+ to NADH in the cytoplasm and the mitochondria to promote the continuation of glycolysis and the ETC. It is reported that in normal rat liver cytoplasm the ratio of NAD+ to NADH 725 and in the mitochondria the ratio is 8 (171). This ratio only changes during times of stress or injury when it becomes difficult to maintain

homeostasis. Therefore, the absence of increased reduction potential following *IDH2* transfection in a normal cell is not surprising and our data indicates the importance of maintaining these ratios. Our final oxidative analysis was of ATP levels following delivery of *IDH2*. We found that delivery of *IDH2* increases ATP/AMP ratio (Figure 36 and Figure 52). This ratio increase corresponds to a potential increase in ATP stores providing oxidative capacity needed to recover from IRI. We believe that increases in membrane potential, SRC, and ATP indicate prevention of a glycolytic shift typically seen following ischemic injuries (172). *IDH2* acts to increase metabolic output in preparation for injury. It is important to point out that mitochondria biogenesis may also be a mechanism by which IDH2 protects against AKI, and is an area of future study. Mitochondria biogenesis, like IPC, is regulated by PGC-1 α, and analyzing changes in this factor may point to the role of IDH2 in both IPC and mitochondria biogenesis (173).

We were able to demonstrate a mechanism by which we can ameliorate and prevent AKI. The critical aspect of hydrodynamic fluid delivery is that it is practical and translatable to the clinic. We believe this tool will one day be used in the clinic not just to reverse AKI, but also to prevent its onset. *IDH2* and *SULT1C2* are only two of the 12 potential candidate proteins that can be used to mimic IPC. Further studies are needed to determine the potential role of these additional candidate proteins in preventing AKI.

REFERENCES

1. Collett JA, Corridon PR, Mehrotra P, Kolb AL, Rhodes GJ, Miller CA, Molitoris BA, Pennington JG, Sandoval RM, Atkinson SJ, et al. Hydrodynamic Isotonic Fluid Delivery Ameliorates Moderate-to-Severe Ischemia-Reperfusion Injury in Rat Kidneys. *J Am Soc Nephrol.* 2017.
2. Basile DP, Anderson MD, and Sutton TA. Pathophysiology of acute kidney injury. *Compr Physiol.* 2012;2(2):1303-53.
3. Chertow GM, Burdick E, Honour M, Bonventre JV, and Bates DW. Acute kidney injury, mortality, length of stay, and costs in hospitalized patients. *J Am Soc Nephrol.* 2005;16(11):3365-70.
4. Silver SA, Long J, Zheng Y, and Chertow GM. Cost of Acute Kidney Injury in Hospitalized Patients. *J Hosp Med.* 2017;12(2):70-6.
5. Canessa M, Adragna N, Solomon HS, Connolly TM, and Tosteson DC. Increased sodium-lithium countertransport in red cells of patients with essential hypertension. *N Engl J Med.* 1980;302(14):772-6.
6. Friedewald JJ, and Rabb H. Inflammatory cells in ischemic acute renal failure. *Kidney Int.* 2004;66(2):486-91.
7. Zhuo JL, and Li XC. Proximal nephron. *Compr Physiol.* 2013;3(3):1079-123.
8. Basile DP, Friedrich JL, Spahic J, Knipe N, Mang H, Leonard EC, Changizi-Ashtiyani S, Bacallao RL, Molitoris BA, and Sutton TA. Impaired endothelial proliferation and mesenchymal transition contribute to vascular rarefaction following acute kidney injury. *Am J Physiol Renal Physiol.* 2011;300(3):F721-33.
9. Basile DP, and Yoder MC. Renal endothelial dysfunction in acute kidney ischemia reperfusion injury. *Cardiovasc Hematol Disord Drug Targets.* 2014;14(1):3-14.
10. Dean R, Zhuo J, Alcorn D, Casley D, and Mendelsohn FA. Cellular distribution of 125I-endothelin-1 binding in rat kidney following in vivo labeling. *Am J Physiol.* 1994;267(5 Pt 2):F845-52.
11. Dean R, Zhuo J, Alcorn D, Casley D, and Mendelsohn FA. Cellular localization of endothelin receptor subtypes in the rat kidney following in vitro labelling. *Clin Exp Pharmacol Physiol.* 1996;23(6-7):524-31.
12. Haberle DA, and von Baeyer H. Characteristics of glomerulotubular balance. *Am J Physiol.* 1983;244(4):F355-66.
13. Kriz W, and Bankir L. A standard nomenclature for structure of the kidney. The Renal Commission of the International Union of Physiological Sciences(IUPS). *Anat Embryol (Berl).* 1988;178(2):N1-8.
14. McDonough AA. Mechanisms of proximal tubule sodium transport regulation that link extracellular fluid volume and blood pressure. *Am J Physiol Regul Integr Comp Physiol.* 2010;298(4):R851-61.
15. Thomson SC, and Blantz RC. Glomerulotubular balance, tubuloglomerular feedback, and salt homeostasis. *J Am Soc Nephrol.* 2008;19(12):2272-5.

16. Mehta RL, Kellum JA, Shah SV, Molitoris BA, Ronco C, Warnock DG, Levin A, and Acute Kidney Injury N. Acute Kidney Injury Network: report of an initiative to improve outcomes in acute kidney injury. *Crit Care.* 2007;11(2):R31.
17. Murugan R, and Kellum JA. Acute kidney injury: what's the prognosis? *Nat Rev Nephrol.* 2011;7(4):209-17.
18. Venkatachalam MA, Griffin KA, Lan R, Geng H, Saikumar P, and Bidani AK. Acute kidney injury: a springboard for progression in chronic kidney disease. *Am J Physiol Renal Physiol.* 2010;298(5):F1078-94.
19. Sutton TA, Mang HE, Campos SB, Sandoval RM, Yoder MC, and Molitoris BA. Injury of the renal microvascular endothelium alters barrier function after ischemia. *Am J Physiol Renal Physiol.* 2003;285(2):F191-8.
20. Sutton TA, and Molitoris BA. Mechanisms of cellular injury in ischemic acute renal failure. *Semin Nephrol.* 1998;18(5):490-7.
21. Bellomo R, Kellum JA, and Ronco C. Acute kidney injury. *Lancet.* 2012;380(9843):756-66.
22. Corridon PR, Rhodes GJ, Leonard EC, Basile DP, Gattone VH, 2nd, Bacallao RL, and Atkinson SJ. A method to facilitate and monitor expression of exogenous genes in the rat kidney using plasmid and viral vectors. *Am J Physiol Renal Physiol.* 2013;304(9):F1217-29.
23. Lameire N, Van Massenhove J, and Van Biesen W. What is the difference between prerenal and renal acute kidney injury? *Acta Clin Belg.* 2012;67(5):309-14.
24. Prowle J, Bagshaw SM, and Bellomo R. Renal blood flow, fractional excretion of sodium and acute kidney injury: time for a new paradigm? *Curr Opin Crit Care.* 2012;18(6):585-92.
25. Sarabu N, and Rahman M. Nephrology Update: Acute Kidney Injury. *FP Essent.* 2016;444(11-7.
26. Yang F, Zhang L, Wu H, Zou H, and Du Y. Clinical analysis of cause, treatment and prognosis in acute kidney injury patients. *PLoS One.* 2014;9(2):e85214.
27. Hoste EA, Bagshaw SM, Bellomo R, Cely CM, Colman R, Cruz DN, Edipidis K, Forni LG, Gomersall CD, Govil D, et al. Epidemiology of acute kidney injury in critically ill patients: the multinational AKI-EPI study. *Intensive Care Med.* 2015;41(8):1411-23.
28. Uchino S, Kellum JA, Bellomo R, Doig GS, Morimatsu H, Morgera S, Schetz M, Tan I, Bouman C, Macedo E, et al. Acute renal failure in critically ill patients: a multinational, multicenter study. *JAMA.* 2005;294(7):813-8.
29. Bezemer R, Legrand M, Klijn E, Heger M, Post IC, van Gulik TM, Payen D, and Ince C. Real-time assessment of renal cortical microvascular perfusion heterogeneities using near-infrared laser speckle imaging. *Opt Express.* 2010;18(14):15054-61.
30. De Backer D, Creteur J, Preiser JC, Dubois MJ, and Vincent JL. Microvascular blood flow is altered in patients with sepsis. *Am J Respir Crit Care Med.* 2002;166(1):98-104.
31. De Backer D, Donadello K, Taccone FS, Ospina-Tascon G, Salgado D, and Vincent JL. Microcirculatory alterations: potential mechanisms and implications for therapy. *Ann Intensive Care.* 2011;1(1):27.

32. Gomez H, and Kellum JA. Sepsis-induced acute kidney injury. *Curr Opin Crit Care.* 2016;22(6):546-53.
33. Seely KA, Holthoff JH, Burns ST, Wang Z, Thakali KM, Gokden N, Rhee SW, and Mayeux PR. Hemodynamic changes in the kidney in a pediatric rat model of sepsis-induced acute kidney injury. *Am J Physiol Renal Physiol.* 2011;301(1):F209-17.
34. Spronk PE, Ince C, Gardien MJ, Mathura KR, Oudemans-van Straaten HM, and Zandstra DF. Nitroglycerin in septic shock after intravascular volume resuscitation. *Lancet.* 2002;360(9343):1395-6.
35. Takasu O, Gaut JP, Watanabe E, To K, Fagley RE, Sato B, Jarman S, Efimov IR, Janks DL, Srivastava A, et al. Mechanisms of cardiac and renal dysfunction in patients dying of sepsis. *Am J Respir Crit Care Med.* 2013;187(5):509-17.
36. Wang Z, Holthoff JH, Seely KA, Pathak E, Spencer HJ, 3rd, Gokden N, and Mayeux PR. Development of oxidative stress in the peritubular capillary microenvironment mediates sepsis-induced renal microcirculatory failure and acute kidney injury. *Am J Pathol.* 2012;180(2):505-16.
37. Bolisetty S, and Agarwal A. Neutrophils in acute kidney injury: not neutral any more. *Kidney Int.* 2009;75(7):674-6.
38. Chen GY, and Nunez G. Sterile inflammation: sensing and reacting to damage. *Nat Rev Immunol.* 2010;10(12):826-37.
39. Kurts C, Panzer U, Anders HJ, and Rees AJ. The immune system and kidney disease: basic concepts and clinical implications. *Nat Rev Immunol.* 2013;13(10):738-53.
40. Medzhitov R. Inflammation 2010: new adventures of an old flame. *Cell.* 2010;140(6):771-6.
41. Valles PG, Lorenzo AG, Bocanegra V, and Valles R. Acute kidney injury: what part do toll-like receptors play? *Int J Nephrol Renovasc Dis.* 2014;7(241-51.
42. Basile DP. The endothelial cell in ischemic acute kidney injury: implications for acute and chronic function. *Kidney Int.* 2007;72(2):151-6.
43. Sutton TA, Fisher CJ, and Molitoris BA. Microvascular endothelial injury and dysfunction during ischemic acute renal failure. *Kidney Int.* 2002;62(5):1539-49.
44. Murry CE, Jennings RB, and Reimer KA. Preconditioning with ischemia: a delay of lethal cell injury in ischemic myocardium. *Circulation.* 1986;74(5):1124-36.
45. Massip-Salcedo M, Rosello-Catafau J, Prieto J, Avila MA, and Peralta C. The response of the hepatocyte to ischemia. *Liver Int.* 2007;27(1):6-16.
46. Wynsen JC, Kenny D, Brooks HL, and Warltier DC. Regional myocardial function after repetitive brief episodes of ischemia: effect of altering the duration of the reperfusion period. *Am Heart J.* 1991;121(5):1331-8.
47. Yokota H, Narayanan SP, Zhang W, Liu H, Rojas M, Xu Z, Lemtalsi T, Nagaoka T, Yoshida A, Brooks SE, et al. Neuroprotection from retinal ischemia/reperfusion injury by NOX2 NADPH oxidase deletion. *Invest Ophthalmol Vis Sci.* 2011;52(11):8123-31.
48. Hausenloy DJ, Tsang A, Mocanu MM, and Yellon DM. Ischemic preconditioning protects by activating prosurvival kinases at reperfusion. *Am J Physiol Heart Circ Physiol.* 2005;288(2):H971-6.

49. Hausenloy DJ, and Yellon DM. New directions for protecting the heart against ischaemia-reperfusion injury: targeting the Reperfusion Injury Salvage Kinase (RISK)-pathway. *Cardiovasc Res.* 2004;61(3):448-60.
50. Zhao Z, and Rivkees SA. Programmed cell death in the developing heart: regulation by BMP4 and FGF2. *Dev Dyn.* 2000;217(4):388-400.
51. Zhao ZQ, Nakamura M, Wang NP, Velez DA, Hewan-Lowe KO, Guyton RA, and Vinten-Johansen J. Dynamic progression of contractile and endothelial dysfunction and infarct extension in the late phase of reperfusion. *J Surg Res.* 2000;94(2):133-44.
52. Zhao ZQ, Nakamura M, Wang NP, Wilcox JN, Shearer S, Ronson RS, Guyton RA, and Vinten-Johansen J. Reperfusion induces myocardial apoptotic cell death. *Cardiovasc Res.* 2000;45(3):651-60.
53. Lecour S. Activation of the protective Survivor Activating Factor Enhancement (SAFE) pathway against reperfusion injury: Does it go beyond the RISK pathway? *J Mol Cell Cardiol.* 2009;47(1):32-40.
54. Lacerda L, Somers S, Opie LH, and Lecour S. Ischaemic postconditioning protects against reperfusion injury via the SAFE pathway. *Cardiovasc Res.* 2009;84(2):201-8.
55. Lecour S. Multiple protective pathways against reperfusion injury: a SAFE path without Aktion? *J Mol Cell Cardiol.* 2009;46(5):607-9.
56. Rodriguez-Sinovas A, Cabestrero A, Lopez D, Torre I, Morente M, Abellan A, Miro E, Ruiz-Meana M, and Garcia-Dorado D. The modulatory effects of connexin 43 on cell death/survival beyond cell coupling. *Prog Biophys Mol Biol.* 2007;94(1-2):219-32.
57. Zager RA, and Baltes LA. Progressive renal insufficiency induces increasing protection against ischemic acute renal failure. *J Lab Clin Med.* 1984;103(4):511-23.
58. Joo JD, Kim M, D'Agati VD, and Lee HT. Ischemic preconditioning provides both acute and delayed protection against renal ischemia and reperfusion injury in mice. *J Am Soc Nephrol.* 2006;17(11):3115-23.
59. Kapitsinou PP, and Haase VH. Molecular mechanisms of ischemic preconditioning in the kidney. *Am J Physiol Renal Physiol.* 2015;309(10):F821-34.
60. Hausenloy DJ. Signalling pathways in ischaemic postconditioning. *Thromb Haemost.* 2009;101(4):626-34.
61. Sarkar K, Rey S, Zhang X, Sebastian R, Marti GP, Fox-Talbot K, Cardona AV, Du J, Tan YS, Liu L, et al. Tie2-dependent knockout of HIF-1 impairs burn wound vascularization and homing of bone marrow-derived angiogenic cells. *Cardiovasc Res.* 2012;93(1):162-9.
62. Jassem W, Fuggle SV, Rela M, Koo DD, and Heaton ND. The role of mitochondria in ischemia/reperfusion injury. *Transplantation.* 2002;73(4):493-9.
63. Reimer KA, Murry CE, and Richard VJ. The role of neutrophils and free radicals in the ischemic-reperfused heart: why the confusion and controversy? *J Mol Cell Cardiol.* 1989;21(12):1225-39.
64. Alberts B. *Molecular biology of the cell.* New York: Garland Science; 2002.

65. Lehninger AL, Nelson DL, and Cox MM. *Lehninger principles of biochemistry.* New York: W.H. Freeman; 2013.
66. Nicholls DG, Ferguson SJ, and ebrary Inc. San Diego, Calif.: Academic Press,; 2002:xviii, 297 p.
67. Kroemer G, Galluzzi L, and Brenner C. Mitochondrial membrane permeabilization in cell death. *Physiol Rev.* 2007;87(1):99-163.
68. Ma L, Chou JW, Snipes JA, Bharadwaj MS, Craddock AL, Cheng D, Weckerle A, Petrovic S, Hicks PJ, Hemal AK, et al. APOL1 Renal-Risk Variants Induce Mitochondrial Dysfunction. *J Am Soc Nephrol.* 2017;28(4):1093-105.
69. Hu CA, Klopfer EI, and Ray PE. Human apolipoprotein L1 (ApoL1) in cancer and chronic kidney disease. *FEBS Lett.* 2012;586(7):947-55.
70. Reeves-Daniel AM, DePalma JA, Bleyer AJ, Rocco MV, Murea M, Adams PL, Langefeld CD, Bowden DW, Hicks PJ, Stratta RJ, et al. The APOL1 gene and allograft survival after kidney transplantation. *Am J Transplant.* 2011;11(5):1025-30.
71. Chan DC. Mitochondria: dynamic organelles in disease, aging, and development. *Cell.* 2006;125(7):1241-52.
72. Dimauro S, and Davidzon G. Mitochondrial DNA and disease. *Ann Med.* 2005;37(3):222-32.
73. Wallace DC. A mitochondrial paradigm of metabolic and degenerative diseases, aging, and cancer: a dawn for evolutionary medicine. *Annu Rev Genet.* 2005;39(359-407.
74. Niaudet P. Mitochondrial disorders and the kidney. *Arch Dis Child.* 1998;78(4):387-90.
75. Hurley JH, Dean AM, Koshland DE, Jr., and Stroud RM. Catalytic mechanism of NADP(+)-dependent isocitrate dehydrogenase: implications from the structures of magnesium-isocitrate and NADP+ complexes. *Biochemistry.* 1991;30(35):8671-8.
76. Kumar SM, Pampa KJ, Manjula M, Abdoh MM, Kunishima N, and Lokanath NK. Crystal structure studies of NADP+ dependent isocitrate dehydrogenase from Thermus thermophilus exhibiting a novel terminal domain. *Biochem Biophys Res Commun.* 2014;449(1):107-13.
77. Minard KI, and McAlister-Henn L. Dependence of peroxisomal beta-oxidation on cytosolic sources of NADPH. *J Biol Chem.* 1999;274(6):3402-6.
78. Ronnebaum SM, Ilkayeva O, Burgess SC, Joseph JW, Lu D, Stevens RD, Becker TC, Sherry AD, Newgard CB, and Jensen MV. A pyruvate cycling pathway involving cytosolic NADP-dependent isocitrate dehydrogenase regulates glucose-stimulated insulin secretion. *J Biol Chem.* 2006;281(41):30593-602.
79. Shechter I, Dai P, Huo L, and Guan G. IDH1 gene transcription is sterol regulated and activated by SREBP-1a and SREBP-2 in human hepatoma HepG2 cells: evidence that IDH1 may regulate lipogenesis in hepatic cells. *J Lipid Res.* 2003;44(11):2169-80.
80. Wen H, Cho HR, Yun T, Kim H, Park CK, Lee SH, Choi SH, and Park S. Metabolomic comparison between cells over-expressing isocitrate dehydrogenase 1 and 2 mutants and the effects of an inhibitor on the metabolism. *J Neurochem.* 2015;132(2):183-93.

81. Comte B, Vincent G, Bouchard B, Benderdour M, and Des Rosiers C. Reverse flux through cardiac NADP(+)-isocitrate dehydrogenase under normoxia and ischemia. *Am J Physiol Heart Circ Physiol.* 2002;283(4):H1505-14.
82. Hartong DT, Dange M, McGee TL, Berson EL, Dryja TP, and Colman RF. Insights from retinitis pigmentosa into the roles of isocitrate dehydrogenases in the Krebs cycle. *Nat Genet.* 2008;40(10):1230-4.
83. Lee SM, Koh HJ, Park DC, Song BJ, Huh TL, and Park JW. Cytosolic NADP(+)-dependent isocitrate dehydrogenase status modulates oxidative damage to cells. *Free Radic Biol Med.* 2002;32(11):1185-96.
84. Lee SM, Park SY, Shin SW, Kil IS, Yang ES, and Park JW. Silencing of cytosolic NADP(+)-dependent isocitrate dehydrogenase by small interfering RNA enhances the sensitivity of HeLa cells toward staurosporine. *Free Radic Res.* 2009;43(2):165-73.
85. Mailloux RJ, Beriault R, Lemire J, Singh R, Chenier DR, Hamel RD, and Appanna VD. The tricarboxylic acid cycle, an ancient metabolic network with a novel twist. *PLoS One.* 2007;2(8):e690.
86. Han SJ, Jang HS, Noh MR, Kim J, Kong MJ, Kim JI, Park JW, and Park KM. Mitochondrial NADP+-Dependent Isocitrate Dehydrogenase Deficiency Exacerbates Mitochondrial and Cell Damage after Kidney Ischemia-Reperfusion Injury. *J Am Soc Nephrol.* 2017;28(4):1200-15.
87. Stoddard BL, Dean A, and Koshland DE, Jr. Structure of isocitrate dehydrogenase with isocitrate, nicotinamide adenine dinucleotide phosphate, and calcium at 2.5-A resolution: a pseudo-Michaelis ternary complex. *Biochemistry.* 1993;32(36):9310-6.
88. Steen IH, Madern D, Karlstrom M, Lien T, Ladenstein R, and Birkeland NK. Comparison of isocitrate dehydrogenase from three hyperthermophiles reveals differences in thermostability, cofactor specificity, oligomeric state, and phylogenetic affiliation. *J Biol Chem.* 2001;276(47):43924-31.
89. Falany CN. Enzymology of human cytosolic sulfotransferases. *FASEB J.* 1997;11(4):206-16.
90. Falany CN. Sulfation and sulfotransferases. Introduction: changing view of sulfation and the cytosolic sulfotransferases. *FASEB J.* 1997;11(1):1-2.
91. Negishi M, Pedersen LG, Petrotchenko E, Shevtsov S, Gorokhov A, Kakuta Y, and Pedersen LC. Structure and function of sulfotransferases. *Archives of biochemistry and biophysics.* 2001;390(2):149-57.
92. Gamage N, Barnett A, Hempel N, Duggleby RG, Windmill KF, Martin JL, and McManus ME. Human sulfotransferases and their role in chemical metabolism. *Toxicol Sci.* 2006;90(1):5-22.
93. Miller AD. Human gene therapy comes of age. *Nature.* 1992;357(6378):455-60.
94. Verma IM, and Somia N. Gene therapy -- promises, problems and prospects. *Nature.* 1997;389(6648):239-42.
95. Gao J, Liu W, Xia Y, Li W, Sun J, Chen H, Li B, Zhang D, Qian W, Meng Y, et al. The promotion of siRNA delivery to breast cancer overexpressing epidermal growth factor receptor through anti-EGFR antibody conjugation by immunoliposomes. *Biomaterials.* 2011;32(13):3459-70.

96. Gao J, Yu Y, Zhang Y, Song J, Chen H, Li W, Qian W, Deng L, Kou G, Chen J, et al. EGFR-specific PEGylated immunoliposomes for active siRNA delivery in hepatocellular carcinoma. *Biomaterials.* 2012;33(1):270-82.
97. Gao Y, Liu XL, and Li XR. Research progress on siRNA delivery with nonviral carriers. *Int J Nanomedicine.* 2011;6(1017-25.
98. Li SD, and Huang L. Targeted delivery of antisense oligodeoxynucleotide and small interference RNA into lung cancer cells. *Mol Pharm.* 2006;3(5):579-88.
99. Shim MS, and Kwon YJ. Efficient and targeted delivery of siRNA in vivo. *FEBS J.* 2010;277(23):4814-27.
100. Tsai LR, Chen MH, Chien CT, Chen MK, Lin FS, Lin KM, Hwu YK, Yang CS, and Lin SY. A single-monomer derived linear-like PEI-co-PEG for siRNA delivery and silencing. *Biomaterials.* 2011;32(14):3647-53.
101. Zhang S, Zhao Y, Zhi D, and Zhang S. Non-viral vectors for the mediation of RNAi. *Bioorg Chem.* 2012;40(1):10-8.
102. Czech MP, Aouadi M, and Tesz GJ. RNAi-based therapeutic strategies for metabolic disease. *Nat Rev Endocrinol.* 2011;7(8):473-84.
103. Judge AD, Bola G, Lee AC, and MacLachlan I. Design of noninflammatory synthetic siRNA mediating potent gene silencing in vivo. *Mol Ther.* 2006;13(3):494-505.
104. Robbins M, Judge A, and MacLachlan I. siRNA and innate immunity. *Oligonucleotides.* 2009;19(2):89-102.
105. Semple SC, Akinc A, Chen J, Sandhu AP, Mui BL, Cho CK, Sah DW, Stebbing D, Crosley EJ, Yaworski E, et al. Rational design of cationic lipids for siRNA delivery. *Nat Biotechnol.* 2010;28(2):172-6.
106. Dai Y, Roman M, Naviaux RK, and Verma IM. Gene therapy via primary myoblasts: long-term expression of factor IX protein following transplantation in vivo. *Proc Natl Acad Sci U S A.* 1992;89(22):10892-5.
107. Fields BN, Knipe DM, Howley PM, Griffin DE, and Lippincott Williams & Wilkins. Philadelphia, PA: Lippincott Williams & Wilkins,; 2002:1 computer laser optical disc.
108. Naldini L, Blomer U, Gage FH, Trono D, and Verma IM. Efficient transfer, integration, and sustained long-term expression of the transgene in adult rat brains injected with a lentiviral vector. *Proc Natl Acad Sci U S A.* 1996;93(21):11382-8.
109. Naldini L, Blomer U, Gallay P, Ory D, Mulligan R, Gage FH, Verma IM, and Trono D. In vivo gene delivery and stable transduction of nondividing cells by a lentiviral vector. *Science.* 1996;272(5259):263-7.
110. Yeh P, and Perricaudet M. Advances in adenoviral vectors: from genetic engineering to their biology. *FASEB J.* 1997;11(8):615-23.
111. Miao CH, Snyder RO, Schowalter DB, Patijn GA, Donahue B, Winther B, and Kay MA. The kinetics of rAAV integration in the liver. *Nat Genet.* 1998;19(1):13-5.
112. Muzyczka N. Adeno-associated virus (AAV) vectors: will they work? *J Clin Invest.* 1994;94(4):1351.
113. Choate KA, and Khavari PA. Direct cutaneous gene delivery in a human genetic skin disease. *Hum Gene Ther.* 1997;8(14):1659-65.

114. Hickman MA, Malone RW, Lehmann-Bruinsma K, Sih TR, Knoell D, Szoka FC, Walzem R, Carlson DM, and Powell JS. Gene expression following direct injection of DNA into liver. *Hum Gene Ther.* 1994;5(12):1477-83.
115. Meyer KB, Thompson MM, Levy MY, Barron LG, and Szoka FC, Jr. Intratracheal gene delivery to the mouse airway: characterization of plasmid DNA expression and pharmacokinetics. *Gene Ther.* 1995;2(7):450-60.
116. Wolff JA, Malone RW, Williams P, Chong W, Acsadi G, Jani A, and Felgner PL. Direct gene transfer into mouse muscle in vivo. *Science.* 1990;247(4949 Pt 1):1465-8.
117. Zhang G, Vargo D, Budker V, Armstrong N, Knechtle S, and Wolff JA. Expression of naked plasmid DNA injected into the afferent and efferent vessels of rodent and dog livers. *Hum Gene Ther.* 1997;8(15):1763-72.
118. Durieux AC, Bonnefoy R, Busso T, and Freyssenet D. In vivo gene electrotransfer into skeletal muscle: effects of plasmid DNA on the occurrence and extent of muscle damage. *J Gene Med.* 2004;6(7):809-16.
119. Heller LC, Ugen K, and Heller R. Electroporation for targeted gene transfer. *Expert Opin Drug Deliv.* 2005;2(2):255-68.
120. Neumann E, Schaefer-Ridder M, Wang Y, and Hofschneider PH. Gene transfer into mouse lyoma cells by electroporation in high electric fields. *EMBO J.* 1982;1(7):841-5.
121. Yang NS, and Sun WH. Gene gun and other non-viral approaches for cancer gene therapy. *Nat Med.* 1995;1(5):481-3.
122. Yang NS, Burkholder J, Roberts B, Martinell B, and McCabe D. In vivo and in vitro gene transfer to mammalian somatic cells by particle bombardment. *Proc Natl Acad Sci U S A.* 1990;87(24):9568-72.
123. J. WAaO. Methods for the collection of fluid from single glomeruli and tubules of the mammalian kidney. . *Am J Physiol.* 1941134):562-79
. 124. AN WJaR. Observations on the composition of glomerular urine, with particular reference to the problem of reabsorption in the renal tubules. *Am J Physiol* 192471):209-27.
125. Lorenz JN. Micropuncture of the kidney: a primer on techniques. *Compr Physiol.* 2012;2(1):621-37.
126. Tanner GA, Sandoval RM, Molitoris BA, Bamburg JR, and Ashworth SL. Micropuncture gene delivery and intravital two-photon visualization of protein expression in rat kidney. *Am J Physiol Renal Physiol.* 2005;289(3):F638-43.
127. Eastman SJ, Baskin KM, Hodges BL, Chu Q, Gates A, Dreusicke R, Anderson S, and Scheule RK. Development of catheter-based procedures for transducing the isolated rabbit liver with plasmid DNA. *Hum Gene Ther.* 2002;13(17):2065-77.
128. Herweijer H, and Wolff JA. Gene therapy progress and prospects: hydrodynamic gene delivery. *Gene Ther.* 2007;14(2):99-107.
129. Liu J, Puckett JL, Takeda T, Jung HY, and Mittal RK. Crural diaphragm inhibition during esophageal distension correlates with contraction of the esophageal longitudinal muscle in cats. *Am J Physiol Gastrointest Liver Physiol.* 2005;288(5):G927-32.

130. Maruyama H, Higuchi N, Nishikawa Y, Hirahara H, Iino N, Kameda S, Kawachi H, Yaoita E, Gejyo F, and Miyazaki J. Kidney-targeted naked DNA transfer by retrograde renal vein injection in rats. *Hum Gene Ther.* 2002;13(3):455-68.
131. Maruyama H, Higuchi N, Nishikawa Y, Kameda S, Iino N, Kazama JJ, Takahashi N, Sugawa M, Hanawa H, Tada N, et al. High-level expression of naked DNA delivered to rat liver via tail vein injection. *J Gene Med.* 2002;4(3):333-41.
132. Wells DJ. Gene therapy progress and prospects: electroporation and other physical methods. *Gene Ther.* 2004;11(18):1363-9.
133. Hall AM, Rhodes GJ, Sandoval RM, Corridon PR, and Molitoris BA. In vivo multiphoton imaging of mitochondrial structure and function during acute kidney injury. *Kidney Int.* 2013;83(1):72-83.
134. Schindelin J, Arganda-Carreras I, Frise E, Kaynig V, Longair M, Pietzsch T, Preibisch S, Rueden C, Saalfeld S, Schmid B, et al. Fiji: an open-source platform for biological-image analysis. *Nat Methods.* 2012;9(7):676-82.
135. Todaro GJ, and Green H. Quantitative studies of the growth of mouse embryo cells in culture and their development into established lines. *J Cell Biol.* 1963;17(299-313.
136. Dunn KW, Sutton TA, and Sandoval RM. Live-animal imaging of renal function by multiphoton microscopy. *Curr Protoc Cytom.* 2012;Chapter 14(Unit12 9.
137. Zheng CY, Petralia RS, Wang YX, and Kachar B. Fluorescence recovery after photobleaching (FRAP) of fluorescence tagged proteins in dendritic spines of cultured hippocampal neurons. *Journal of visualized experiments : JoVE.* 201150).
138. Basile DP, Dwinell MR, Wang SJ, Shames BD, Donohoe DL, Chen S, Sreedharan R, and Van Why SK. Chromosome substitution modulates resistance to ischemia reperfusion injury in Brown Norway rats. *Kidney international.* 2013;83(2):242-50.
139. Mehrotra P, Patel JB, Ivancic CM, Collett JA, and Basile DP. Th-17 cell activation in response to high salt following acute kidney injury is associated with progressive fibrosis and attenuated by AT-1R antagonism. *Kidney international.* 2015;88(4):776-84.
140. Barreto R, Mandili G, Witzmann FA, Novelli F, Zimmers TA, and Bonetto A. Cancer and Chemotherapy Contribute to Muscle Loss by Activating Common Signaling Pathways. *Front Physiol.* 2016;7(472.
141. Lai X, Wang L, Tang H, and Witzmann FA. A novel alignment method and multiple filters for exclusion of unqualified peptides to enhance label-free quantification using peptide intensity in LC-MS/MS. *J Proteome Res.* 2011;10(10):4799-812.
142. Bacallao R, Antony C, Dotti C, Karsenti E, Stelzer EH, and Simons K. The subcellular organization of Madin-Darby canine kidney cells during the formation of a polarized epithelium. *The Journal of cell biology.* 1989;109(6 Pt 1):2817-32.
143. Dunn KW, Kamocka MM, and McDonald JH. A practical guide to evaluating colocalization in biological microscopy. *Am J Physiol Cell Physiol.* 2011;300(4):C723-42.

144. Kelly KJ, Sandoval RM, Dunn KW, Molitoris BA, and Dagher PC. A novel method to determine specificity and sensitivity of the TUNEL reaction in the quantitation of apoptosis. *Am J Physiol Cell Physiol.* 2003;284(5):C1309-18.
145. Gnaiger E. Capacity of oxidative phosphorylation in human skeletal muscle: new perspectives of mitochondrial physiology. *Int J Biochem Cell Biol.* 2009;41(10):1837-45.
146. Lores-Arnaiz S, Lombardi P, Karadayian AG, Orgambide F, Cicerchia D, and Bustamante J. Brain cortex mitochondrial bioenergetics in synaptosomes and non-synaptic mitochondria during aging. *Neurochem Res.* 2016;41(1-2):353-63.
147. Yoshino J, and Imai S. Accurate measurement of nicotinamide adenine dinucleotide (NAD(+)) with high-performance liquid chromatography. *Methods Mol Biol.* 2013;1077(203-15.
148. Lv Q, Xing S, Li Z, Li J, Gong P, Xu X, Chang L, Jin X, Gao F, Li W, et al. Altered expression levels of IDH2 are involved in the development of colon cancer. *Exp Ther Med.* 2012;4(5):801-6.
149. Abbate M, Zoja C, and Remuzzi G. How does proteinuria cause progressive renal damage? *J Am Soc Nephrol.* 2006;17(11):2974-84.
150. Winfree S, Hato T, and Day RN. Intravital microscopy of biosensor activities and intrinsic metabolic states. *Methods.* 2017.
151. Digman MA, Caiolfa VR, Zamai M, and Gratton E. The phasor approach to fluorescence lifetime imaging analysis. *Biophys J.* 2008;94(2):L14-6.
152. Carden DL, and Granger DN. Pathophysiology of ischaemia-reperfusion injury. *J Pathol.* 2000;190(3):255-66.
153. Molitoris BA, Sandoval R, and Sutton TA. Endothelial injury and dysfunction in ischemic acute renal failure. *Crit Care Med.* 2002;30(5 Suppl):S235-40.
154. Molitoris BA, and Sutton TA. Endothelial injury and dysfunction: role in the extension phase of acute renal failure. *Kidney Int.* 2004;66(2):496-9.
155. Luke DR, Berens KL, and Verani RR. Role of vascular decongestion in ischemic acute renal failure defined by postinsult administration of pentoxifylline. *Ren Fail.* 1989;11(4):187-94.
156. Mason J, Torhorst J, and Welsch J. Role of the medullary perfusion defect in the pathogenesis of ischemic renal failure. *Kidney Int.* 1984;26(3):283-93.
157. Lin J, Handschin C, and Spiegelman BM. Metabolic control through the PGC-1 family of transcription coactivators. *Cell Metab.* 2005;1(6):361-70.
158. Condello M, Caraglia M, Castellano M, Arancia G, and Meschini S. Structural and functional alterations of cellular components as revealed by electron microscopy. *Microsc Res Tech.* 2013;76(10):1057-69.
159. Kaunitz JD, Cummins VP, Mishler D, and Nagami GT. Inhibition of gentamicin uptake into cultured mouse proximal tubule epithelial cells by L-lysine. *J Clin Pharmacol.* 1993;33(1):63-9.
160. Kroning R, Katz D, Lichtenstein AK, and Nagami GT. Differential effects of cisplatin in proximal and distal renal tubule epithelial cell lines. *Br J Cancer.* 1999;79(2):293-9.
161. Janosevic D, Axis J, Bacallao RL, and Amsler K. Occludin Content Modulates Hydrogen Peroxide-Induced Increase in Renal Epithelial Paracellular Permeability. *J Cell Biochem.* 2016;117(3):769-79.

162. Kwon O, Nelson WJ, Sibley R, Huie P, Scandling JD, Dafoe D, Alfrey E, and Myers BD. Backleak, tight junctions, and cell- cell adhesion in postischemic injury to the renal allograft. *The Journal of clinical investigation.* 1998;101(10):2054-64.
163. Meyer TN, Schwesinger C, Ye J, Denker BM, and Nigam SK. Reassembly of the tight junction after oxidative stress depends on tyrosine kinase activity. *J Biol Chem.* 2001;276(25):22048-55.
164. Yu W, Beaudry S, Negoro H, Boucher I, Tran M, Kong T, and Denker BM. H2O2 activates G protein, alpha 12 to disrupt the junctional complex and enhance ischemia reperfusion injury. *Proceedings of the National Academy of Sciences of the United States of America.* 2012;109(17):6680-5.
165. Chiara F, Castellaro D, Marin O, Petronilli V, Brusilow WS, Juhaszova M, Sollott SJ, Forte M, Bernardi P, and Rasola A. Hexokinase II detachment from mitochondria triggers apoptosis through the permeability transition pore independent of voltage-dependent anion channels. *PLoS One.* 2008;3(3):e1852.
166. Rasola A, and Bernardi P. The mitochondrial permeability transition pore and its involvement in cell death and in disease pathogenesis. *Apoptosis.* 2007;12(5):815-33.
167. Dhingra R, and Kirshenbaum LA. Succinate dehydrogenase/complex II activity obligatorily links mitochondrial reserve respiratory capacity to cell survival in cardiac myocytes. *Cell Death Dis.* 2015;6(e1956.
168. Nickens KP, Wikstrom JD, Shirihai OS, Patierno SR, and Ceryak S. A bioenergetic profile of non-transformed fibroblasts uncovers a link between death-resistance and enhanced spare respiratory capacity. *Mitochondrion.* 2013;13(6):662-7.
169. Pfleger J, He M, and Abdellatif M. Mitochondrial complex II is a source of the reserve respiratory capacity that is regulated by metabolic sensors and promotes cell survival. *Cell Death Dis.* 2015;6(e1835.
170. Sriskanthadevan S, Jeyaraju DV, Chung TE, Prabha S, Xu W, Skrtic M, Jhas B, Hurren R, Gronda M, Wang X, et al. AML cells have low spare reserve capacity in their respiratory chain that renders them susceptible to oxidative metabolic stress. *Blood.* 2015;125(13):2120-30.
171. Williamson DH, Lund P, and Krebs HA. The redox state of free nicotinamide-adenine dinucleotide in the cytoplasm and mitochondria of rat liver. *Biochem J.* 1967;103(2):514-27.
172. Lan R, Geng H, Singha PK, Saikumar P, Bottinger EP, Weinberg JM, and Venkatachalam MA. Mitochondrial Pathology and Glycolytic Shift during Proximal Tubule Atrophy after Ischemic AKI. *J Am Soc Nephrol.* 2016;27(11):3356-67.
173. Ventura-Clapier R, Garnier A, and Veksler V. Transcriptional control of mitochondrial biogenesis: the central role of PGC-1alpha. *Cardiovasc Res.* 2008;79(2):208-17.

VITA

CAREER SUMMARY

I am an accomplished medical-scientific professional with an exceptional blend of research and development and analysis expertise to support and further the development of treatments and methodologies to address medical challenges. I have experience overseeing and managing initiatives to evaluate the efficacy of methodologies and procedures and employing findings to develop solutions.

I am adept in building strong working partnerships with academic professionals, industry experts, fellow research scientists, and staff at all levels. I have excellent communication and leadership capabilities. I am skilled in aligning R&D and medical efforts to achieve overall strategic vision and goals.

CORE COMPETENCIES

- Research & Development
- Evaluation Methodologies
- Grant Submission & Administration
- Strategy Development & Implementation
- Laboratory & Experiment Analysis
- Treatment Development & Tests
- Assay/ Experiment Development & Execution
- Best Practices & Quality Control

LABORATORY AND RESEARCH EXPERIENCE

INDIANA UNIVERSITY PURDUE UNIVERSITY INDIANAPOLIS (2013 – 2017)

DOCTORAL STUDENT, NEPHROLOGY LABORATORY – PRINCIPAL INVESTIGATOR, DR. SIMON ATKINSON (2013 – 2017)

Partnered with Dr. George Rhodes in learning and performing animal surgeries, including hydrodynamic delivery and bilateral renal pedicle clamping to induce ischemic injury.

Determined hydrodynamic delivery pressures during injection in collaboration with Dr. Jason Collett.

Supported further research by working with Ms. Shijun Zhang and Ms. Keyin Lu on western blotting and imaging, mitochondrial protein purification and quantification, mitochondrial respiration assay, plasmid purification, endotoxin quantification and removal, laurdan assay, and serum creatinine measuring.

Imaged the kidney for fluorescent plasmids and heavy weight molecular dye uptake, employing confocal and 2 photon microscopy.

Performed fluorescence recovery after photo-bleaching (FRAP) to study membrane turnover subsequent to ischemia reperfusion injury using a confocal microscope.

Oversaw cell work conducted in the Atkinson laboratory, including transfection and transduction of mouse S3 proximal tubule cells, human embryonic kidney 293 cells, and mitochondrial energetics of the cells using a seahorse machine.

Held full accountability for all animal surgeries performed in the Atkinson laboratory and ensured adherence to all methodologies and best practices.

INDIANA UNIVERSITY PURDUE UNIVERSITY INDIANAPOLIS (Continued)

DOCTORAL ROTATION, LIVER PHYSIOLOGY LABORATORY – PRINCIPAL INVESTIGATOR, DR. GUOLI DAI (2013)

Collaborated with Mr. Joonyong Lee and Mr. Shashank Nambiar on immunohistochemistry, agarose gel preparation and electrophoresis, and PCR techniques for liver DNA and RNA analysis.

DOCTORAL ROTATION, IMMUNOLOGY LABORATORY – PRINCIPAL INVESTIGATOR, DR. HUA-CHEN CHANG (2013)

Worked with Dr. Chun Yu Tung in learning methodologies associated with flow cytometry, antibody purification and labeling, natural killer cell isolation, and Elisa essay.

TEACHING EXPERIENCE

INDIANA UNIVERSITY PURDUE UNIVERSITY INDIANAPOLIS, (2013-2017)

ASSOCIATE INSTRUCTOR, GRADUATE STUDENT (2014 – 2017)

Assisted biochemistry students in mastering topics covered in class, including enzymes and enzyme kinetics, cellular metabolism, carbohydrates, proteins, and nucleotides. I supported students in individual and group settings to ensure an understanding and application of materials, driving positive student outcomes.

LABORATORY TEACHING ASSISTANT, INTRODUCTORY BIOLOGY (2014)

Led and instructed students in laboratory experiments to further and deepen knowledge and understanding of concepts and materials learned in the classroom setting.

Assisted and taught student's laboratory procedures related to pipetting and microscope use, taxonomy, enzyme kinetics, agarose gel electrophoresis, and mitosis and meiosis. Developed and executed one laboratory session weekly for 30 students, graded quizzes, and evaluated laboratory reports.

EDUCATIONAL AND PROFEESIONAL DEVELOPMENT

INDIANA UNIVERSITY PURDUE UNIVERSITY INDIANAPOLIS, Indianapolis, Indiana

PHD IN BIOLOGY (GRADUATION: AUGUST 2017)

Dissertation: Studies on Hydrodynamic Delivery as a Treatment for Acute Kidney Injury

MASTER OF SCIENCE IN BIOLOGY (2010) | GPA 3.9

Relevant Coursework: Molecular Biology; Biochemistry; Biotechnology; Immune System Disorders; Bone Molecular Biology; Plant Molecular Biology; Developmental Biology; Endocrinology; Molecular Biology of Cancer; and Regenerative Biology and Medicine

UNIVERSITY OF MARYLAND BALTIMORE COUNTY, Baltimore, Maryland

BACHELOR OF ARTS IN BIOLOGY (2010) | GPA 3.0

PUBLICATIONS AND PRESENTATIONS

Exogenous gene transmission of mitochondrial NADP+ Isocitrate Dehydrogenase II mimics ischemia preconditioning (Manuscript Under Review)

Renal Vein Hydrodynamic Fluid Delivery Ameliorates Established Renal Injury following Ischemia/Reperfusion Injury, JASN, January 2017

Ischemia leads to Increases in Tight Junction Mobility following FRAP in vivo, Experimental Biology, April 2017

Hydrodynamic delivery of IDH2 Mimics Ischemia Preconditioning, Experimental Biology, April 2017

Hydrodynamic delivery of IDH2 for the treatment of AKI, Indiana Physiological Society, February 2016

AWARDS

American Society of Nephrology Kidneys Stars Selection (2015)
American Society of Nephrology Kidneys Stars Selection (2016)

PROFESSIONAL AFFILIATIONS

Member: November 3 2015-present American Society of Nephrology Member
Member: February 15, 2017-present American Society for Biochemistry and Molecular Biology

TECHNICAL SKILLS

Methodologies: DNA Transfection; FRAP; Adenoviral Expansion and Hydrodynamic Delivery of BSL2 Agents; IHC/IF; Protein Separation; and IACUC (animal use) Protocol Preperation
Software: Image J and Microsoft Excel, PowerPoint, and Word
Research Tools: Medline and Pubmed